Graduate School of Engineering, Nagoya University
Department of Electrical Engineering

A dissertation submitted for the degree of
Doctor of Engineering
2023

Photovoltaic Power System Control to Increase the Flexibility of Frequency Control in Electric Power System

Supervisor: Takeyoshi Kato

Noha Mamdouh Ali Hassan Harag
Student ID: 482041052
harag.noha.mamdouh.ali.hassan.w3@s.mail.nagoya-u.ac.jp
noha.harag@gmail.com

Table of Contents

List of Figures

1. Introduction

1.1. General Background

1.1.1. Increasing renewable energy generation in the world

In the face of the climate crisis, 136 countries around the world have pledged to reach net zero carbon emissions by 2050. In order to achieve this goal, one of the most promising solutions is the massive installation of renewable energy sources (RES). Therefore, the world is experiencing a remarkable increase in the adoption and expansion of RES, marking a significant shift in the global energy landscape. As of the most recent data available, the global capacity of renewable energy installations has witnessed substantial growth. As of the year 2022, the total installed capacity of RES including the conventional hydro power reached an impressive 3372 GW worldwide which represents about 40% of the total installed capacity of all power supply resources [1]. This increase can be attributed to the remarkable progress made in various RES, including solar, wind, geothermal, and biomass.

Photovoltaic power generation (PV) system installations have experienced a particularly notable increase in global capacity. As by the end 2021, the global PV installed capacity represented 945 GW, playing a significant role in the renewable energy mix [2], [3]. Factors contributing to this expansion include the declining costs of PV panels, advancements in PV inverters' technology, and supportive government policies. Likewise, the installations of wind turbine have seen impressive growth. As of 2022, the global installed capacity of wind power stood at approximately 906 GW, with both onshore and offshore wind farms contributing to this progress [4]. Technological advancements, increased investments, and favorable policies promoting wind energy have been instrumental in driving this expansion.

Looking towards the future, experts and industry forecasts suggest that the global renewable energy sector will continue to grow. Projections indicate that the worldwide energy supply is expected to reach 60% of the global electricity in 2050, representing a substantial increase compared to current levels [5]. In the coming three decades, PV system is expected to

become the largest source of renewable electricity generation worldwide in terms of the installed capacity. By 2050, the capacity of installed PV power is expected to surpass 4.6 TW and wind power is expected to rank second after the PV system, with about 2.3 TW, followed by hydropower [6]. These projections consider anticipated advancements in renewable energy technologies, the expansion of supportive policies and regulations, and the growing global demand for clean and sustainable energy sources.

1.1.2. Increasing renewable energy generation in Japan

In order to realize a carbon neutrality by 2050, Japanese government has stated an interim goal of reducing greenhouse gas (GHG) emissions by 46% compared to 2013 levels by 2030 [7]. One reason is that after the Fukushima nuclear accident in 2011, most of the nuclear power plants have been suspended, and replaced with fossil fuel generation. Another reason is that the increase in energy self-sufficiency is also important, and hence RES will be introduced in a large scale into power systems.

In Japan, to accelerate renewable energy deployment, Renewable Portfolio Standard (RPS) policy was once introduced in 2003. The policy requires electric power companies to provide a certain amount of renewable energy to electricity users [8]. As a result, electric energy provided by RES increased from 50,000 GWh in 2004 to 130,000 GWh in 2011, while RES capacity rose from 3 GW to 9 GW [9]. The policy was eventually called off due to low targets. After that, FIT (feed-in-tariff) was introduced in 2012. FIT policy is the most widely used policy around the world. Unlike the RPS policy, FIT policy guarantees an above-market price for renewable energy producers, which gives them incentives to introduce renewable energy into the power system [8].

In Figure 1-1, the left-hand column shows the 2019 power-generation shares of renewable energy (including hydro), nuclear, natural gas, coal, and oil (which includes oil products) in Japan. Specifically, Japan's current capacity of PV system is approximately 70 GW while wind power capacity currently reached 5 GW. The second column portrays the 2030 goals and in the far right-hand column, the figure provides a break-down of renewable energy via a summary of the relative contributions from geothermal, biomass, and other

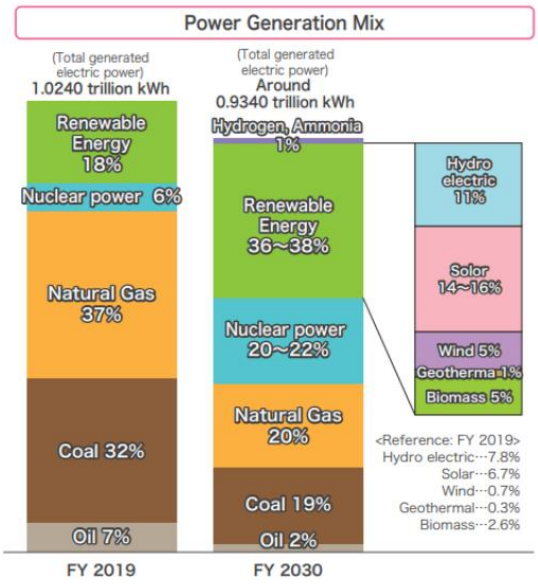

Figure 1-1 Breakdown of total power generation facilities by 2019 and 2030 [10]

renewables. This figure indicates that the current Strategic Energy Plan goals for 2030 project a moderate increase in renewables to about 40% where the PV power contributes to the highest percentage among the other renewables [10].

With more progression in the future, the maximum technical potential of PV system in Japan can be 542 GW by 2050 [11]. The target capacity is 300 GW by Japan Photovoltaic Energy Association (JPEA) while wind is predicted to reach almost 88 GW in 2050 [12]. PV systems are introduced as the main RES in Japan, due to less restriction like land use and weather, compared with wind power and geothermal power generation [13].

1.2. Power system control

1.2.1. General overview of power system control

Voltage and frequency control are essential aspects of power system operation and stability. The power system operator ensures that the voltage levels and frequency of the power system are maintained within acceptable limits for the reliable and efficient operation of the system. Voltage control involves regulating the voltage levels at various points in the power system to ensure they remain within acceptable limits. The standard

voltage level for most power systems is typically defined as the nominal voltage. Voltage control is necessary due to variations in the electricity demand, changes in power generation, and transmission losses. The primary methods of voltage control include, generator voltage control, transformer tap changers, reactive power source including both conventional type and inverter based voltage regulators, etc. [14].

Frequency control involves not only maintaining the power system frequency at the nominal value, usually 50 Hz or 60 Hz, depending on the region, but also recovering the frequency quickly in disturbances. The frequency is determined by the balance between the total generated power and the total consumed power in the system. Frequency control is critical because violation from the acceptable frequency range can lead to synchronization issues, equipment damage, and instability in the power system [15].

The difficulty lies in the fact that electricity demand changes both in the short and long term. To maintain the above balance, the frequency deviations must be controlled within certain limits [15]. However, renewable energy systems, such as PV and wind power, can increase fluctuations in the power system due to their inherent variability. Thus, this will increase the difficulty in maintaining the frequency deviations within these certain limits in various factors shown by the following subsections; the operation on the day, unit commitment scheduling and the future situation of power system with increased PV systems.

1.2.2. Operation on the day

- Supply and demand balancing controls

In a power system operation, it becomes an important issue to keep supply and demand balance with proper frequency due to the uncertain renewable energy output fluctuation. For this, various control methods, i.e. economic dispatching control (EDC), load-frequency control (LFC), and governor-free (GF) control have been considered to properly manage the balancing issue. The relation between these methods is explained as follows by using Figure 1-2, which is called AGC30 model and developed by the Institute of Electrical Engineers of Japan (IEEJ) in 2016 for analyzing and developing the

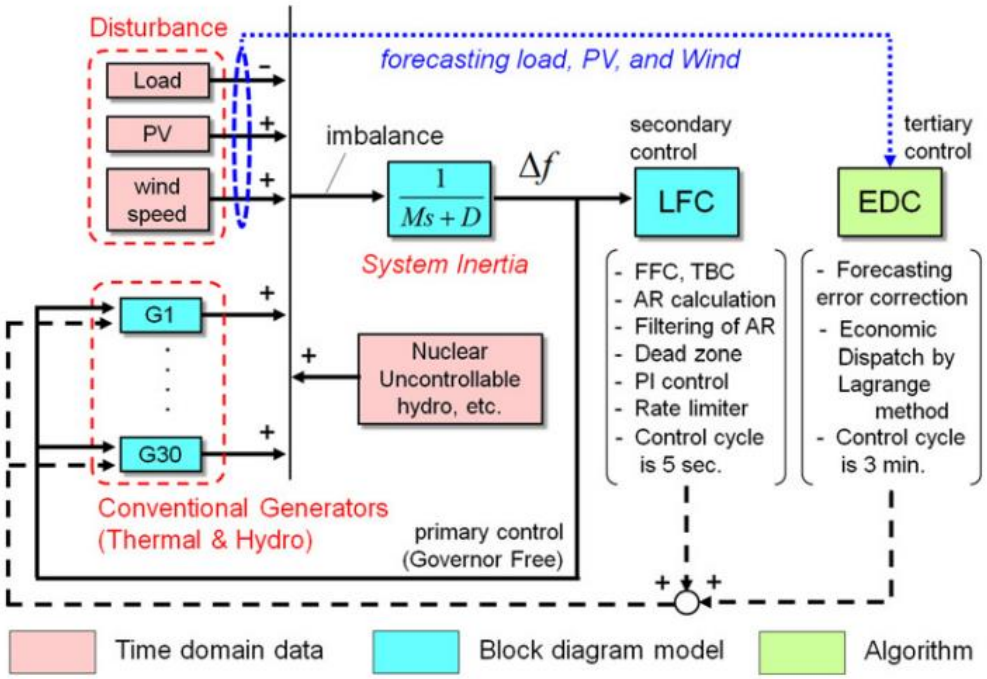

Figure 1-2 AGC30 Model [16]

advanced supply and demand control considering EDC, LFC and GF [16].

This model consists of element models such as conventional power plants, inertia model, tie-line power flow, and time domain data about fluctuation of load and renewable energy output together with the control block of LFC, EDC and GF.

Against long-period demand fluctuation whose time cycle is longer than 20 min, EDC will dispatch the least-costly generation as soon as possible to adjust the imbalance fluctuation based on the short-term loading forecasting. Against short-period demand fluctuation during the control cycle of EDC in several minutes, LFC is applied to compensate the supply/demand imbalance based on the measurement of frequency deviation and tie-line power flow. LFC mainly works to compensate the short-period fluctuation whose time cycle is from several minutes to 20 minutes. Finally, GF control is used to suppress instant frequency violations. Figure 1-2 shows the range in demand fluctuation cycle in which each method mainly work. The following paragraphs are representing the specific mechanisms of EDC, LFC and GF [17].

- EDC

EDC is a method used by power system operators to optimize the allocation of available power generation resources in order to meet electricity demand at the lowest possible cost. It involves determining the most cost-effective combination of power plants to operate, considering factors such as fuel costs, generation capacities, and transmission constraints. By utilizing EDC, operators can ensure efficient utilization of resources, minimize operational costs, and maintain grid reliability while meeting the electricity demand in real-time.

- LFC

LFC is a control mechanism in the power system that uses a central regulator to adjust the active power set points of generating units. Its purpose is to restore power interchanges with adjacent control areas to their programmed values and bring the system frequency back to its set-point value.

Under normal operating conditions, LFC continuously adjusts power based on varying power demand with few minutes as shown in Figure 1-3. It requires a central regulator, systems for measuring interchanged power and system frequency, and a means to transmit regulator signals to relevant generating units. The central regulator minimizes the system

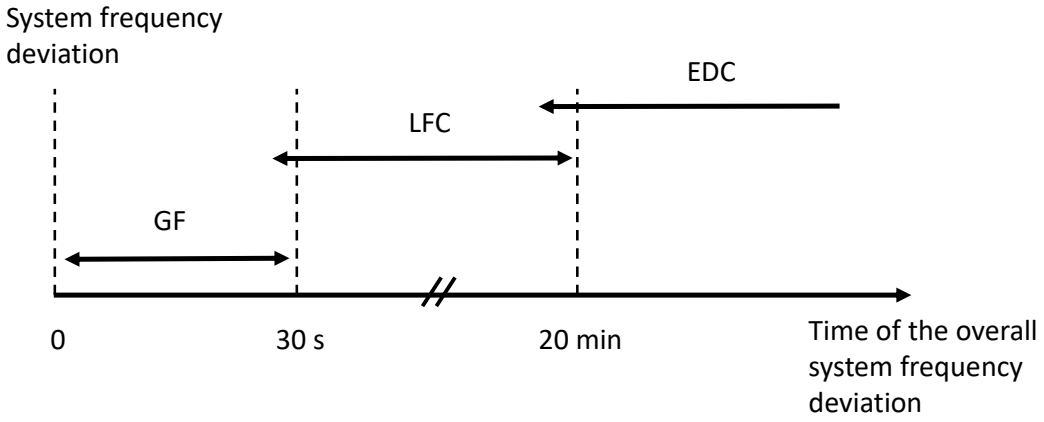

Figure 1-3 The timing of the GF, LFC and EDC ranges in a power system

control error in real-time, considering factors such as measured power interchanges on tie-lines, system frequency, and set-point frequency.

For effective LFC, the generating units involved must have sufficient power reserve to respond to regulator signals by adjusting generated power and the rate of change. The rate of change in the power output at the generator terminals significantly depends on the generation technique. Typically, for oil or gas-fired power stations this rate is about 8% per min, for hard-coal-fired power stations it is up to 2% and 5% per min, respectively, and for nuclear power stations this rate is up to 5% per min. Even in the case of reservoir power stations the rate is 2.5% of the rated plant output per second [19].

- GF control

GF control is a control mechanism in the power system that adjusts a generating unit's power output in response to frequency deviations. GF provides regulation, when the turbo-generator is on bars, by controlling the steam inflow to the turbine. The regulation is envisaged by various control logics and by operating the control valves in the turbine. The speed or power of the steam turbine is controlled by varying the steam flow to the turbine. The GF control action occurs within 0 to 30 seconds after a disturbance affects the power balance as shown in Figure 1-3.

In steady state, GF maintains the system frequency at the nominal value by adjusting the power output. This is done by sensing the rotational speed, comparing it to the desired value, generating a control signal, and adjusting the governing mechanism to correct the frequency deviation.

In non-steady state conditions, the GF responds to transient events like load changes or faults. It detects rotational speed deviations, generates an error signal, and adjusts the governing mechanism to restore the generator's rotational speed and power output. This helps stabilize the system frequency and minimize deviations caused by transient events [20]. This continues until a new balance between power generation and consumption is achieved. Once the balance is restored, the system frequency stabilizes at a quasi-steady-

state value, which differs from the nominal frequency due to generator droop. Then, the controller of that system activate appropriate LFC power to restore the nominal frequency and scheduled power exchanges.

The quasi-steady-state frequency deviation is determined by the disturbance amplitude and the system's stiffness. The effectiveness of GF control relies on the generator's droop characteristics and the availability of GF control reserve in the system. It is essential to have an adequate level of GF control reserve distributed across numerous generating units, ready to be activated within seconds of detecting rotational speed deviations from the nominal value.

1.2.3. Unit Commitment (UC) scheduling

To maintain the electricity supply/demand balance properly throughout the day, the suitable number of operating units should be turned on and off as needed. Scheduling for what units should be online during the day are made in advance based on demand forecasts. Such a scheduling is called a unit commitment (UC) [21]-[23]. Hence, the control variables that are determined a day-ahead are the output of power plants, the amount of GF, LFC and EDC reserves, the charge/discharge power of storage batteries, and the amount of PV and wind power output curtailment, the planned power flow of the interconnection line, and the amount of control power interchanged with the interconnector.

Specifically, requirement of flexibility reserve is determined based on the forecasting of the electricity demand variability in the LFC time zone, which is assumed as the representative value of ±2% of the hourly value of forecasted demand according to the Power System Working Group government committee [24]. In addition, PV and wind are considered as a negative demand because they are forms of renewable energy that are variable and intermittent in nature, and when they generate excess power that exceeds the demand and this excess power cannot be stored is it referred to as negative demand. The variability of PV power output is assumed as ±10% of the corresponding output and the variability of wind power output is assumed as ±5% of the installed capacity [24]. The

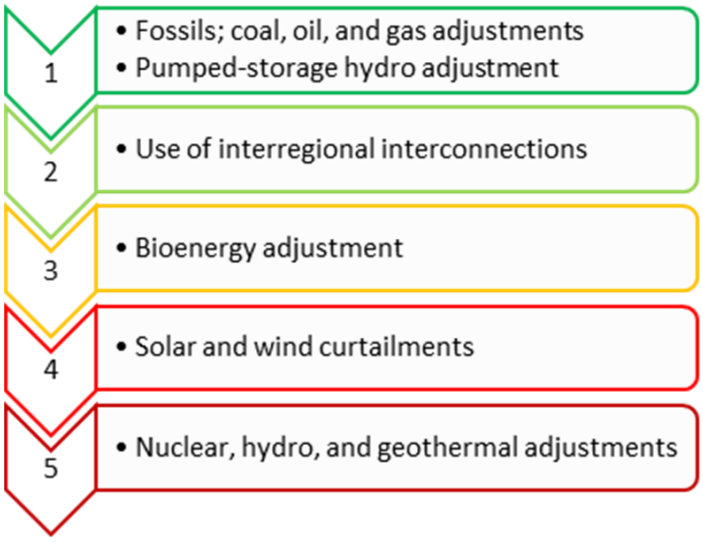

Figure 1-4 Simplified presentation of the rule of priority of power supply in Japan [24]

requirement of flexibility can be determined in terms of these variabilities of the demand, PV and wind power outputs.

The available reserve flexibility analyzed is the balancing capacity in the LFC time zone is represented in several studies [21]-[24]. For example, as for conventional generators, LFC capacity is a total of ±5% of the rated capacity in operation, ±20% of hydro power plant in operation, ±20% of pumped storage hydro at power generation and ±20% of pumped storage hydro with variable speed pump during pumping.

In UC scheduling, when the surplus power supply is anticipated based on the forecast of demand and renewable power supply, the rule of priority of power supply in Japan as shown in Figure 1-4 is implemented to reach the supply/demand balance and to preserve the margin for flexibility that is used to maintain the grid frequency [24]. When the electricity demand is forecasted within a certain period of time, firstly the thermal power plants power output will be adjusted at the minimum operation limit in consideration to providing a margin of flexibility reserve. If thermal power plants at the minimum operation limit are providing more power than that needed for achieving the supply/demand balance, the interregional interconnections and bioenergy will be reduced for the adjustment of power. After that comes the curtailment of PV and wind power

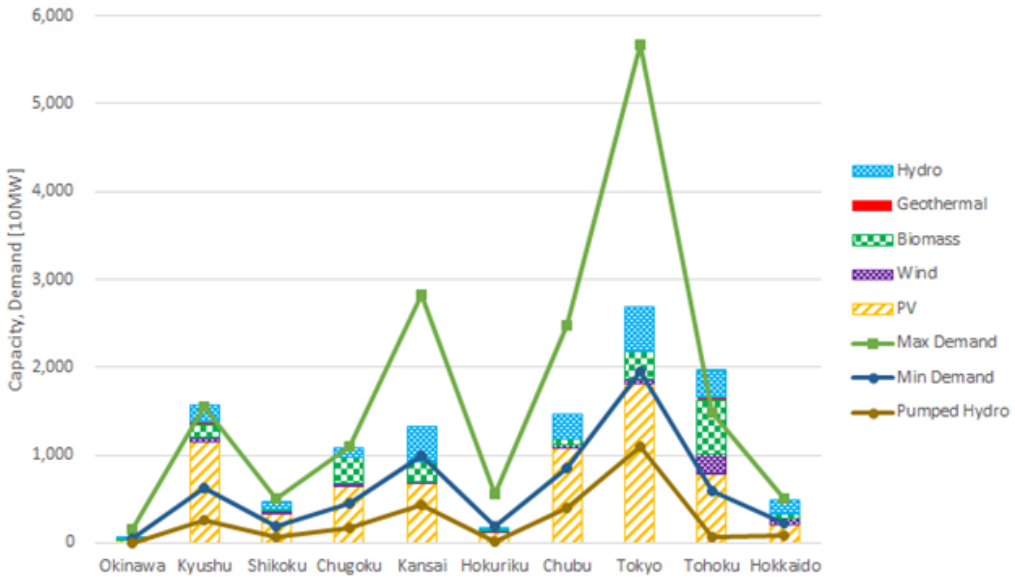

Figure 1-5 Grid Connection Status by Area (End of Dec. 2022)

Source: Compiled from data of general transmission and distribution companies

outputs and finally the nuclear, hydro and geothermal power adjustments. Refer to the appendix for a detailed example regarding the demand variability and cases where the supply balance out the demand as well as preserve LFC flexibility.

Power curtailment is an important tool for operational planning which enables the power system operators manage the variability of RES such as PV, wind and bioenergy as mentioned above. As PV systems abundancy is witnessed in Japan as mentioned in Subsection 1.1.2, fluctuating PV power output will increase the variability of the system frequency, which increases the requirement of flexibility reserve. Hence, curtailing the fluctuating PV power output can be used to reduce the required flexibility reserve.

In the Kyushu area, 11.4 GW of PV power plants have already been connected to the power grid under the FIT system as of the end of December 2022, and together with 630 MW of wind power plants, the variable RES connected capacity exceeds 12 GW as shown in Figure 1-5. While maximum and minimum demand is realized to be 16 GW and 7 GW, respectively [25].

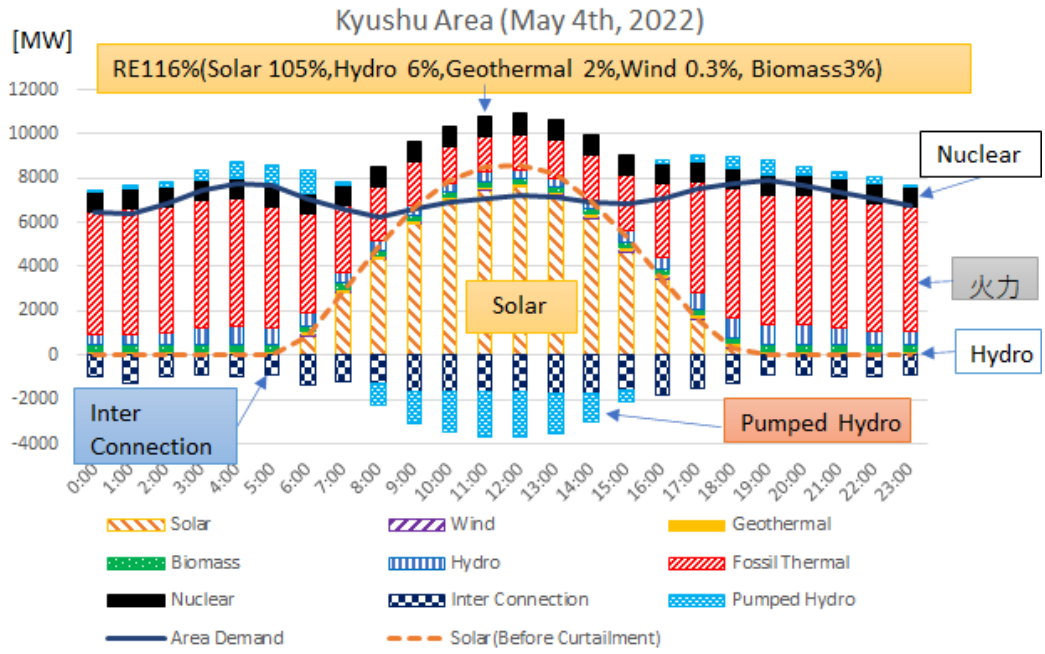

Figure 1-6 Kyushu Area Electricity Supply and Demand (May 4, 2022)

Source: Prepared from Kyushu Electric Power Transmission and Distribution's electricity supply and demand data

These statistical figures are highlighting the abundance of RES in Kyushu area especially the PV power output that usually encounters curtailment. Therefore, in Japan, in the Kyushu area, variable RES curtailment has been taking place since 2018 among all areas in Japan, and the variable RES curtailment rate for the whole year of 2022 was 1.4%. Figure 1-6 shows an example when the power output curtailment occurs as the share of PV power has reached a maximum of 104.9% during the peak hourly period at 11:00 a.m. on May 4th, 2022. At this time, wind power accounted for 0.3%, and the RES share 116% [25]. Power curtailment actions are expanding to be implemented in other regions such as the central region where the electricity demand is high. As of 2023, PV power curtailment is applied in Chubu area and next year it will be applied in Tokyo and Kansai areas.

1.2.4. Future situation of power system with increased PV systems

As mentioned in Subsection 1.1.2, Japanese government has set targets to achieve a substantial increase in renewable energy capacity by 2030, encouraging the development of renewable projects and the deployment of advanced technologies. In addition, towards

2050, the most abundant expected RES which is PV system is anticipated to reach a capacity of 300 GW [12].

The extreme increase of PV system penetration will lead to various challenges for stable operation [12]. Preserving the requirement of flexibility resources for maintaining grid frequency is one of the challenges. The requirement of flexibility resources would be increased, because PV systems currently undergo the maximum power point tracking (MPPT) control and its unstable power output property depending on irradiance fluctuation will increase the fluctuation of residual electricity load in overall power system [26].

As high penetration rate of intermittent PV power output becomes more prevalent, there is a growing concern about the potential for significant power output curtailment, leading to a wastage of energy. This issue arises due to various challenges associated with managing the variability and intermittency of PV power output [27].

Addressing these challenges associated with the increased penetration of PV system into the power system requires a combination of technological advancements. By adopting a holistic approach that considers grid flexibility, forecasting, and inverters' control upgrades, it is possible to ensure the stable operation of the power system while maximizing the benefits of PV systems.

One potential solution to minimize PV power output curtailment and optimize the use of PV system is to utilize PV power for frequency regulation. Frequency regulation is a critical aspect of grid stability, ensuring that the supply and demand of electricity remain balanced. Traditionally, this role has been fulfilled by conventional power plants, but with the increasing adoption of PV systems, PV systems can also contribute to frequency regulation [28].

To implement PV-based frequency regulation effectively, it requires the integration of smart grid technologies and advanced control systems. These technologies allow for real-

time monitoring and control of PV systems, enabling them to respond rapidly to grid frequency fluctuations. Additionally, appropriate market mechanisms and regulatory frameworks need to be in place to incentivize and facilitate the participation of PV systems in frequency regulation services. This approach not only optimizes the use of PV power but also contributes to the stability and reliability of the power system [29].

1.3. PV systems supporting grid frequency control

1.3.1. Current functionalities of PV inverter

Conventional PV inverter scheme employ a maximum power point tracking (MPPT) control to continuously optimize the power output of PV panels. By tracking the MPP of the I-V curve and P-V curve of a PV module shown in Figure 1-7, MPPT control ensures that the system operates at its peak efficiency, even under varying weather conditions or shading [30]. The parameters in this figure are short-circuit current (I_{SC}), open-circuit voltage (V_{OC}), The MPP is at the knee of the I-V curve where the product of voltage and current reaches the maximum. The voltage at MPP is V_R, and the current at MPP is I_R. The aim is that PV module operate at MPP to extract the highest amount of power from it.

As the grid infrastructure is advancing, power system operators may employ advanced

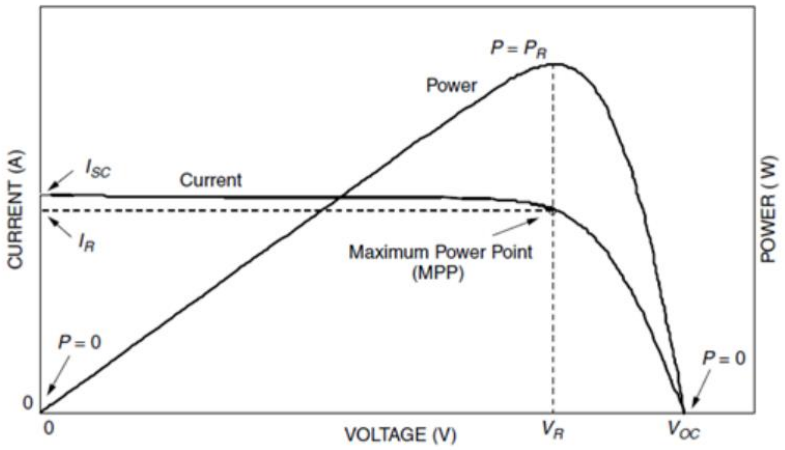

Figure 1-7 I-V curve and P-V curve for a PV module [30]

control strategies, energy storage systems, or grid support functionalities within the PV inverter schemes to enhance the stability and resilience of the grid during periods of varying PV power output. Generally, the power system operators need to adhere to relevant regulations, policies, and interconnection standards imposed by regulatory authorities. Compliance with these guidelines ensures the safe and efficient integration of PV systems into the existing power infrastructure [31].

Therefore, advanced PV inverter scheme has the ability to operate efficiently and autonomously with limited operator intervention required. This scheme implemented in some countries where it offers a range of advanced functionalities that enhance the performance and efficiency of PV more than the interactive inverter scheme, however this control scheme is still not widely implemented [32]-[33]. Key functionalities of this PV advanced inverter include:

- Monitoring and Data Communication: PV inverters come equipped with monitoring capabilities that provide real-time data on system performance, energy production, and other key parameters. Many inverters offer built-in communication protocols to enable remote monitoring and control of the PV power system.
- Demand Response and Grid Services: Certain PV inverters have the capability to participate in demand response programs or grid services. They can receive signals from utilities and adjust their power output accordingly, helping to manage grid load and support the grid.

1.3.2. Future functionalities of PV smart inverter

Smart inverters can enable more dynamic and flexible grid management. Through communication and coordination with power system operators, smart inverters can respond to real-time grid conditions and adjust their operation accordingly. This dynamic grid management can help manage frequency fluctuations, voltage fluctuations, and enhance overall grid performance.

Smart inverters, equipped with advanced control capabilities can set the upper limit of PV power (i.e. curtail PV power output) and utilize the curtailed power to apply droop

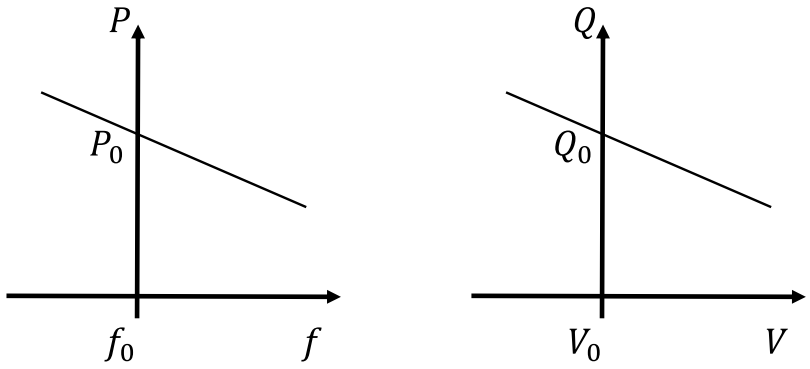

Figure 1-8 Simple droop frequency control and droop voltage control

characteristics similar to synchronous generators [26], [34]. Droop control is an important feature offered by smart inverters to enhance the stability and coordination of distributed energy resources within a grid-connected system or a microgrid. Droop control, also known as droop frequency control or droop voltage control are shown in Figure 1-8, is used to regulate power output and maintain grid frequency or adjust the reactive power and to regulate the voltage, respectively [35].

Typically, droop control is implemented using a proportional control scheme. The power output of each smart inverter is modulated based on the difference between its local frequency or voltage measurement and the reference frequency or voltage. The droop characteristic is defined by a slope or a droop coefficient, which determines the rate of change in power output in response to variations in frequency or voltage [36].

Another advancement of smart invert is the virtual inertia control that involves the use of power electronics and advanced control algorithms in inverters to emulate the inertia response of traditional generators. When a disturbance occurs, these systems can dynamically adjust their power output to provide an instantaneous response and support the grid frequency. By injecting or absorbing power in response to frequency deviations, virtual inertia control helps regulate the system frequency and dampen oscillations, enhancing grid stability [37], [38].

One of the advantages of droop control over virtual inertia control is that the droop control

does not require complex algorithms or communication protocols. The control action is based solely on the local measurements of voltage or frequency and the predetermined droop slope. This simplicity eliminates the need for sophisticated control algorithms or extensive communication infrastructure [39]. Also, another advantage of droop control by smart inverters is its decentralized nature. Each inverter autonomously adjusts its power output based on local measurements, reducing the need for centralized control systems. This decentralized approach enhances the flexibility of small-scale distributed generators such as residential PV systems [40].

Studies have shown the efficiency of droop control in mitigating the sudden frequency deviations that are detected by the wind smart inverter in case of emergency such as sudden load change or conventional generator dropout. In [41], the fast primary frequency regulation mechanism is triggered within a wind farm system, resulting in a significantly improved frequency response. The involvement of wind power in providing primary frequency regulation through its reserved capacity has been explored in previous works [42]-[44]. In contrast, the contribution of PV inverters to fast frequency response control schemes is comparatively limited when compared to wind power's capabilities in this aspect.

The main reason for the disparity in contributions between wind power and PV inverters is the inherent nature of the two technologies. Wind turbines can initially use the rotor’s inertia to provide extra power. Moreover, Wind power can emulate the behavior of inertia to contribute to grid stability and frequency control. This concept is known as synthetic inertia [44].

The following studies represented active power-frequency (*p-f*) droop control providing fast frequency response by PV inverters. For instance, [45] has focused on providing frequency reserve using autonomous *p-f* functions that modify active power during contingencies only. It also discussed the design of the *p-f* curve for the curtailment, dead band and droop setting. Moreover, [46] investigated the use of grid support functions to improve grid frequency response using a frequency-watt function for an island grid. The

proposed approach dampens frequency disturbances associated with contingency events. These studies confirmed the importance of *p-f* droop control of PV to regulate frequency during contingencies, yet they lack *p-f* droop control designed to mitigate normal frequency deviations caused by frequent disturbances in load or generation [47].

The idea of smart-inverters contributing the normal changes in grid frequency lacks in recent studies. Thus, modern inverter-interfaced PV generators should respond to normal frequency changes i.e., they should be fully capable of providing various forms of active power control and in time frames even faster than conventional generators [48].

Therefore, the challenge here is the formation of a *p-f* control that can accommodate both normal and emergency changes in frequency. That leads to different mechanisms of measuring the frequency deviations and forming a corresponding controls to these different measurements. Another issue will be how these controls will work in coherence without affecting the impact of one another.

Another aspect that has been addressed in prior studies is that the implementation of these *p-f* control schemes is primarily focused on large-scale PV systems. For instance, in [49], large-scale PV systems are utilized to perform simultaneous fast frequency control and power oscillation damping, effectively enhancing frequency regulation. Additionally, the feasibility of achieving fast frequency response by a 300 MW PV plant in California, controlled by the power system operator, is examined in [50]. However, to make a more comprehensive contribution to the grid's stability, it is essential for frequency control to be extended beyond large-scale PV systems. Medium and small-scale PV systems should also be able to provide such control, allowing for a more widespread integration of PV-generated power and ensuring a robust and resilient power system.

The number of installed small-scale PV systems in urban areas has increased along with the growth of the global PV market [51]-[53]. Hence, increased PV installations may require less dependence on the operator to provide control signals to adjust the magnitude of their response to disturbances and this independence can cause a more efficient and

economical operation of the power system. Therefore, active power should be adjusted autonomously by an effective control scheme in response to the frequency deviation challenge in renewable integrated power systems.

With the expansion of the global PV market, there has been a notable rise in the installation of small-scale PV systems in urban areas [51]-[53]. As a result of this trend, there is a potential for reduced reliance on operators to supply control signals for adjusting the response magnitude to disturbances. This greater independence can lead to a more efficient and cost-effective operation of the power system. Consequently, it becomes imperative to develop effective control schemes that allow active power to be autonomously adjusted in response to frequency deviations, especially in renewable integrated power systems.

1.3.3. Increasing the effectiveness of PV power output curtailment

The current PV power output curtailment scheme in Japan is that the power **s**ystem operators forecast the PV power output and plan PV power output curtailment in a day-ahead UC scheduling. They communicate the curtailment plans to PV plant operators to ensure coordinated curtailment. Particularly, the power system operator will randomly communicate with PV plants to be disconnected based on the curtailment plan. Consequently, the aggregated PV power output will be reduced meanwhile, the aggregated PV fluctuations characteristics will still exist. However, in the future, the curtailment scheme will be changed to determine the upper limit of PV smart inverters power output. This will reduce the aggregated PV power output as well as the aggregated PV fluctuations. Hence, reduced aggregated PV fluctuations will reduce the required flexibility capacity [54].

Therefore, it is essential to determine the curtailment level (CL) of each PV power output so that the fluctuations in the aggregated PV power output are further minimized as it is a major cause of frequency fluctuations. When the required flexibility capacity is reduced, the requirement of curtailment can be reduced, hence mitigating the waste of PV power output. Refer to the example in appendix 3 showing as example of PV power curtailment that reduced required flexibility capacity by the demand.

Forecasting the PV power output is used a tool for determining the CL. Many studies have been conducted to a day-ahead forecast PV power output from different perspectives, including various forecasting models based on statistical, mathematical, physical, machine learning or hybrid [55]–[59]. With higher PV penetration, the short-term forecasting becomes more crucial for guaranteeing the achievement of the required PV power output on each hour on the operation day. Highly accurate short-term forecasting can lead to further adjustment of CL compared to the pre-determined CL by the UC scheduling. Currently, the forecasting of the average value of PV power output in short-term, ranging from few minutes to few hours, is feasible and different methods are discussed in [60] to be mainly divided into physical and data-driven methods. Whereas [61] followed data-driven methods to cooperate neural network model with deep learning technology to predict the short-term average value of PV power output, achieving a high level of accuracy.

On the other hand, the forecasting of time-series change in PV power output still remains challenging with a considerable amount of error even though machine learning algorithms and other advanced modeling techniques are used [62]–[66]. However, the fluctuation characteristics such as fluctuation range can be practically feasible. If available, the forecasted fluctuation characteristics of each region can be used to allocate optimal CL value for each region. Depending on the number of regions to which the optimal CL value is allocated, the allocation process can still be time-consuming, and needs a sophisticated but practically feasible approach.

1.4. Objectives of this dissertation

To enhance the involvement of PV systems in grid frequency regulation and further promote their integration, a more effective approach would entail integrating diverse control schemes into a single PV-based control synthesis problem. Additionally, optimizing the curtailment of PV power output can play a pivotal role in achieving seamless grid integration. By combining these strategies, the contribution of PV systems to grid stability can increase.

As described above, The PV system has the capability to incorporate two control schemes. The first one is aimed at mitigating frequent fluctuations caused by load or generation disturbances. The second scheme focuses on suppressing frequency deviations during contingencies. The crucial aspect is to implement both control schemes simultaneously for optimal performance. Therefore, the first objective of this dissertation is to develop an autonomous active power control based on a dual active power–frequency (*p–f*) droop control which can respond to normal and sudden frequency fluctuations, and to demonstrate that it can work well without a negative dynamic conflict by using a numerical simulation.

The second objective is to propose PV power curtailment scheme so that CL in each region is optimally allocated to minimize the fluctuation of aggregated PV power output without precisely forecasting the time-series of PV power output. In this proposal, a more simple straightforward approach should be adopted assuming that the fluctuation characteristics can be predicted in the short-term forecasting and be expressed in several typical patterns. Thus, instead of using huge accurate forecasted time-series PV power output for each region, each region will be given a typical prepared pattern that reflects its level of fluctuations based on the short-term forecasting.

1.5. Structure of the dissertation

The structure of this thesis is as follows:
Chapter 2 presents an active power control mechanism for PV systems, contributing to both fast and slow frequency responses in a power system. The proposed approach involves an autonomous active power control based on a dual active power-frequency (*p-f*) droop control, which can dynamically adjust the droop characteristics depending on the magnitude of frequency change. The primary goal of this study is to introduce an efficient PV system control that can effectively respond to both slow and fast frequency fluctuations. Notably, the proposed dual *p-f* droop control demonstrates harmonious operation without any negative dynamic conflicts. To evaluate its performance, two simulation tests are conducted. The first test examines load-generation imbalance using a

simplified version of the AGC30 model [29], while the second test simulates generation dropout. In each test, the PV systems are assessed under the application of the dual *p-f* droop control, demonstrating its simplicity and effectiveness as a control scheme.

Chapter 3 introduces a proposal of optimal allocation of CL levels among different regions using typical prepared patterns that reflects their PV power output behaviors. The study involves the preparation of these patterns through the formation of statistical relations of average value and maximum fluctuation against different CL, respectively, these relations are used to distinguish each region PV power output behavior in short-term. Secondly, using these relations, this study proposes an optimization of different CL to be allocated to each region. In this approach, the optimal CL in each region will minimize the fluctuation of aggregated PV power output without precisely forecasting the time-series of PV power output. As a result, the proposed method can contribute to the reduction of the control burden needed to eliminate the frequency fluctuations and hence reducing the required resources for frequency control in the power system.

Chapter 4 describes the summary of conclusions of this study and the applications of these studies and suggested improvement of the studies. Finally, suggested build up ideas of the studies are proposed as well.

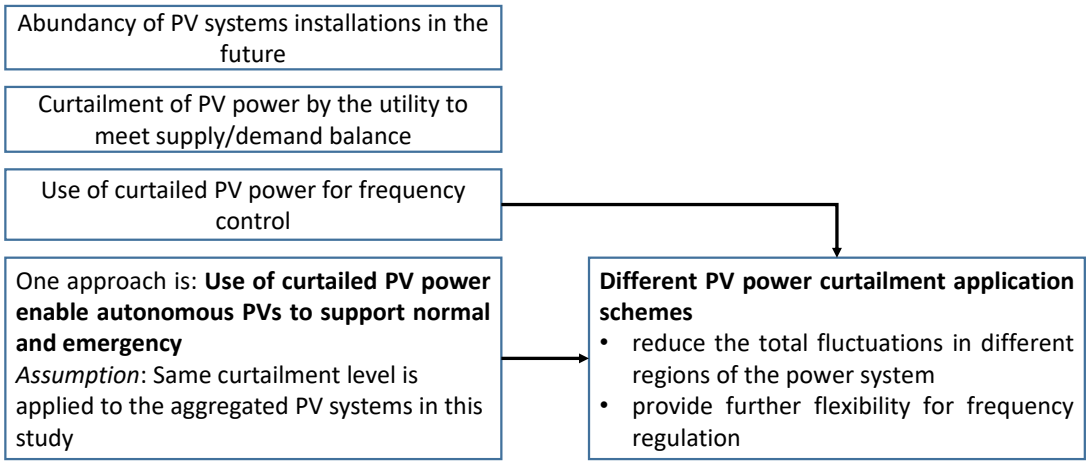

Figure 1-9 Structure of the thesis

References

[1] International renewable energy agency (IRENA), “Record Growing Renewables Achieved despite Energy Crisis,” 21 March 2023. [Online]. Available: https://www.irena.org/News/pressreleases/2023/Mar/Record-9-point-6-Percentage-Growth-in-Renewables-Achieved-Despite-Energy-Crisis.

[2] Energy transition, “More than a third of the world’s electricity will come com renewables in 2050, World Economic Forum,” 16 March 2023, [Online]. Available: https://www.weforum.org/agenda/2023/03/electricity-generation-renewables-power iea/#:~:text=Renewable%20energy%20will%20produce%2035,2025%3A%20IEA%20%7C%20World%20Economic%20Forum

[3] Technology collaboration program, “Trends in Photovoltaic applications,” REPORT IEA PVPS T1-43:2022, International Energy Agency, 2022. [Online]. Available: https://iea-pvps.org/wp-content/uploads/2023/02/PVPS_Trend_Report_2022.pdf

[4] Global Wind Energy Council (GWEC), “Global Wind Report 2023,” 2023. [Online]. Available: https://gwec.net/globalwindreport2023/

[5] International renewable energy agency (IRENA), “Global Energy Transformation,” 2018. [Online]. Available: https://www.irena.org/-/media/Files/IRENA/Agency/Publication/2018/Apr/IRENA_Report_GET_2018.pdf

[6] Lucia Fernandez, “renewables generation capacity outlook 2020-2050,” 8 February 2023. [Online]. Available: https://www.statista.com/statistics/217270/projected-global-installed-renewable-generation-capacity/

[7] Davos, “How Japan is accelerating efforts towards a carbon-neutral society,” World Economic Forum, 2023. [Online]. Available: https://www.weforum.org/agenda/2023/01/davos23-japan-accelerate-efforts-carbon-neutral-society/X

[8] NREL, “Feed-in Tariff Policy: Design, Implementation, and RPS Policy Interaction,” 2019. [Online]. Available: https://www.nrel.gov/docs/fy09osti/45549.pdf

[9] 資源エネルギー庁：「電気事業者による新エネルギー等の利用に関する特別措置法の平成２３年度の施行状況について」[Online]. Available: https://www.rps.go.jp/RPS/new-contents/pdf/rps_H23.pdf

[10] Andrew DeWit, “The Japan Renewable energy Institute’s Proposal for the 2030 Energy Mix,” *The Asia-Pacific Journal*, vol. 18, no. 17, Sep. 2020

[11] Renewable Energy Institute, “Renewable pathways to climate-neutral Japan,” March 2021. [Online]. Available: https://www.renewable-ei.org/pdfdownload/activities/LUT-Agora-REI_2021_study.pdf

[12] Renewable Energy Institute, “2050: Decarbonizing Grid Systems with Renewables,” April 2023. [Online]. Available: https://www.renewable-ei.org/en/activities/reports/20230407.php

[13] 荻本和彦：「出力が変動する再生可能エネルギー発電の大量導入と電力システムの進化（1）」, 日本原子力学会誌, pp. 24-29, 2014.

[14] Soundarrajan A, Sumathi S, Sivamurugan G., " Voltage and frequency control in power generating system using hybrid evolutionary algorithms," in *Journal of Vibration and Control*, vol. 18, pp. 214-227, 2012.

[15] Renewable Energy Institute, "Integrating renewables into the Japanese power grid by 2030," Dec. 2018. [Online]. Available: https://www.renewable-ei.org/pdfdownload/activities/REI_Agora_Japan_grid_study_FullReport_EN_WEB.pdf

[16] Investigating R&D Committee on recommended practice for simulation models for automatic generation control: "Recommended practice for simulation models for automatic generation control." No. 1386, IEEJ Technical Report, 20 Dec. 2016.

[17] Farsi, F.N., *et al.*, "Economic Dispatch in power systems," in the *Proceedings of the IEEE 8th GCC Conference and Exhibition GCCCE,* 2015.

[18] Sarker, Md and Hasan, Kamrul. "Load Frequency Control in Power System," *ResearchGate*, vol. 10, pp. 23-30. 2016.

[19] N. Sumie *et al.*, "Analysis of value of flexibility in Japan's power system with increased VRE," in *Clean Energy*, 2018.

[20] J. Undrill, "Primary Frequency Response and Control of Power System Frequency," Berkeley lab, Feb. 2018. [Online]. Available: https://escholarship.org/content/qt46122362/qt46122362_noSplash_235a7a6a96700f91db14b19722ffba37.pdf

[21] L. Montero, A. Bello, and J. Reneses, "A Review on the unit commitment problem: approaches, techniques, and resolution methods," in *Energies*, vol. 15, no. 4, p. 1296, Feb. 2022.

[22] H. Sangrody, N. Zhou and Z. Zhang, "Similarity-Based Models for Day-Ahead Solar PV Generation Forecasting," in *IEEE Access*, vol. 8, pp. 104469–104478, Jun. 2020.

[23] B. Lu and M. Shahidehpour, "Unit commitment with flexible generating units," in *IEEE Transactions on Power Systems*, vol. 20, no. 2, pp. 1022–1034, May 2005.

[24] Roman Zissler, "Renewable Energy Curtailment in Japan- Room for improvement," Renewable Energy Institute, 9 April 2019. [Online]. Available: https://www.renewable-ei.org/en/activities/column/REupdate/20190409.php

[25] Institute for sustainable energy policies, "Share of Electricity from Renewable Energy Sources in Japan (Preliminary)～Solar power generation to reach 10%, further expansion of renewables urged in Japan," 14 Apr. 2023. [Online]. Available: https://www.isep.or.jp/en/1436/

[26] M. J. Abbass, R. Lis, and F. Saleem, "The Maximum Power Point Tracking (MPPT) of a Partially Shaded PV Array for Optimization Using the Antlion Algorithm," in *Energies*, vol. 16, no. 5, p. 2380, Mar. 2023, doi: 10.3390/en16052380.

[27] S. Asiaban *et al.*, "Wind and Solar Intermittency and the Associated Integration Challenges: A Comprehensive Review Including the Status in the Belgian Power System," in *Energies*, vol. 14, no. 9, p. 2630, May 2021, doi: 10.3390/en14092630.

[28] L. Cristaldi, M. Faifer, C. Laurano, R. Ottoboni, E. Petkovski and S. Toscani, "Power Generation Control Algorithm for the Participation of Photovoltaic Panels in Network Stability," in *IEEE Transactions on*

Instrumentation and Measurement, vol. 72, pp. 1-9, 2023, Art no. 9000809, doi: 10.1109/TIM.2023.3238745.

[29] A. F. Hoke, M. Shirazi, S. Chakraborty, E. Muljadi and D. Maksimovic, "Rapid Active Power Control of Photovoltaic Systems for Grid Frequency Support," in *IEEE Journal of Emerging and Selected Topics in Power Electronics*, vol. 5, no. 3, pp. 1154-1163, Sept. 2017, doi: 10.1109/JESTPE.2017.2669299.

[30] C. R. Jeevandoss, M. Kumaravel and V. J. Kumar, "Sunlight based I-V characterization of solar PV cells," in the *Proceeding 2011 IEEE International Instrumentation and Measurement Technology Conference*, Hangzhou, China, 2011, pp. 1-4, doi: 10.1109/IMTC.2011.5944061.

[31] K.N. Nwaigwe, P. Mutabilwa, E. Dintwa,, "An overview of solar power (PV systems) integration into electricity grids," in *Materials Science for Energy Technologies*, Vol. 2, no. 3, pp. 629-633, Dec. 2019, , https://doi.org/10.1016/j.mset.2019.07.002.

[32] D. K. Dash and P. K. Sadhu, "A Review on the Use of Active Power Filter for Grid-Connected," in Power Electronics for Energy Transition and Renewable Energy Conversion Process," vol. 11, no. 5, p. 1467, May 2023, doi: 10.3390/pr11051467.

[33] Colin Schader, "Advanced Inverter Technology for High Penetration Levels of PV Generation in Distribution Systems," national renewable energy laboratory (NREL), March 2014.

[34] R. B. Godoy et al., "Procedure to Match the Dynamic Response of MPPT and Droop-Controlled Microinverters," in *IEEE Transactions on Industry Applications*, vol. 53, no. 3, pp. 2358-2368, May-June 2017, doi: 10.1109/TIA.2016.2642883.

[35] Ruisheng Li,Chapter 2 - Grid-connected power conversion of distributed resources, Editor(s): Ruisheng Li, Distributed Power Resources, Academic Press, 2019, pp. 19-50, ISBN 9780128174470.

[36] K. De Brabandere, B. Bolsens, J. Van den Keybus, A. Woyte, J. Driesen and R. Belmans, "A Voltage and Frequency Droop Control Method for Parallel Inverters," in *IEEE Transactions on Power Electronics*, vol. 22, no. 4, pp. 1107-1115, July 2007, doi: 10.1109/TPEL.2007.900456.

[37] D. Sun, H. Liu, S. Gao, L. Wu, P. Song and X. Wang, "Comparison of Different Virtual Inertia Control Methods for Inverter-based Generators," in *Journal of Modern Power Systems and Clean Energy*, vol. 8, no. 4, pp. 768-777, July 2020, doi: 10.35833/MPCE.2019.000330.

[38] R. Ofir, U. Markovic, P. Aristidou and G. Hug, "Droop vs. virtual inertia: Comparison from the perspective of converter operation mode," in the *Proceedings of 2018 IEEE International Energy Conference (ENERGYCON)*, Limassol, Cyprus, 2018, pp. 1-6, doi: 10.1109/ENERGYCON.2018.8398752.

[39] IEEE PES Industry Technical Support Leadership Committee, Impact of IEEE 1547 Standard on Smart Inverters and the Applications in Power Systems, technical report, August 2020.

[40] M. Easley, S. Jain, M. Shadmand and H. Abu-Rub, "Autonomous Model Predictive Controlled Smart Inverter With Proactive Grid Fault Ride-Through Capability," in *IEEE Transactions on Energy Conversion*, vol. 35, no. 4, pp. 1825-1836, Dec. 2020, doi: 10.1109/TEC.2020.2998501.

[41] W. Bo, S. Chong, S. Weichneng, Z. Guangru and D. Kaigsong, "Actual Measurement and Analysis of Wind Power Plant Participating in Power Grid Fast Frequency Modulation Base on Droop Characteristic," in the

Proceeding of International Conference on Power System Technology (POWERCON), Guangzhou, pp. 1552-1557, 2018.

[42] J. Morren, S. W. H. de Haan, W. L. Kling and J. A. Ferreira, "Wind turbines emulating inertia and supporting primary frequency control," in *IEEE Transactions on Power Systems*, vol. 21, no. 1, pp. 433-434, Feb. 2006.

[43] P. Yang *et al*., "Research on Primary Frequency Regulation Control Strategy of Wind-thermal Power Coordination," in *IEEE Access*, vol. 7, pp. 144766-144776, 2019.

[44] Y. Wang *et al*., "Methods for Assessing Available Wind Primary Power Reserve," in *IEEE Transactions on Sustainable Energy*, vol. 6, no. 1, pp. 272-280, Jan. 2015.

[45] J. Johnson, J. C. Neely, J. J. Delhotal and M. Lave, "Photovoltaic Frequency–Watt Curve Design for Frequency Regulation and Fast Contingency Reserves," in *IEEE Journal of Photovoltaics*, vol. 6, no. 6, pp. 1611-1618, Nov. 2016.

[46] J. Neely, J. Johnson, J. Delhotal, S. Gonzalez and M. Lave, "Evaluation of PV frequency-watt function for fast frequency reserves," in *IEEE Applied Power Electronics Conference and Exposition (APEC)*, Long Beach, CA, pp. 1926-1933, 2016.

[47] H. Bevrani, *Robust Power System Frequency Control*, 2nd Ed., Springer, 2014.

[48] V. Gevorgian, and B. O'Neill, "Advanced Grid-Friendly Controls Demonstration Project for Utility-Scale PV Power Plant", Technical Report NREL/TP-5D00-65368, 2016

[49] R. K. Varma and M. Akbari, "Simultaneous Fast Frequency Control and Power Oscillation Damping by Utilizing PV Solar System as PV-STATCOM," in *IEEE Transactions on Sustainable Energy*, vol. 11, no. 1, pp. 415-425, Jan. 2020.

[50] R. Golden and B.Paulos, "Curtailment of Renewable Energy in California and beyond", in *The Electricity Journal*, vol. 28, no. 6, pp. 36-50, ISSN 1040-6190, 2015.

[51] Psomopoulos, Constantinos S. *et al.* "Electricity Production from Small-Scale Photovoltaics in Urban Areas." Renewable and Alternative Energy: Concepts, Methodologies, Tools, and Applications, edited by Information Resources Management Association, IGI Global, pp. 618-656, 2017.

[52] A. B. Eltantawy and M. M. A. Salama, "Management Scheme for Increasing the Connectivity of Small-Scale Renewable DG," in IEEE Transactions on Sustainable Energy, vol. 5, no. 4, pp. 1108-1115, Oct. 2014.

[53] S. Cobben, B. Gaiddon and H. Laukamp, "Impact of Photovoltaic Generation on Power Quality in Urban Areas with High PV Population", 2008. [Online]. Available: https://www.acdemia.edu/1439223/IMPACT_OF_PHOTOVOLTAIC_GENERATION_ON_POWER_QUALITY_IN_URBAN_AREAS_WITH_HIGH_PV_POPULATION_Results_from_Monitoring_Campaigns

[54] L. Montero, A. Bello, and J. Reneses, "A Review on the unit commitment problem: approaches, techniques, and resolution methods," in *Energies*, vol. 15, no. 4, p. 1296, Feb. 2022.

[55] U. K. Das et al., "Forecasting of photovoltaic power generation and model optimization: A review," in *Renewable and Sustainable Energy Reviews*, vol. 81, pp. 912–928, Jan. 2018.

[56] L. Gigoni et al., “Day-ahead hourly forecasting of power generation from photovoltaic plants, ” in *IEEE Transactions on Sustainable Energy*, vol. 9, no. 2, pp. 831–842, Apr. 2018.

[57] E. Lorenz et al., “Irradiance forecasting for the power prediction of grid-connected photovoltaic systems,” in *IEEE Journal of Selected Topics in Applied Earth Observations and Remote Sensing*, vol. 2, no. 1, pp. 2–10, Mar. 2009.

[58] J. H. Kim et al., “The WRF-Solar ensemble prediction system to provide solar irradiance probabilistic forecasts,” in *IEEE Journal of Photovoltaics*, vol. 12, no. 1, pp. 141–144, Jan. 2022.

[59] J. Shi et al., “Forecasting power output of photovoltaic systems based on weather classification and support vector machines,” in *IEEE Transactions on Industry Applications*, vol. 48, no. 3, pp. 1064–1069, Jun. 2012.

[60] I. Kaaya, and J. Ascencio-Vásquez, “Photovoltaic power forecasting methods,” in Solar Radiation - Measurement, Modeling and Forecasting Techniques for Photovoltaic Solar Energy Applications. London, United Kingdom, Intech Open, Apr. 2021. [Online]. Available: https://www.intechopen.com/chapters/76055

[61] W. Hu, X. Zhang, L. Zhu and Z. Li, “Short-term photovoltaic power prediction based on similar days and improved SOA-DBN model,” in *IEEE Access*, vol. 9, pp. 1958–1971, Dec. 2021.

[62] J. Yan *et al.*, “Frequency-domain decomposition and deep learning based solar PV power ultra-short-term forecasting model,” in *IEEE Transactions on Industry Applications*, vol. 57, no. 4, pp. 3282–3295, Aug. 2021.

[63] Z. Zhen *et al.*, “Deep learning based surface irradiance mapping model for solar PV power forecasting using sky image,” in *IEEE Transactions on Industry Applications*, vol. 56, no. 4, pp. 3385–3396, Aug. 2020.

[64] M. S. Hossain and H. Mahmood, “Short-term photovoltaic power forecasting using an LSTM neural network and synthetic weather forecast,” in *IEEE Access*, vol. 8, pp. 172524–172533, Sep. 2020.

[65] C. -J. Huang and P. -H. Kuo, “Multiple-input deep convolutional neural network model for short-term photovoltaic power forecasting,” in *IEEE Access*, vol. 7, pp. 74822–74834, Jun. 2019.

[66] B. D. Dimd, S. Völler, U. Cali and O. -M. Midtgård, “A review of machine learning-based photovoltaic output power forecasting: Nordic context,” in *IEEE Access*, vol. 10, pp. 26404–26425, Mar. 2022.

2. An Autonomous Dual Active Power-Frequency Control in a Grid with Small-Scale Photovoltaic Power Generation

2.1. Introduction

As mentioned in Chapter 1, the contribution of PV systems to frequency control had generally not been considered until a few years ago, since PV system using MPPT control as shown above in Figure 1-7 is not controllable generator and had not been expected to be installed in such a significant proportion as it is today. Therefore, in few studies [1]-[3], PV systems are currently only obliged to adjust their power output when severe power system instabilities occur. This is currently the only technical requirement for PV systems concerning frequency control. In the normal operating state of the power system, where control reserve is applied in order to stabilize grid frequency, PV systems have not been involved yet [4].

To enhance the role of PV systems in grid frequency regulation and accommodate the further increase in PV active power penetration, a more advanced approach involves implementing multiple control schemes simultaneously within single PV systems using smart inverters. By employing various control schemes, PV inverters can effectively respond to both normal frequency fluctuations and emergency situations. This capability is not limited to large-scale PV systems; it should also be extended to medium-scale and small-scale PV systems.

As the number of small-scale PV installations continues to grow, their combined capacity can become substantial. Small-scale PV systems are often dispersed across the grid, bringing power generation closer to the point of consumption. This decentralization improves grid resilience and reduces the risk of large-scale grid disruptions. Also, Small-scale PV systems can respond rapidly to changes in grid conditions due to their simple and modular design. This agility allows them to provide frequency support quickly when needed.

Considering the expected surge in installed small-scale PV systems in the future, PV systems may require less dependence on the operator to provide control signals to adjust the magnitude of their response to disturbances and this independence can cause a more efficient and economical operation of the power system. Therefore, active power should be adjusted autonomously by an effective control scheme in response to the frequency deviation challenge in renewable integrated power systems.

As a result of this trend, there is a potential for reduced reliance on operators to supply control signals for adjusting the response magnitude to disturbances. This greater independence can lead to a more efficient and cost-effective operation of the power system. Consequently, it becomes imperative to develop effective control schemes that allow active power to be autonomously adjusted in response to frequency deviations, especially in renewable integrated power systems.

The main goal of this study is to develop an autonomous active power control system for small-scale PV systems, capable of contributing to both normal and emergency frequency changes in a power system. To achieve this, the study proposes an autonomous active power control based on a dual active power-frequency (*p-f*) droop control, wherein the droop characteristics are dynamically adjusted depending on the magnitude of frequency change. This chapter aims to demonstrate the effectiveness of the proposed dual *p-f* droop control for PV systems, showcasing its ability to respond to both slow and fast frequency fluctuations while ensuring seamless coordination between the fast and slow control mechanisms.

To achieve this objective, two simulation tests are conducted to compare two methods of dual *p-f* droop control, aiming to derive an efficient control scheme. The first simulation test, employing the simplified AGC30 model [5], illustrates how the power supply/demand balancing can be improved. The second test demonstrates how the frequency drop resulting from the disconnection of conventional thermal power plants can be mitigated. By conducting these simulation tests, the study seeks to validate the

efficacy of the dual *p-f* droop control scheme for small-scale PV systems, showcasing its potential in effectively contributing to grid frequency regulation under both normal and emergency scenarios.

This study is divided as follows, Section 2.2 represents the two advanced methods to realize dual *P-f* droop control supporting the grid frequency. Sections 2.3 and 2.4 are the simulation tests to evaluate the effect on the power supply/demand balancing and the inertial supporting generator dropout. In each test, the two enhanced methods of *p-f* droop control are applied, followed by their results. Section 2.5 represents some parameters that affects the *p-f* droop control. Finally, Section 2.6 summarizes the outcomes of the study.

2.2. Proposals of dual *p-f* droop control for supporting grid frequency

2.2.1. Basic idea of dual *p-f* droop control

The proposed control is based on the power output curtailment control, which maintains the pre-set point of active power output P_0 at a lower level that the expected maximum power output $P_{\underline{mpp}}$ using maximum power point tracking (MPPT) control. The difference between P_{mpp} and P_0 can be utilized as a control reserve for adjusting the active power output according to the fluctuation of the grid frequency.

Forecasting P_{mpp} of PV systems can be a challenging task due to the intermittent and highly dependent nature of solar energy generation. Accurate P_{mpp} forecasting is crucial for efficient grid integration and reliable energy management. Several state-of-the-art approaches have been developed to address this challenge. Physical equations to simulate the behavior of PV systems under varying environmental conditions. They consider factors like solar irradiance, temperature, and panel characteristics. While physical models can provide accurate predictions, they require detailed data and can be computationally intensive. Also, Statistical approaches use historical data of PV system performance and environmental conditions to identify patterns and trends. Integrating real-time weather forecasts into forecasting models allows for better predictions, as it considers future changes in solar irradiance and weather conditions.

The proposed control scheme aims to optimize the P_0 of the PV system by using the difference between the P_{mpp} and P_0 as a control reserve. Instead of setting a fixed P_0, the control algorithm estimates prospective P_{mpp} based on the PV system's predetermined I-V characteristics. It utilizes additional sensors to observe short circuit current (I_{sc}) and open-circuit voltage (V_{oc}) that are influenced by irradiance and module temperature, respectively. This approach is expected to provide a more accurate estimation of P_{mpp} compared to using PV irradiance or I_{sc} alone.

In the proposed dual *p-f* droop control, the large frequency change of frequency can be detected immediately by the direct measurement (fast frequency measurement), while small frequency change of frequency within the regulation range is measured with low-pass filter for the stable measurement (slow frequency measurement). According to these measurements, in case of small fluctuations within regulation range, slow response control is activated, and PV system should respond properly, which should be addressed by LFC in power system. In case of detection of fluctuations exceeding the regulation range, fast response control becomes essential however, fast response control might cause higher fluctuations after the suppression of occasional violation of frequency threshold. Hence, slow frequency response will be required to operate simultaneously with fast response control to avoid these violations.

The proposed control is based on switching between different droop characteristics according to the magnitude of frequency deviation. In this study, a combination of two different droop characteristics for slow-frequency and fast-frequency responses is proposed through three designs, e.g., Method-0 is a basic initial design proposal and Method-1 and Method-2 are the enhanced design proposals.

2.2.2. Initial proposal of dual *p-f* droop control (Method-0)

Figure 2-1 shows a dual *p-f* droop control of Method-0, where *df* is the measurement of the change of frequency. The frequency deviation for slow-frequency droop control df_{slow} is calculated based on the observed terminal voltage using several hundred previous

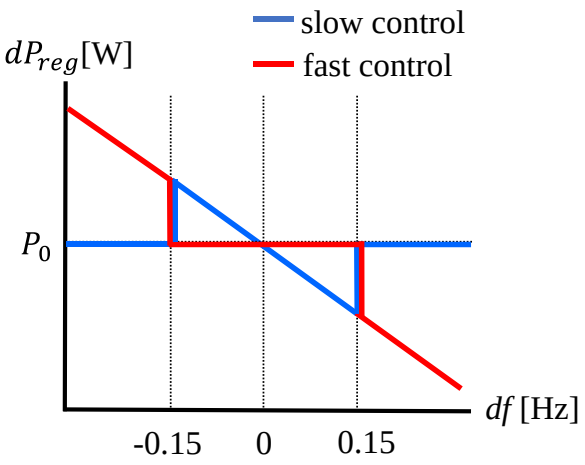

Figure 2-1 Dual *p-f* droop control of Method-0

cycles through a low-pass filter. On the other hand, large frequency fluctuation within a short time span is caused by power plant failures or the disconnection of large loads. In this situation, the immediate activation of fast-frequency response is desirable to mitigate the maximum frequency deviation. Therefore, the frequency deviation used in the fast-frequency control df_{fast} is calculated based on the observed voltage in the last few cycles.

This is a simple combination of two droop characteristics operating in two different modes in terms of frequency deviation separated between small and large frequency deviation ranges determined by the threshold values of $\pm df_{th}$. Method-0 is a simple design proposal where the two droop controls are placed together and changes based on $\pm df_{th}$ of ±0.15 Hz. The simplicity of this method comes from when one control is operating, the other will not be operating.

Based on the measured frequency deviation used in slow-frequency control df_{slow} and fast-frequency control df_{fast}, the corresponding active power change is given as follows.

$$dP_{fast} = -\frac{1}{D} \cdot \frac{P_{mpp}}{f_0} \cdot df_{fast} \quad \textbf{(2.1)}$$

$$dP_{slow} = -\frac{1}{D} \cdot \frac{P_{mpp}}{f_0} \cdot df_{slow} \quad \textbf{(2.2)}$$

where dP_{slow} and dP_{fast} are the power deviations due to df_{slow} and df_{fast}, respectively; D is the droop setting of 4%; P_{mpp} is the power due to MPPT control; and f_0 is the nominal frequency of the power grid, which is 60 Hz in this study. Although the formulas of dP_{slow} and dP_{fast} are the same, the time-series change in dP_{slow} and dP_{fast} is different because of the difference in measurement method of df_{slow} and df_{fast}.

The frequency deviation for slow-frequency droop control df_{slow} is calculated based on the observed terminal voltage using several hundred previous cycles through a low-pass filter. In this study paper, 400 cycles are used. The frequency measurement df_{slow} slowly follows the system frequency. This measurement will not be as quick as frequency variations which can detect all changes in the system frequency. While, the frequency deviation used in the fast-frequency control df_{fast} is calculated based on the observed voltage in the last few cycles. In this study, 20 cycles are used. The frequency measurement df_{fast} quickly follows the system frequency and it is used to detect any changes in the system frequency.

Figure 2-2 shows the time-series assumption of frequency deviation and the corresponding measurements of frequencies df_{slow} and df_{fast}. df is changed to -0.25 Hz at 2 s, recovered to -0.05 Hz at 10 s, and returned to 0 Hz at 20 s. Figure 2-3 shows the corresponding change in dP_{slow} and dP_{fast} applying Method-0. df_{fast} overlaps df due to a small delay of measurement and df_{slow} follows df with about 7 s delay. During such a change in df, the slow-frequency control, the fast-frequency control, and the switching from slow to fast and from fast to slow work as described below.

- Method-0 uses the slow frequency measurement to activate the slow-frequency control when the frequency deviation is within the range of ±0.15 Hz. These deviations are caused by the change in electricity demand. The normal frequency deviation range is reported to be ±0.2 Hz in the power system in Japan [6]. However, in this study, a slightly lower range, i.e., ±0.15 Hz is selected, to reduce the possibility of its violation beyond the agreed-upon frequency range. Generally, the frequency

thresholds can be decided by the system operator based on the grid code. The frequency threshold divides the region between the normal and abnormal frequency deviations, hence the value of the frequency threshold determines which frequency control operates within or beyond that threshold.

- The quick response of frequency measurement is used to activate the fast-frequency control when the frequency deviation exceeds the range of ±0.15 Hz as shown in Figure 2-2. In other words, the droop characteristics of fast-frequency control contain

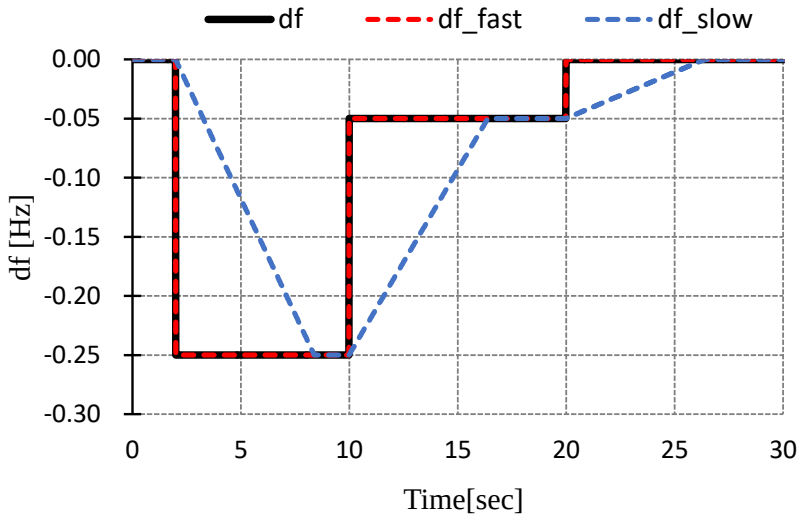

Figure 2-2 Time-series assumption of frequency deviation

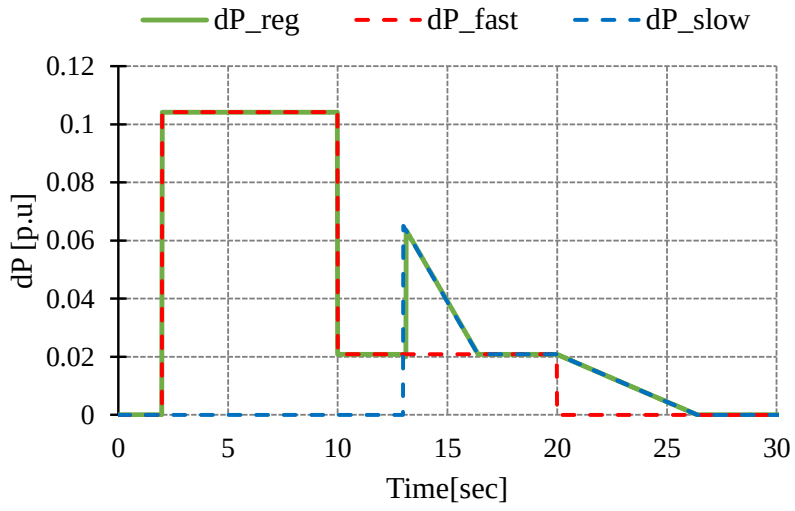

Figure 2-3 Time-series operation of dual droop control (Method-0)

a large dead band to prevent the fast-frequency control when the frequency deviation is small. When the fast-frequency control is activated, the droop setting in the slow-frequency control becomes zero, resulting in no contribution by the slow-frequency control.

- In Figure 2-3, the response to large frequency deviation that occurred at 2 seconds becomes fast because the fast-frequency is activated immediately for large frequency deviation. Regulation power dP_{reg} which is the sum of dP_{fast} and dP_{slow} will only be equal dP_{fast} as only fast-frequency control is activated.

- The same droop setting (D) is used for both slow-frequency and fast-frequency controls. In the case of switching from fast-frequency to slow-frequency controls in the recovery phase that starts from 10 seconds, there is a difference between the measured frequency for df_{slow} and df_{fast}. If dP_{slow} is suddenly activated when df_{fast} is below 0.1 Hz and the fast-frequency control is deactivated, there will be a sudden change in dP_{reg}. This sudden change in power output should be avoided in the recovery phase to normal operation. To reduce this sudden change in dP_{reg}, an enhanced control design is introduced.

2.2.3. Enhanced proposal of dual *p-f* droop control (Method-1)

Method-1 is enhanced compared to Method-0 in two points. At first, to prevent frequent switching between fast- and slow-frequency controls at ±0.15 Hz, a hysteresis is implemented as shown in Figure 2-4 under the switching condition from fast- to slow-frequency responses as recovery phase. This is done by replacing the droop characteristics of Figure 2-1 with that of Figure 2-5(b) for the recovery phase. The droop characteristics under the switching condition for slow-frequency to fast-frequency responses is the same as Method-0 as shown in Figure 2-5(a). In these figures, arrows are added in to show the switch of frequency deviation threshold $\pm df_{th}$ in terms of the direction of frequency deviations.

As described in Method-0, in the case of switching from fast-frequency to slow-frequency

controls, the sudden change in power output should be avoided in the recovery phase to normal operation because of the difference between the measured frequency for df_{slow} and df_{fast}. Note that dP_{slow} is determined by (2.1) without any limitation (or threshold), although dP_{slow} is still zero when df_{fast} decreases to ±0.1 Hz in Figure 2-5(b). In Method-1, to reduce the aforementioned sudden change in dP_{reg}, the proposed control approach introduces that the temporal power output dP_{trans} is the power deviation due to transition mode signal as:

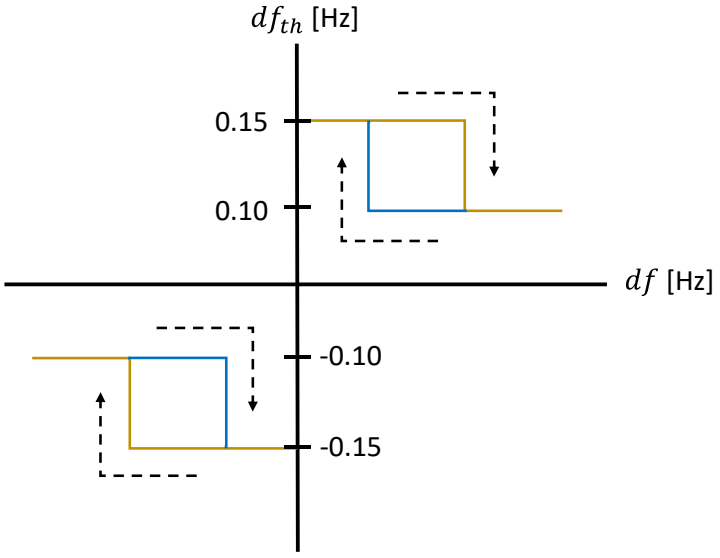

Figure 2-4 Change of frequency threshold in Method-1

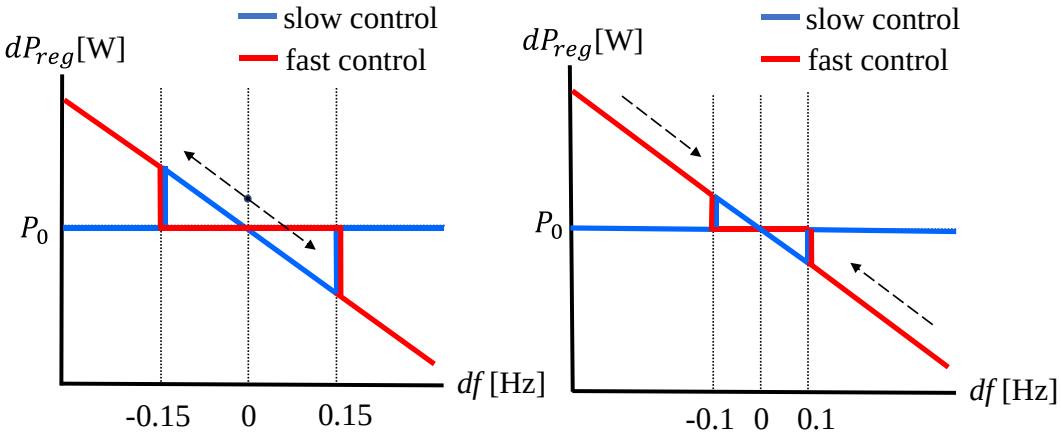

(a) df within ±0.15 Hz (b) after df exceeds ± 0.15 Hz

Figure 2-5 Dual *P-f* droop control of Method-1

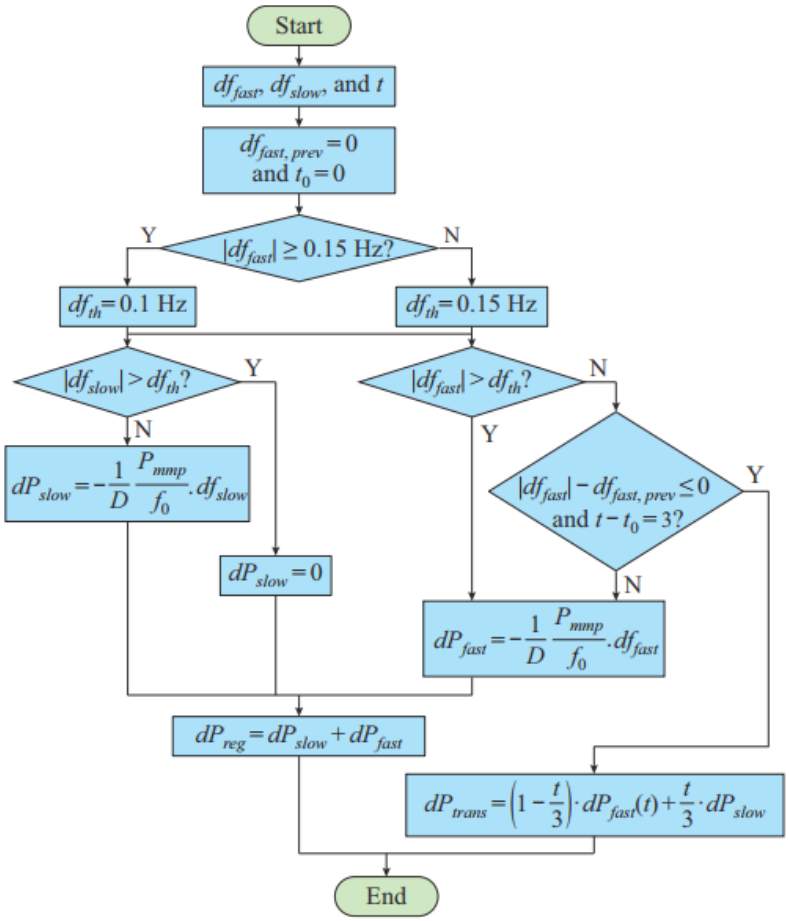

Figure 2-6 Flowchart of Method-1 of dual *p-f* droop control

$$P_{trans} = \left(1 - \frac{1}{x}t\right) \times P_{fast} + \frac{1}{x}t \times P_{slow} \tag{2.3}$$

The sudden change in dP_{reg} can be avoided by changing the addition into a temporal time-variant equation in terms of dP_{fast} and dP_{slow}. Then dP_{reg} will be called dP_{trans} in the transition phase only. Accordingly, dP_{trans} will lead to a smooth transition from fast-frequency to slow-frequency controls without any step increase. Since an equation is created to achieve a smooth transition from fast- to slow-frequency controls, it should be an equation that has a proportional distribution between dP_{fast} and dP_{slow}. The ratio between dP_{fast} and dP_{slow} keeps changing according to the time of transition t until dP_{trans} shifts gradually from df_{slow} towards dP_{fast}.

The operation of Method-1 is explained in Figure 2-6 including the change of frequency thresholds and the calculation of dP_{reg} which can be calculated as dP_{trans} during the recovery phase.

2.2.4. Enhanced proposal of dual *p-f* droop control (Method-2)

Although Method-1 seems to be simple as it just switches between the two modes, some complications are observed at the PV regulation power output. These complications include the variations of threshold depending on the measured df_{fast} after switching from slow-frequency to fast-frequency responses and vice versa in the recovery phase. Therefore, this design is proposed to avoid these complications.

The combination of the two droop characteristics is expressed in the following manner, where only the slow-frequency response is activated within the threshold value $\pm df_{th}$ and both fast- and slow-frequency responses operate beyond this threshold as shown in Figure 2-7. In particular, when df_{fast} exceeds the threshold, dP_{fast} is expressed as a linear equation as stated in (2.1) while dP_{slow} is expressed with a similar equation in (2.2) but df_{slow} will be equal to df_{th}. Hence, dP_{slow} will be a constant value beyond the threshold. Finally, dP_{reg} will be represented in terms of both dP_{fast} and dP_{slow}.

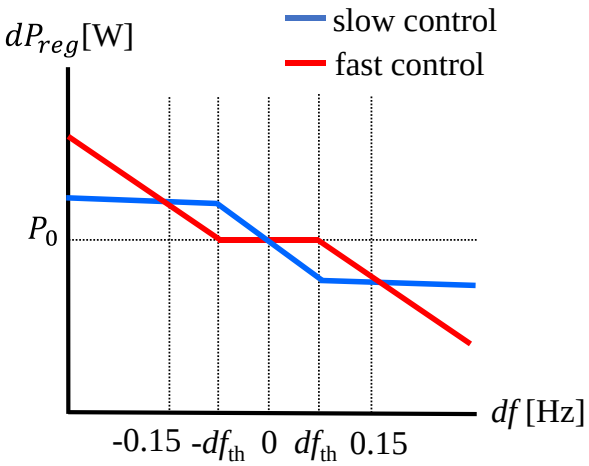

Figure 2-7 Dual *p-f* droop control of Method-2

One of the complications involves time settings of t in Eq. (2.3) for transient signal in Method-1. To prevent this and provide smooth recovery phase, Method-2 has only df_{slow} being activated within the threshold $\pm df_{th}$, and both df_{fast} and df_{slow} are enabled when df_{fast} is more than df_{th}. A transient signal is not necessary since there is no discrete change in the fast-droop and slow-droop characteristics, and the design of the control scheme becomes simpler than that in Method-1. Compared to Method-1, Method-2 is anticipated to have a delay when at sudden frequency violation of the threshold as both slow and fast frequency controls are operating and this delay will be tested in the next section.

2.2.5. Curtailment method assumed in this study

As for the pre-set point of active power output P_0, (or curtailed power output in other words), the upper limit control of power output relative to the rated inverter capacity can be used. However, in this scheme, the difference between P_{mpp} and P_0 cannot be utilized as a control reserve when the irradiance fluctuation is very large. Therefore, the proposed control assumes to employ the setting of P_0 based on the estimation of prospective P_{mpp} on the actual operation by employing the predetermined I-V characteristics for PV system to be controlled, and the observations of the short circuit current I_{sc} and the open-circuit voltage V_{oc} by using additional silicon sensor with the same I-V characteristics. A similar method using an additional measurement of PV irradiance is proposed by [7]. Because, I_{sc} and V_{oc} dominantly dependent on the irradiance and the module temperature, respectively, the estimation of P_{mpp} is expected to be more accurate than the estimation solely by the PV irradiance or I_{sc}. Based on the assumption that the setting of P_0 based on the estimation of P_{mpp}, in the following studies, the time-series data of PV power output curtailed by fixed ratio to the power output MPPT is used.

2.3. Contribution of slow response of dual *p-f* droop control to support load-frequency control (LFC)

The PV system with the enhanced dual *p-f* droop control of Method-1 and Method-2 is expected to contribute to both frequency controls in a normal situation and fast inertial response in case of severe disturbances. In the following sections, these situations will be

tested to conduct a comparison between both methods. Specifically, the interaction between the slow-dynamic and fast-dynamic responses in the two enhanced methods will be compared. The first simulation test highlights the importance of slow-frequency response in both methods whereas the second test shows the influence of fast response.

2.3.1. AGC30 model by the Institute of Electrical Engineers of Japan (IEEJ)

The IEEJ has developed a simulation model for frequency regulation called AGC30, which is possible to simulate the supply and demand balance control considering both EDC and LFC, as shown in Figure 1-2 in Chapter 1.

AGC30 model consists of each element model such as conventional power plants, LFC, EDC, inertia, tie-line power flow, and time domain data about fluctuation of load and renewable energy output.

In AGC30 model, two sets of power demand data are prepared with consideration of average characteristics of fluctuations of ten power system areas in Japan on the days

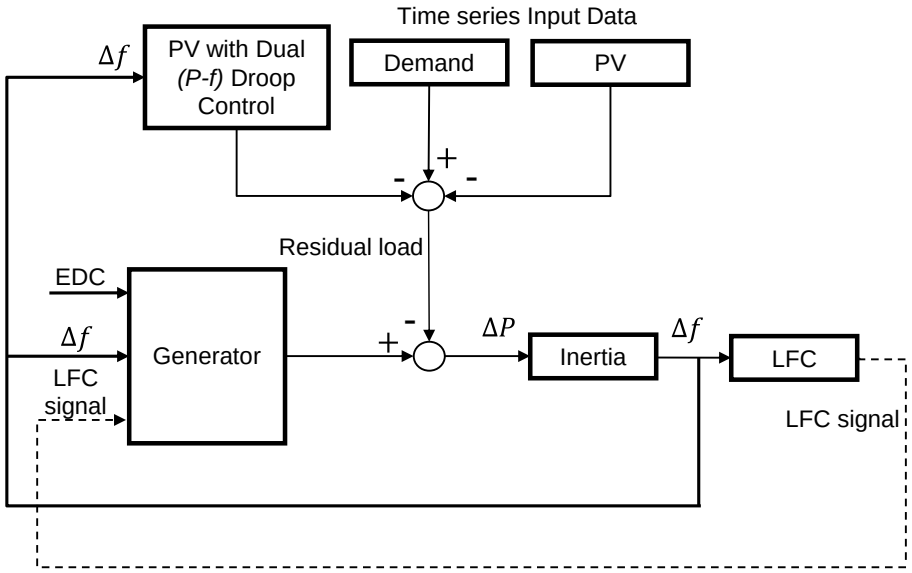

Figure 2-8 Supply-demand frequency simulation model

with a large power demand in the summer season and a small power demand in spring and autumn season.

As for irradiance, six sets of time-series data with different weather conditions are prepared. Six patterns of large fluctuations are extracted for different weather conditions during the daytime and used as standard data. Since the PV power output data is usually inaccurate, smoothing effect is considered to remove the influence of local cloud movements. However, it is extremely difficult to measure all the power outputs of many individual PV power plants installed in the area and add them up. Therefore, it is desirable to create the standard data, which are used in this chapter since PV power output are multi-point PV radiation data acquired from the Ministry of Economy, Trade, and Industry's subsidized project [8]. In addition, the standard data are the average PV radiation intensity in the area where the smoothing effect is taken into consideration, and the power generation output is calculated by multiplying the assumed installed capacity and the system efficiency.

2.3.2. Simulation model in this study

This study utilizes a simplified AGC30 model shown in Figure 2-8 where the PV power with the proposed dual *p-f* droop control block is added. The model is simplified in a way that there is one block generator block representing the parameters of different generators in an averaged manner, and EDC is simply a constant input signal in the simplified model. The proposed control is introduced to investigate the contribution of regulation power dP_{reg} of the dual *p-f* droop control when the demand and PV power output data are fluctuating.

2.3.3. Time-series data of demand and PV power output

In this case study, the semi-clear day pattern time-series data of PV have been prepared by IEEJ [5]. Figure 2-9 shows the time-series data of demand, residual load, and PV power for 600 s from 10:00 to 10:10 of semi-clear day in summer. The simulation interval

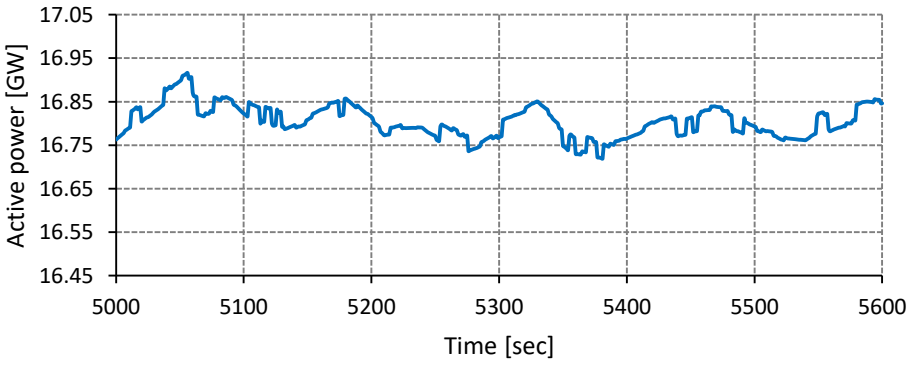

(a) Demand

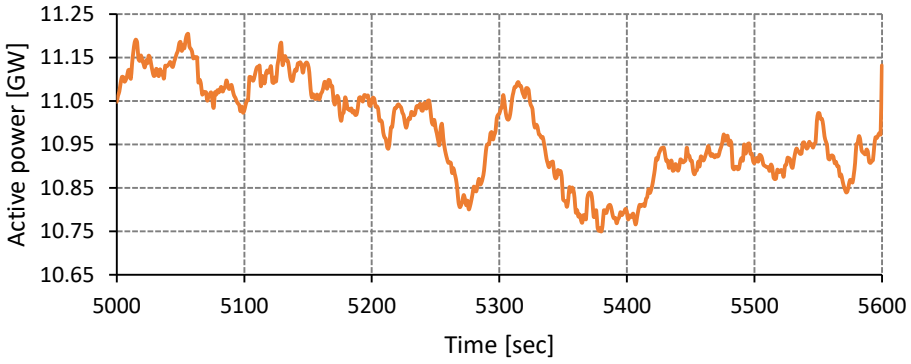

(b) Residual load

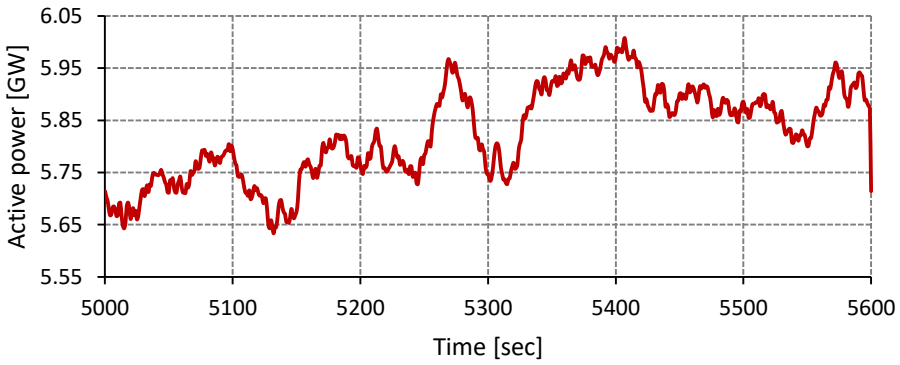

(c) PV power

Figure 2-9 Time-series data of demand, residual load, and PV power.

of running this model is 0.1 s, which is the same as that of the original AGC30 model. Although the demand is nearly constant as shown in Figure 2-9(a), the fluctuations of the PV power output in Figure 2-9(c) have yielded changes in the residual load as in Figure

2-9(b) hence the measured frequency of this system is anticipated to be fluctuating.

The power system operator can set the duration of the power output of aggregated PV system using dual *p-f* droop control. The duration can be for several minutes during certain time of a day. Therefore, the time-series data are almost smooth and steady for this short period. If the irradiance is changed, the time-series data can be obtained at higher or lower steady power output for that short period.

As shown in Figure 2-9(a), the power demand is almost constant at 16.8 GW with small fluctuations ranging between 16.75 and 16.90 GW. The maximum output data can be obtained from (2.4). When the maximum PV radiation is 1000 W/m^2, PV irradiance I is multiplied by the installed capacity of PV power S and PV power system output coefficient η = 0.8 to get P_{mpp}, which is the PV data in Figure 2-9(c). The residual load, i.e., P_{mpp} data subtracted from demand data, is shown in Figure 2-9(b).

$$P_{mpp} = \eta \cdot S \cdot \frac{I}{1000} \tag{2.4}$$

The capacity of the PV system is 10 GW and the average PV output P_{mpp} is 5800 MW, which is the yield of irradiance. The prospective P_{mpp} is estimated by employing the I-V characteristics for PV system, and the observations of the short-term I_{sc} and the open circuit V_{oc} by using silicon sensor with the same I-V characteristics. This P_{mpp} is curtailed by 20% using the generation of a fixed portion of available production approach to 4600 MW [9], thus it is assumed that 10% of the curtailed PV power which is 464 MW is available to be used for dual *p-f* droop control. Specifically for this amount of PV power penetration, only 10% is sufficient to contribute to frequency regulation, whereas the increase in this percentage is expected to cause more violations in the power system. Therefore, the variations in this percentage and its influence on the model can be investigated in future work.

The droop setting *D*, which determines the *p-f* characteristic of a generating unit, is generally expressed as a percentage [10]. The speed drooping characteristic is obtained

by adding a steady-state feedback gain, 1/*D*, in the turbine-governor transfer function. The action of droop in a generating unit is to decrease the power reference of the prime mover as the frequency increases. The grid codes of various countries stipulate governor droop settings between 3% and 6%, for all units participating in the system frequency regulation [11]. The droop setting used in the turbine-governor is 4% which is considered to be a typical value of droop setting for thermal generators [12]. The same setting is chosen for the proposed control.

2.3.4. Setting of components

Figure 2-10 shows the inertial model with a set of parameters given in Table II, which are previously set by the AGC30 model [5]. They are considered to be a mixture of thermal power generation model. Each one has an inertia ranging from 8 MWs/MVA to 11 MWs/MVA. Therefore, the assumed inertia is 9 MWs/MVA which is the average of that range.

Figure 2-11 shows the generic governor model but the transfer function of $1/(1 + 0.2s)$ will be omitted to eliminate any delay in the simulation. In this simplified AGC30 model, the capacity of aggregated synchronous generator model is set to be 20 GW, it is assumed that each generator has a rated capacity of 1 GW and which means that 20 generation units are used.

The LFC system model in Figure 2-12 is applied to compensate the supply/demand imbalance by using the frequency deviation and tie-line power flow. The inputs of this model are the actual frequency deviations. These signals will undergo area requirement (AR) calculation, and then the output will be smoothed. The control signal might have some delay causing the system to be unstable as a result of increasing oscillations. This is often avoided by providing a dead zone to the extent that the system can tolerate it. Also, a proportional-integral (PI) controller is used to eliminate any steady-state deviation. To avoid overshooting, the appropriate values for PI controller parameters are stated in Table III. Then, the signal will follow a ramp rate of 2% per minute, and it is assumed

that the majority of used thermal generating units are coal power plants. Afterwards, the LFC signal is fed back to the generator model. Finally, the EDC is considered as a constant signal. The EDC is equivalent to the value of the average residual load (11 GW) divided by the capacity of generators (20 GW), which is 0.55.

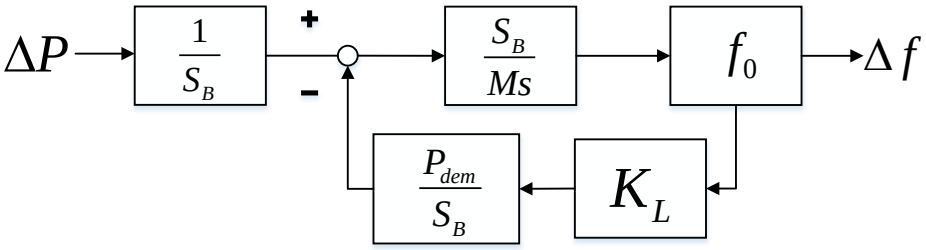

Figure 2-10 Block Diagram of Inertial model

TABLE II

INERTIA PARAMETERS SETTING

Variables	Set Value
Inertia M	9 [MW*s/MVA]
Selected power base in volt-amperes S_B	1000 [MVA]
Load frequency capacity K_L	2 [%MW/%Hz]
Nominal frequency f_0	60 [Hz]
Time increment Δt	0.01 [second]

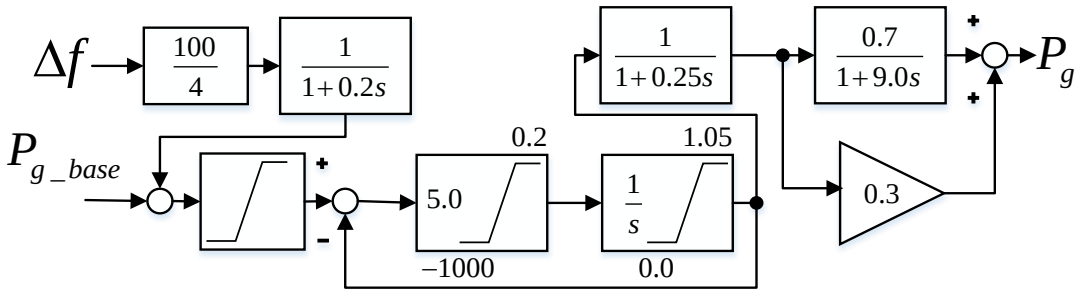

Figure 2-11 AGC30 turbine-governor model

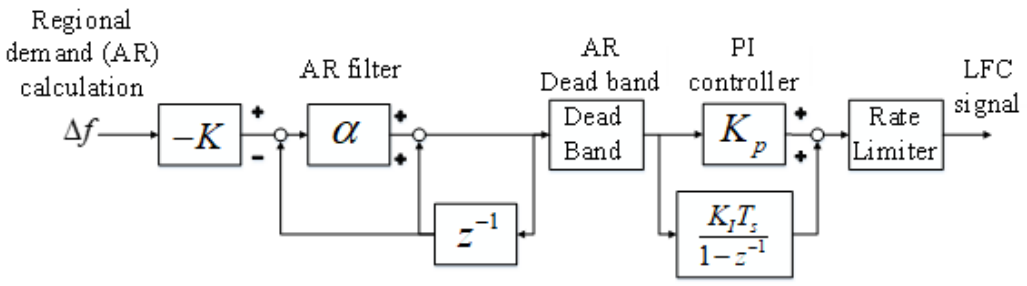

Figure 2-12 Block Diagram of LFC model

TABLE III

LFC PARAMETERS SETTING

Variables		Set Values
AR Calculation	Control cycle T_s	5s
	System constant K	10%MW/Hz
AR smoothing	Smoothing factor α	0.3
Dead zone	Dead zone width	±10MW
	Δf dead zone	±0.01Hz
PI Controller	Proportional gain	1.0
	Integral gain	0.003

The chosen LFC ramp rate is 2% per minute, which means that 2% of the generator capacity, which is 400 MW of the synchronous generator per minute, is available to support the LFC. In the first case study when the frequency fluctuation rate is higher than 400 MW/min, the fast-frequency control of dual droop control is able to provide frequency regulation so that the frequency fluctuations are mitigated when the fluctuations violate the frequency threshold value.

The slow-frequency control is activated within the frequency threshold region to support the LFC and mitigate the small fluctuations further to diminish the chances of higher rates of frequency deviations that cross the threshold and are beyond the region where the LFC can be applied. It is also preferable to always contain the fluctuations in this region, since the fast-frequency control might cause fluctuations by changing the response of generators after being activated.

2.3.5. Results of Method-1

Figure 2-13 shows frequency deviation with and without the proposed dual *p-f* droop control. In all cases, the system frequency fluctuates due to the imbalance between PV power output and demand while the power output of generators is adjusted to compensate for the imbalance. Without the proposed dual *p-f* droop control, the maximum frequency deviation reaches 0.284 Hz at 5354 s. Then, the operation of 464 MW of PV power with the proposed dual *p-f* droop control results in further mitigation of the frequency to 0.178 Hz due to the influence of the fast-frequency response of Method-1 and Method-2. The frequency fluctuations are small within ±0.15 Hz, the fluctuations are generally mitigated by the slow-frequency response of the proposed control. Method-1 and Method-2 have almost the same values of frequency deviation, due to their overlapping responses

In Figure 2-14, the application of the proposed control enables the distinction between the frequency measurements due to fast-frequency and slow-frequency responses The measured frequency due to fast-frequency response almost follows the actual frequency of the system while the measured frequency due to slow-frequency response has a delay from the actual frequency by a few seconds.

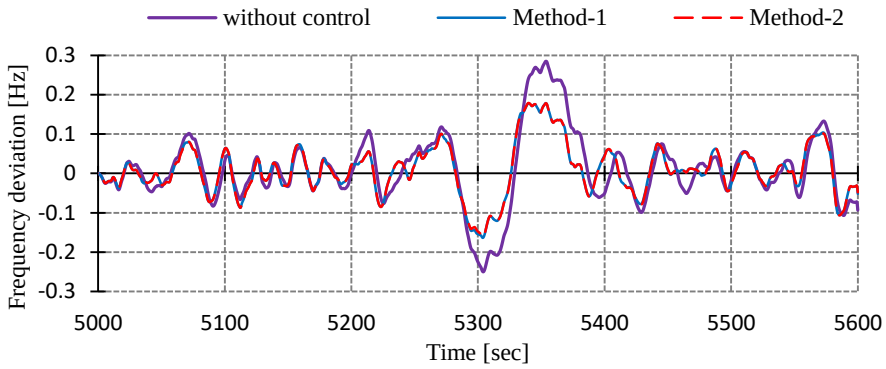

Figure 2-13 Frequency deviation with and without the proposed dual *P-f* droop control methods

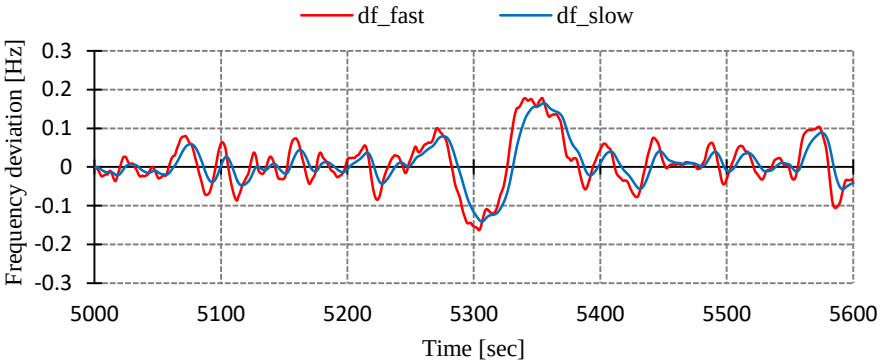

Figure 2-14 Measured Frequency Deviation due to slow and fast response of Method-1

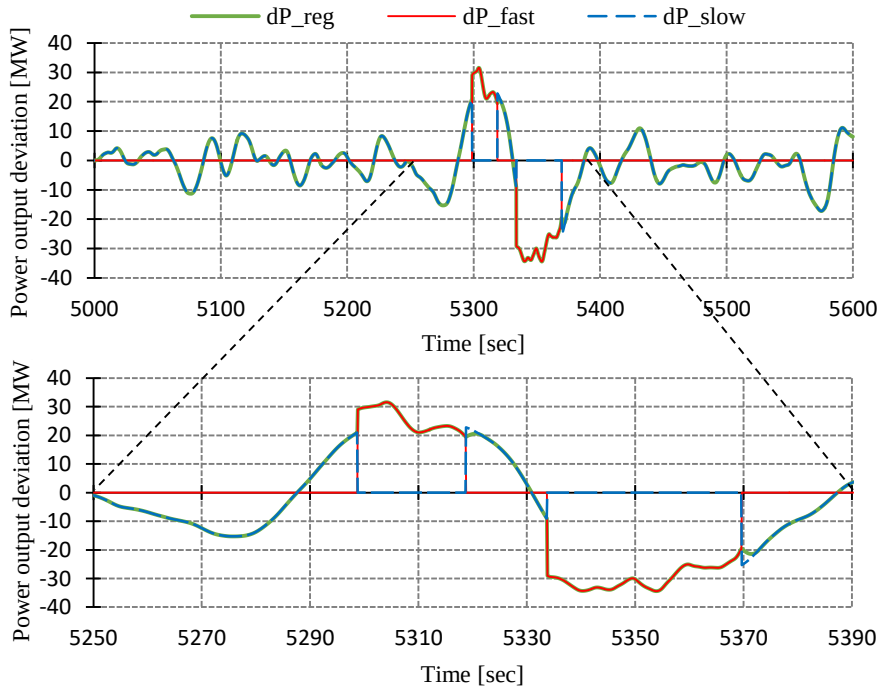

Figure 2-15 PV power output deviation due to slow and fast response applying Method-1

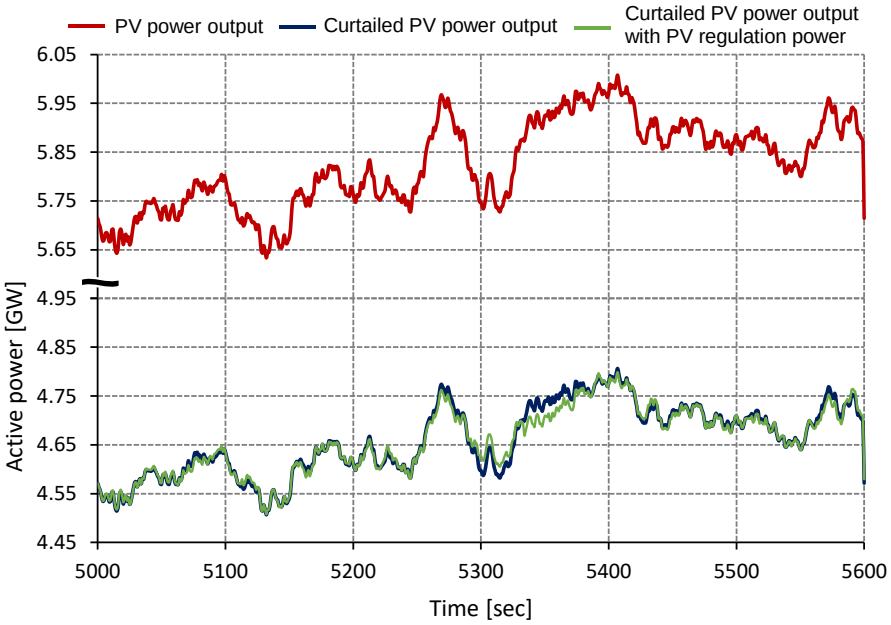

Figure 2-16 PV power output with regulation applying Method-1

When Method-1 is implemented in this model, it will result in dP_{reg}, as shown in Figure 2-15. dP_{slow} is the output as long as the frequency deviation is within ±0.15 Hz. Once the deviation exceeds ±0.15 Hz, which occasionally happens, dP_{fast} is activated and the new $\pm df_{th}$ becomes ±0.1 Hz. Therefore, dP_{fast} will have an output from the time when it exceeds ±0.15 Hz until the frequency reaches the new threshold of ±0.1 Hz. The maximum frequency deviation of 0.178 Hz at 5354 s will lead to a maximum power deviation of -34.4 MW due to the activation of fast-frequency response only.

The reduction below the threshold point of ±0.1 Hz will enable slow-frequency response again and only dP_{slow} contributes to the output. It is also observed that at the frequency recovery phase, when switching between fast-frequency and slow-frequency modes occur in Figure 2-15, dP_{reg} is no longer equal to the sum of dP_{slow} and dP_{fast}. However, it is the yield of the dP_{trans} where dP_{fast} will change to dP_{slow} as stated in Section 2.3 for only 3 seconds. During this period, dP_{reg} increases slightly from -19.6 MW to -21.4 MW instead of -25.4 MW if no transition signal is introduced. After 3 s, dP_{reg} is calculated as the sum of dP_{slow} and dP_{fast} again.

Figure 2-16 shows the PV power output, the curtailed PV power output and curtailed PV power in addition to the changes of dP_{reg}. Although the demand is nearly constant as shown in Figure 2-9(a), the fluctuations of the PV power output have yielded changes in the measured frequency as in Figure 2-14. These changes in frequency is mitigated as shown in Figure 2-13 by the dP_{reg} of the dual *p-f* droop control

2.3.6. Results of Method-2

Figure 2-17 shows PV power output deviation due to slow-frequency and fast-frequency responses applying Method-2. In Figure 2-14, when $\pm df$ is within ±0.1 Hz, dP_{reg} will be a result of slow-frequency response. Once the frequency crosses the threshold of 0.1 Hz, both the slow-frequency and fast-frequency responses will be activated so the maximum power deviation is -34.4 MW at 5354 s. Method-2 is proposed to prevent the switching of PV power outputs between slow-frequency and fast-frequency responses and eliminates the time detection used for the transition mode signal at the recovery period.

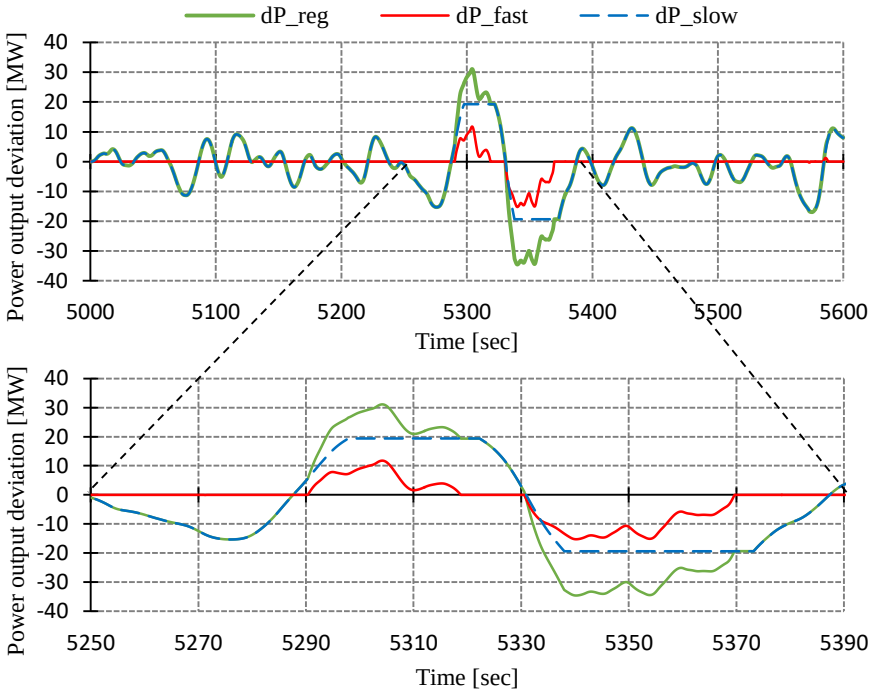

Figure 2-17 PV power output Deviation due to slow and fast response applying Method-2

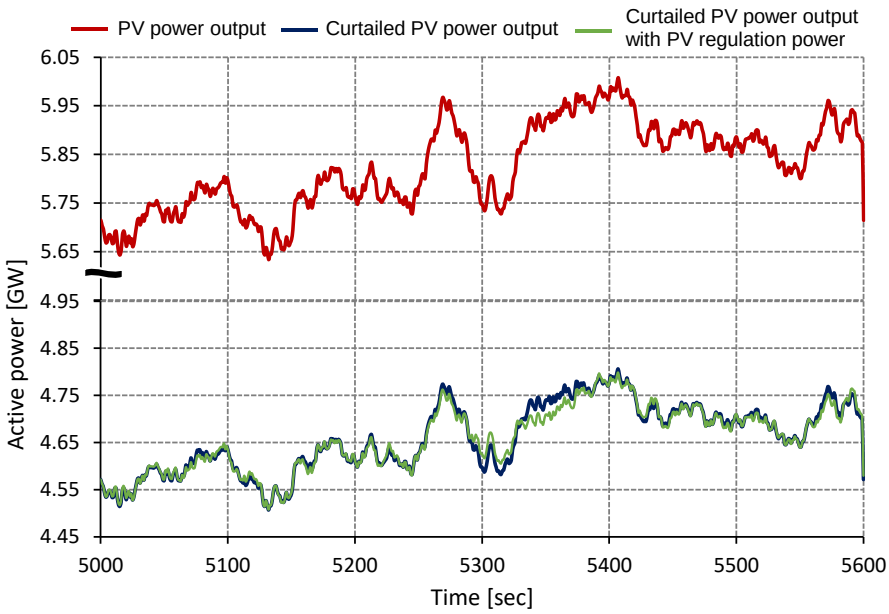

Figure 2-18 PV power output with regulation applying Method-2

Thus, dP_{reg} is always expressed in terms of the sum of both dP_{slow} and dP_{fast}. Accordingly, when the frequency recovers, dP_{reg} shows a gradual decrease to -19.33 MW at 5370 s due to the influence of slow-frequency response when it operates simultaneously with fast-frequency response. Figure 2-18 also shows the PV power output in addition to the changes of dP_{reg} that mitigated the frequency as shown in Figure 2-13. This is similar to Figure 2-16 to prove that Method-2 operate similarly as Method-1 in providing the same regulation power but in a simpler operation mechanism.

2.3.7. Effect of slow response in dual *p-f* droop control

Power output has a quicker increase in dP_{reg} than Method-1 in an abnormal situation. This is caused by the sole operation of fast-frequency response in Method-1 in an abnormal situation whereas both slow-frequency and fast-frequency responses occur simultaneously in Method-2, which slows down the operation of Method-2 at that phase. The slightly delayed response of Method-2 in abnormal situations leads to conduct another simulation that detects whether such delay is significant or not.

Referring to Figure 2-19, at the infrequent incidents of violating df_{th}, only fast-frequency

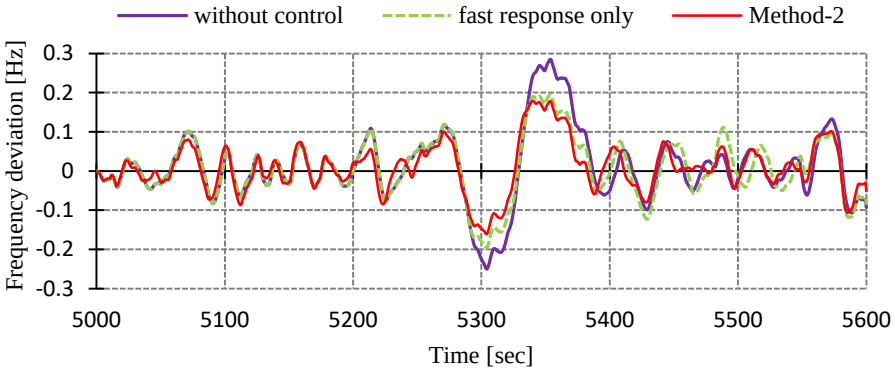

Figure 2-19 Frequency deviation due to fast response only and with dual *p-f* droop control of Method-2.

response will reduce the frequency deviation to 0.182 Hz. As stated previously, Method-2 further mitigates the frequency deviation to 0.178 Hz. After 5380 s, the occasional mitigation of frequency by the fast-frequency response generates higher variations in frequency following that mitigation. These variations are even more than the case without control. That is because the operation of the thermal generator has changed after that mitigation by fast-frequency response, hence the frequency fluctuation becomes different and larger than the case without control. This negative effect is suppressed by slow-frequency response using Method-2 to witness a lower frequency deviation, emphasizing the importance of slow-frequency response of the proposed dual *p-f* droop control. This affirms the idea that slow-frequency response working along with the fast-frequency response can maintain the frequency deviation at a lower level compared to the other studies mentioned in Subsection 1.3.2 where fast-frequency response only where used.

2.4. Support of fast response of dual *p-f* droop control to inertial response of synchronous generators

2.4.1. Simulation Model

The proposed control is tested when the generator trips and it is assumed that demand and PV input data are constant in this scenario by using the model in Figure 2-20 which is a more simplified model of AGC30 than that used in the previous section. This model

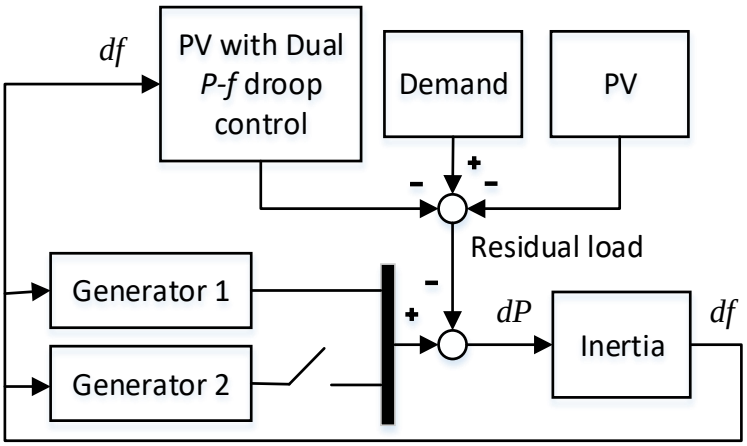

Figure 2-20 Supply-Demand Frequency Simulation Model

involves the same components as the previous test model but LFC controller is excluded so that this test model is concerned on the primary frequency response only. The simulation time interval is 0.01 s to realize the sudden incident of generator tripping and frequency drop.

The constant demand is rated to be 16.8 GW. The capacity of the PV is 10 GW and the power utilized by the dual *p-f* droop control is equivalent to 464 MW. The droop setting of the dual *p-f* droop control is also 4%. These are the same assumptions as considered in the previous test of Section 2.3.

The settings of parameters of the inertial model are the same as those shown in Table II. Both generators in the model have a total capacity of 20 GW. The capacity of generator 2 corresponds to 5% of the overall capacity which is equivalent to 1 GW in this test. The generator model is slightly different from that used in the previous model because when the generator trips, we have to observe a few seconds that immediately follow this drop. Accordingly, the generic model of the turbine governor will be used without the omission of the transfer function to observe the reaction of the frequency in a shorter time interval and distinguish the influence of dual *p-f* droop control. In this model, the frequency is not restored to its nominal value of 60 Hz due to the absence of the LFC system.

2.4.2. Results of Method-1 and Method-2

In Figure 2-21, without implementing the proposed control, which emulates the test of free-governor control only, the frequency deviation of the system will drop to -0.435 Hz and the frequency is recovered to a deviation of -0.162 Hz due to the absence of the LFC. While the mere application of slow-frequency control results in a frequency deviation of -0.397 Hz and recovers to -0.117 Hz quicker than the proposed control. The power due to slow-frequency response will be higher since the slow-frequency measurement is slightly delayed. Therefore, it detects higher frequency change.

When dual *p-f* droop control is implemented, the frequency deviation is mitigated to -0.353 Hz and -0.360 Hz by Method-1 and Method-2, respectively, and it is recovered to -0.117 Hz. It is also observed that the frequency deviation values of both methods are almost the same, which leads to the values overlapping from 115 s.

Fast-frequency response of Method-1 causes regulation power to increase steeply to 71 MW, as shown in Figure 2-22. Regulation power due to fast-frequency response is supposed to stop when it hits df_{th} of -0.15 Hz. However, regulation power continues till df_{th} of -0.1 Hz, which is the new value of df_{th}, following the characteristics of Method-1. The power starts to decrease, hitting the peak when the largest frequency occurs. Contrarily, due to the slow-manner of frequency detection of slow-frequency control, it will still be activated even though df is less than -0.1 Hz (df_{th}), resulting in a significant power increase in dP_{reg}. It reaches 544 MW. Eventually, the power due to slow-frequency response will drop to zero power deviation that will lead to a slightly steep decrease in dP_{reg} as shown in Figure 2-23.

The application of Method-2 of dual *p-f* droop control has shown that power output due to fast-frequency response in Figure 2-22 will increase to 53 MW. Regulation power due to slow-frequency response is provided when df decreases below -0.1 Hz. Fast- and slow-frequency responses will operate concurrently beyond df_{th} which results in the fact that dP_{reg} is the sum of power due to fast- and slow-frequency responses equivalent to 536

MW. As a result, dP_{reg} in method-2 in Figure 2-23 seems to have a smoother increase than that in Method-1. Then, the supply of dP_{reg} due to both methods almost overlaps since the droop settings used in both methods are the same.

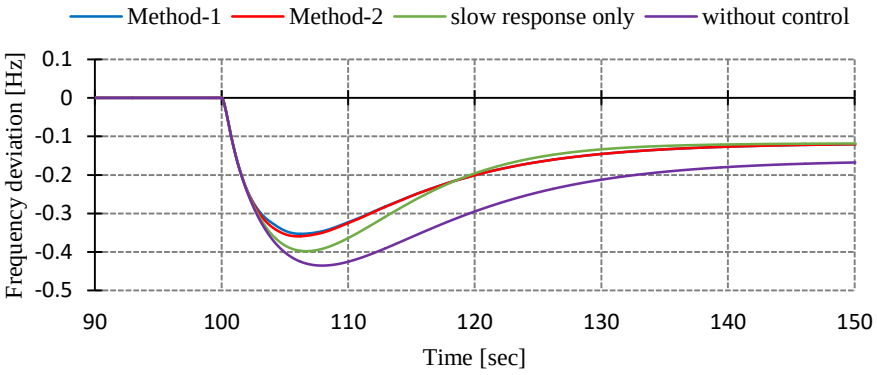

Figure 2-21 Frequency deviation response in the absence of LFC system

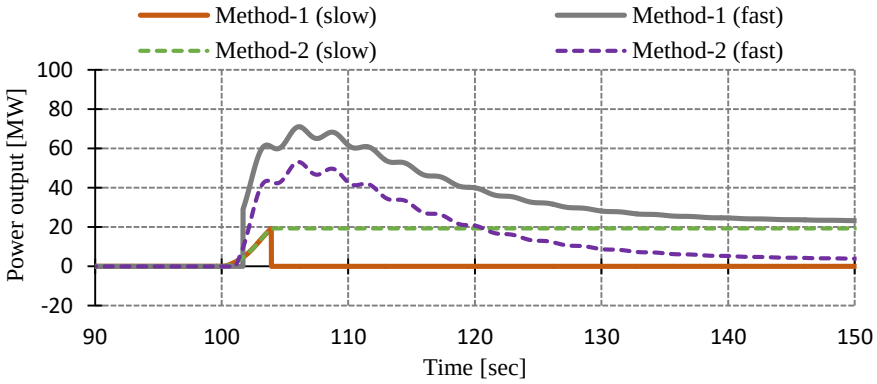

Figure 2-22 PV power output due to the slow and fast responses of Method-1 and Method-2

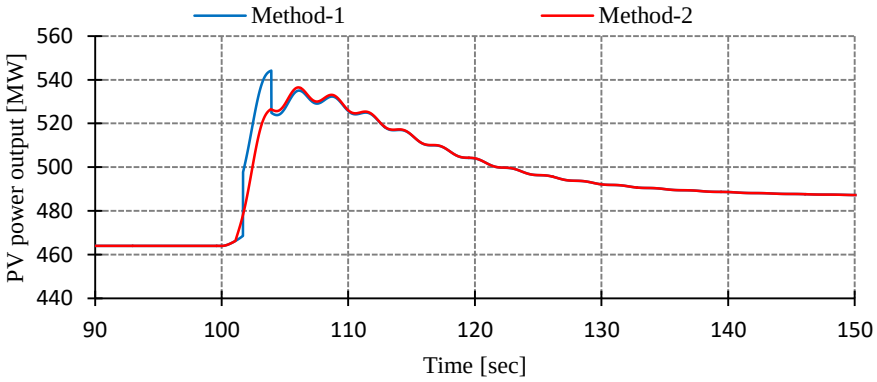

Figure 2-23 Total PV regulation power output using Method-1 and Method-2

The maximum frequency deviation occurs when no control is applied which simulates the condition of the inertial response of the existing generator. When the slow-response suppresses the frequency deviations, it is further suppressed by the proposed control due to the activation of the fast-frequency response. The positive influence of fast-frequency response in the proposed control confirms a rapid recovery and further a reduction in frequency deviation.

There is a slight difference between frequency deviation due to the application of Method-1 and Method-2 at 103 s. The reason is that the activation of only fast-frequency response in Method-1 and the simultaneous operation of slow-frequency response along with fast-frequency response in Method-2 in abnormal operation state delays the quick action of fast-frequency response to be marginally slower than that of Method-1. However, this slight difference is considered insignificant since Method-2 still has a quicker reaction compared with the inertia of the generator in the system without the proposed control.

Moreover, the results of dP_{reg} have revealed a surge of power output when using method 1 due to the switching from fast- to slow-frequency responses. Therefore, the proposal of a simple control scheme such as Method-2 proves a smooth PV power output due to the operation of slow-frequency and fast-frequency responses, simultaneously.

2.5. Parameters affecting dual *p-f* droop control

In the numerical simulations of Sections 2.3 and 2.4, some parameters' values were assumed within a reasonable range. However, it is necessary to adjust these parameters. These parameters are:

- The slope of the droop characteristics which is the droop setting and it is expressed in the proposed control by *dP/df*. The droop setting (*D*) was assumed to be 4%. If the droop setting is reduced, the reaction of the dual *p-f* droop control is expected to be faster and the frequency deviations will be mitigated faster. However, by realizing such a quick response of the dual *p-f* droop control, the dual *p-f* droop control can cause unexpected disturbances in the system hence it is preferable to conduct a sensitivity analysis for the purpose of testing the most effective range of the droop

setting.

- The frequency threshold where the two control changes that was ±0.15 Hz. However if less threshold value is used, fast response will be frequently activated to suppress these frequency deviations. However, the quick and frequent activation of fast response of the dual *p-f* droop control can cause unexpected disturbances in the system which lead to the idea of conducting a sensitivity analysis for the purpose of testing the most effective frequency threshold value.
- The number of measured cycles for fast and slow controls, i.e. for fast control, it is 20 cycles and for slow control, it is 400 cycles. The number of cycles for fast control is already considered as a rapid measurement. On the other hand, if the number of cycles of frequency measurement to a lower for slow control measurement, it might further mitigate the normal frequent fluctuations. The slow response supports the LFC and in the actual LFC scheme, the signal is dispatched to generators every 5 signals to adjust their power, while time of slow control measurement is about 6.5 seconds. However, further investigation can be conducted to find the optimum number of cycles that does not disturb the system meanwhile support the LFC efficiently.
- The dual *p-f* droop control in this study is primarily created using portion of the curtailed PV power output to provide regulation power. PV power output curtailment of 20% was applied to the average of the aggregated PV power output rather than application of curtailment to each region in the power system which can be an optimistic assumption. In addition, 10% of the curtailed PV power was used for the dual *p-f* droop control. Another investigation should be done to test the impact of dual *p-f* droop control against different power curtailment approaches.

Chapter 2 introduced a simplified idea of PV using the dual *p-f* droop control that involves different parameters. Since these parameters should to be further investigated, the next study is used to deepen the investigation of PV power curtailment which is one of the aforementioned parameters by proposing different curtailment application schemes.

2.6. Conclusion

Autonomous active power control for supporting LFC and the inertial response of synchronous generators is proposed by creating two different characteristics for slow- and fast-frequency dynamic responses provided by small-scale PV systems. Two simple control methods of dual *p-f* droop control are designed to achieve a smooth transition between slow- to fast-frequency responses according to the change in frequency.

Firstly, a basic idea that combines fast-frequency and slow-frequency droop controls is proposed. In literature, fast-frequency droop control is already implemented as discussed in Subsection 1.3.2. However, slow-frequency control is preferably added to enhance the droop control in tackling normal disturbances in the power system, and a dual *p-f* droop control can be formed. Method-1 is an enhanced design of dual *p-f* droop control where besides the simple turning on one frequency control while turning off the other, as the frequency deviation changes, it has an additional control such as transition signal as well as switching of frequency thresholds. However, Method-2 provides a complementary simpler idea to improve the operation of fast-frequency and slow-frequency controls, i.e., both frequency controls can operate simultaneously. A summary of advantages and disadvantages of these methods is shown in Table I.

Two simulation models are conducted to highlight the importance of slow- and fast-frequency responses of enhanced proposed methods. The results reveal that the slow- and fast-frequency controls can work independently. The switching between slow- and fast-frequency controls in emergency and recovery phases has shown that Method-2 of the proposed control provides smoother transitions than method 1. This proves that method 2 outperforms method 1 as an effective control for supporting frequency by small-scale PV systems.

As future work, the proposed dual *p-f* droop control should be tested using a detailed model in consideration of the existence of various types of generators, different irradiance fluctuations among different regions, different control schemes such as dual *p-f* droop control and other direct controls by the system operator, etc. Then, a sensitivity analysis

will be also done for some factors such as the used frequency threshold, and the degree of changing the PV power experiencing dual *p-f* droop control. Accordingly, the impact of this variability on the system frequency deviation will be investigated. Finally, various changes in demand data especially their surge will reflect the future inflation of demand, thus the effectiveness of the proposed control under this condition should be tested.

TABLE I
SUMMARY OF DUAL P-F DROOP METHODS

Methods of dual *P-f* droop control	Advantages	Disadvantages
Basic idea	• fast frequency control is solely activated when $\left\|df_{fast}\right\| > df_{th}$ • The regulation power (dP_{reg}) increase immediately when frequency drops.	There is a difference between df_{fast} and df_{slow} which will lead to a step increase in dP_{reg}
Method-1	• same as the basic idea • smoother transition from dP_{fast} to dP_{slow} than that of Method-0	To solve the step increase in method-0, dP_{reg} will be calculated as dP_{trans} for few seconds to create a smooth transition from dP_{fast} to dP_{slow}. In addition, switching of frequency thresholds is used. These two additional mechanisms complicate this method
Method-2	• Since both fast frequency control and slow frequency control are operating, switching between the two control-modes (switching from dP_{fast} to dP_{slow} and vice versa) does not exist. • Therefore, dP_{reg} will always be calculated as the summation of dP_{fast} and dP_{slow} which makes Method-2 a simpler dual *P-f* droop control	• Both fast frequency control and slow frequency control are operating when $\left\|df_{fast}\right\| > df_{th}$ • The regulation power increase slowly: This slow increase is to be investigated in the second case study to prove its insignificance

References

[1] J. Johnson, J. C. Neely, J. J. Delhotal and M. Lave, “Photovoltaic Frequency–Watt Curve Design for Frequency Regulation and Fast Contingency Reserves,” in *IEEE Journal of Photovoltaics*, vol. 6, no. 6, pp. 1611-1618, Nov. 2016.

[2] H. Xin, Y. Liu, Z. Wang, D. Gan and T. Yang, “A New Frequency Regulation Strategy for Photovoltaic Systems Without Energy Storage,” in *IEEE Transactions on Sustainable Energy*, vol. 4, no. 4, pp. 985-993, Oct. 2013.

[3] A. F. Hoke, M. Shirazi, S. Chakraborty, E. Muljadi and D. Maksimovic, “Rapid Active Power Control of Photovoltaic Systems for Grid Frequency Support,” in *IEEE Journal of Emerging and Selected Topics in Power Electronics*, vol. 5, no. 3, pp. 1154-1163, Sept. 2017.

[4] J.Seidel, F. Rauscher, B. Engel, “Enhanced contribution of photovoltaic power systems to frequency control in future power systems”, in *IET renewable power generation*, May 2021.

[5] Investigating R&D Committee on recommended practice for simulation models for automatic generation control: ‘Recommended practice for simulation models for automatic generation control’. No. 1386, IEEJ Technical Report, 20 December 2016.

[6] Organization for Cross-regional Coordination of Transmission Operators, Nov.,2018. Report on the quality of electricity supply. [Online]. Available: https://www.occto.or.jp/en/information_disclosure/miscellaneous/files/170203_qualityofelectricity.pdf

[7] C. R. Jeevandoss, M. Kumaravel and V. J. Kumar, “Sunlight based I-V characterization of solar PV cells,” in the *Proceedings of 2011 IEEE International Instrumentation and Measurement Technology Conference*, Hangzhou, China, 2011, pp. 1-4, doi: 10.1109/IMTC.2011.5944061.

[8] IEEJ, “Recommended practice for simulation models for automatic generation control,” Japan. Tech. Rep. Dec. 2016.

[9] M. Rossi, G. Viganò, D. Moneta, D. Clerici and C. Carlini, “Analysis of active power curtailment strategies for renewable distributed generation,” in the *Proceedings of 2016 AEIT International Annual Conference (AEIT)*, Capri, pp. 1-6, 2016.

[10] P. Kundur, “Power System Stability and Control”, McGraw-Hill, Inc., 1994.

[11] K. V. Vidyanandan and N. Senroy, “Primary frequency regulation by deloaded wind turbines using variable droop,” in *IEEE Transactions on Power Systems*, vol. 28, no. 2, pp. 837-846, May 2013.

[12] R. E. Cosse, M. D. Alford, M. Hajiaghajani and E. R. Hamilton, “Turbine/generator governor droop/isochronous fundamentals - A graphical approach,” 2011 Record of Conference Papers Industry Applications Society 58th Annual IEEE Petroleum and Chemical Industry Conference (PCIC), Toronto, ON, pp. 1-8, 2011.

3. Optimal Allocation of Curtailment Levels of PV Power Output in Different Regions in Consideration of Reduction of Aggregated Fluctuations

3.1. Introduction

As mentioned in Chapter 1, in a day-ahead UC scheduling of required generation resources based on a day-ahead forecast of electricity demand and various renewable power generation, the curtailment level (CL) of the aggregated PV power output is determined [1]–[3]. The curtailed PV power output deliberately contributes to maintaining the supply-demand balance of the power system as well as to providing adequate capacity for the frequency control [4], [5]. In the actual application of PV power output curtailment in Japan and many studies regarding UC scheduling, the CL of the aggregated PV power output is determined regardless of the distinctive fluctuating behavior of each region in the power system service area [1]-[3]. However, different CL among each region should be applied to reduce the fluctuations in the aggregated PV power output. This will contribute to maintaining the frequency variations within the acceptable ranges determined by the grid codes, reducing the requirement of frequency regulation. Therefore, the main objective of this study is to propose an optimal allocation of CL among each region.

Here, in consideration of the optimal CL allocation, there are two major challenges, i.e., the improvement of short-term forecasting of power output fluctuation characteristics as well as the power output average value and the development of method to optimize CL based on the short-term forecasting. This study tackles the later one as described below.

As for the former one, numerous studies have been conducted to a day-ahead forecast PV power output from different perspectives, including various forecasting models based on statistical, mathematical, physical, machine learning or hybrid [6]–[11]. With higher PV penetration, the short-term forecasting becomes more crucial for guaranteeing the

achievement of the required PV power output on each hour on the operation day. Highly accurate short-term forecasting can lead to further adjustment of CL compared to the pre-determined CL by the UC scheduling. Currently, the forecasting of the average value of PV power output in short-term, ranging from few minutes to few hours, is feasible and different methods are discussed in [12] to be mainly divided into physical and data-driven methods. Whereas [13] followed data-driven methods to cooperate neural network model with deep learning technology to predict the short-term average value of PV power output, achieving a high level of accuracy. On the other hand, the forecasting of short-term fluctuations of PV power output still remains challenging with a considerable amount of error even though machine learning algorithms and other advanced modeling techniques are used [14]–[18].

Short-term forecasting data with high accuracy can be challenging. Yet, if available, each region short-term time-series power output data can be used to allocate an optimal CL value. Yet this approach that involves huge time-series data can be a sophisticated and time-consuming. Therefore, this study tackles this issue through a more straightforward novel approach assuming that the fluctuation characteristics can be predicted in the short-term forecasting and be expressed in several typical patterns. Thus, instead of using huge accurate forecasted time-series data for each region, each region will be given a typical prepared pattern that reflects its level of fluctuations based on the short-term forecasting.

Therefore, the objectives of this study, firstly is the formation of statistical relations of average value and maximum fluctuation against different CL, respectively, these relations are used to distinguish each region PV power output behavior in short-term. Secondly, based on the short-term forecasting, each region will have a specific relation, thus, using these relations this study proposes an optimization of different CL to be allocated to each region. In this approach, the optimal CL in each region will minimize the fluctuation of aggregated PV power output without precisely forecasting the time-series of PV power output. As a result, the proposed method can contribute to the reduction of the control burden needed to eliminate the frequency fluctuations and hence reducing the required resources for frequency control or secondary control in the power system.

This chapter is divided as follows, Section 3.2 describes the irradiance data used in this study. Section 3.3 discusses the concept of five different methods of CL adjustment together with three methods for comparison. Section 3.4 demonstrates an example used to show the procedure of data preparation and calculation process for the proposed methods of CL adjustment. Using the example of Section 3.4, Section 3.5 represents the application of all the adjustment methods on the day of operation. Finally, Section 3.6 is dedicated to the results and discussion of the application of all methods over an entire year data.

3.2. Data under investigation

Although the numbers of PVs are installed in each region of the power system service area, the time-series data of either PV power output or irradiance of fine temporal resolution might be available only at specific sites in each region. Therefore, in order to estimate the aggregated power output data observed at the limited number of location, a low-pass filter (LPF) model should be applied [19]. In the LPF model, a so called

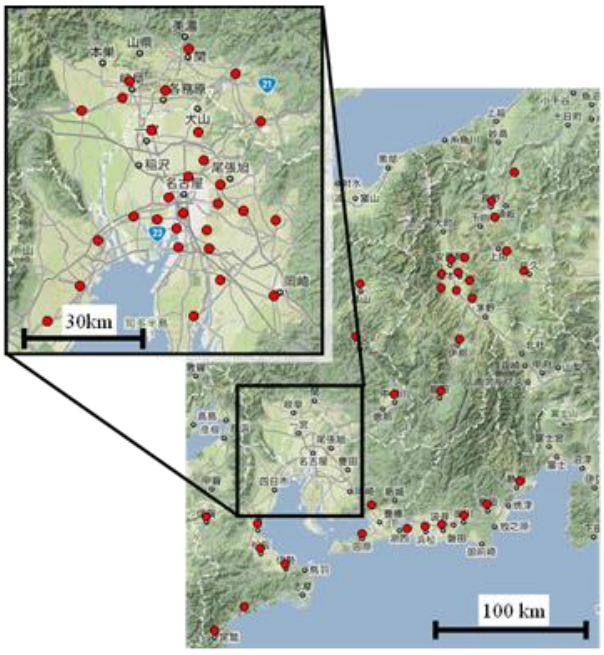

Figure 3-1 Location of multi observation points of PV power output in Chubu region, Japan.

smoothing effect among different fluctuations in a certain region is taken into account according to the geographical size of the representative region of each observation point, in which the aggregated fluctuations becomes smaller than that at single point.

To calculate the aggregated PV power output, this study utilizes the irradiance data observed at 61 points shown in Figure 3-1. The 61 observation points are dispersed almost evenly according to the population distribution with mountain areas excluded in the central region of Japan which is called Chubu region, except for Nagoya City that is enlarged in Figure 3-1. The distance between each pair of the neighboring observation points varies between 4.2 km and 138 km, and the average distance is 22 km. The 61 representative regions of each observation point is determined by applying Voronoi decomposition [19].

The irradiance data are observed in 363 days from September 2010 to August 2011.The data have a fine temporal resolution of one minute for an entire year. As these data are obtained from 61 points in one specific region in Japan, it is considered to be an advantageous point of this study. The aggregated time-series data of curtailed PV power output for a certain period is $P_{agg}^{CL}(t)$ and it is expressed as the weighted sum of PV power output of each region after the curtailment application as shown in

$$P_{agg}^{CL}(t) = \sum_{i=1}^{6\,1} \omega_i P_i^{CL}(t) = \sum_{i=1}^{6\,1} \omega_i \frac{I_i(t)}{I_{max}} CL_i \qquad \textbf{(3.1)}$$

where, $P_i^{CL}(t)$ is the time series curtailed PV power output for individual region i, ω_i is the weighted factor based on each region's installed capacity, $I_i(t)$ is the time series irradiance of each region, I_{max} is the maximum irradiance, thus 1000 W/m^2, and CL_i is the curtailment level applied for each region. Because ω_i is determined in consideration to the aggregated capacity of PV in the power system service area, P_{agg}^{CL} and P_i^{CL} are expressed in per unit (p.u.).

Considering that the curtailment will be applied when PV power output is high usually in the period from 10:00 to 14:00, the proposed methods are tested for one hour from 12:00 to 13:00 for the entire days of the year. This one hour gives a reasonable representation to the different PV power output behaviors of the 61 regions for every day at every season. For instance, in Japan, the temporal resolution of irradiance forecast is one hour, and in one hour time horizon, variability and uncertainty of PV power output still exist. In this hour, 61 regions can exhibit high average PV power output and low fluctuations in few days of summer season or low average PV power output and low fluctuations in few days in winter or wide ranges of low average PV power output and fluctuations in spring and autumn. Therefore, the statistical analysis on the performance of proposed method is available even with the data of one hour for each day instead of using data of longer period for each day. The following sections will demonstrate the different methods of CL adjustment.

3.3. CL adjustment methods

The unit commitment scheduling is proceeded a day-ahead to determine the supply requirements of different generation resources based on the forecasted demand for the next day. In the current day-ahead UC scheduling, the CL of the aggregated PV power output is determined regardless of the distinctive fluctuating behavior of each region in the power system service area. However, different CL among each region should be applied to reduce the fluctuations in the aggregated PV power output. Therefore, as explained below, the proposed method further adjust the CL in the real-time operation of the day based on the short-term forecasting of PV power output in each region.

3.3.1. Proposed CL adjustment methods

Method-1: Short-term adjustment of CL based on short-term forecasting of hourly average output

The main purpose of CL adjustment in Method-1 is to obtain hourly average value of resultant P_{agg}^{CL}, which is referred to as Avg_{agg}^{CL} equal to the predetermined average by the system operator (Avg_{pre}) in the short-term. Although Method-1 is not intended to reduce the

fluctuations of the aggregated PV power output, Method-2, which is the main proposal in this study, is developed based on Method-1. Therefore, Method-1 is explained as a part of proposed method. Avg_{agg}^{CL} is simply defined in Eq. (2) where T is 60 minutes.

$$Avg_{agg}^{CL} = \frac{1}{T}\sum_{t=0}^{59} P_{agg}^{CL}(t) \tag{3.2}$$

Considering the fluctuations within one hour, Avg_{agg}^{CL} is not a simple linear function of CL. Therefore, in the proposed Method-1, when short-term (i.e. few hours ahead) forecasting of PV power output in each region takes place, the adjusted CL is allocated to each region distinctively based on the relation between CL and the corresponding hourly average curtailed PV power output for each region (Avg_i^{CL}) where Avg_i^{CL} is simply defined in Eq. (3). The relations between Avg_i^{CL} and CL are called Avg-CL patterns and the concept of these patterns is shown in Figure 3-2(a)

$$Avg_i^{CL} = \frac{1}{T}\sum_{t=0}^{59} P_i^{CL}(t) \tag{3.3}$$

The Avg-CL patterns are prepared based on the analysis of the observed PV power output in the past. The three patterns of Avg-CL can be expressed to range from high Avg to low Avg modes. Thus, instead of exact Avg_i^{CL} forecasting, the prediction of the mode to which the value can be categorized is enough for the proposed method. By predicting Avg

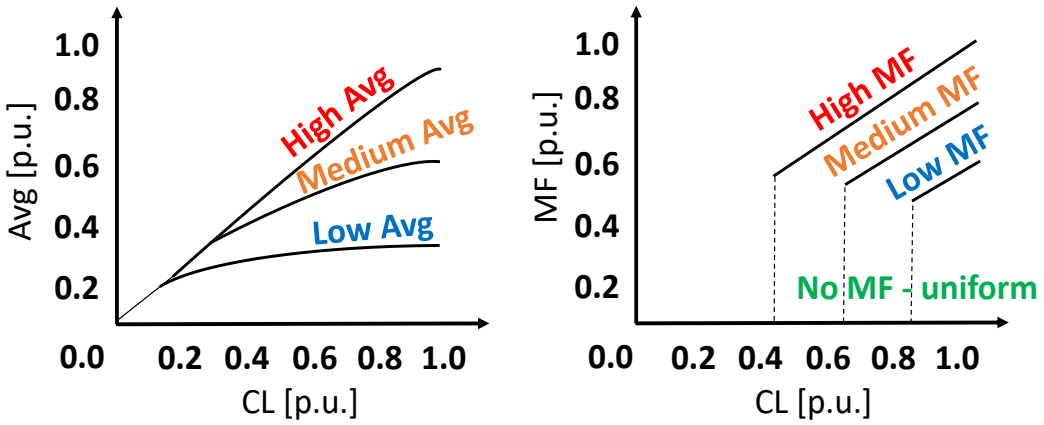

(a) Avg-CL (b) MF-CL

Figure 3-2 Concept of hourly average and maximum fluctuation of PV power output as a function of CL

mode, CL is adjusted and the Avg_{agg}^{CL} can be more accurate compared to the Avg_{pre} determined a day-ahead.

It is noted that Method-1 indirectly gives an insight into the characteristics of PV power output fluctuations. For instance, the medium Avg mode reflects the case when fluctuations are high at either low or high PV power output. Therefore, to precisely adjust CL, more information about the fluctuations becomes crucial and hence the next method is proposed. Figure 3-3 includes the CL adjustment procedures of Method-1 in blue. They are composed of two main steps: preparation of Avg-CL patterns in Section 3.3, and the utilization of these patterns to apply CL adjustment methods on the day of operation in Section 3.4.

Method-2: Short-term adjustment of CL based on short-term forecasting of hourly average output and maximum fluctuations

The main purpose of CL adjustment in Method-2 is to minimize the maximum fluctuations of the aggregated PV power output (MF_{agg}^{CL}) as long as the predetermined Avg_{pre} is met. MF is basically the difference between the maximum and minimum time-series PV power in 20-minute moving window. The approach of calculating MF is further elaborated in Section 3.4.2. CL adjustment in this method undergoes a more advanced approach than Method-1 by considering the PV power output fluctuations directly. Despite the fact that the forecasting of actual fluctuations is challenging, this study assumes that the forecasting of typical fluctuation patterns can be available.

The relations between hourly maximum fluctuations of PV power output for each region MF_i^{CL} and CL are called MF-CL patterns and the concept of these patterns is shown in Figure 3-2(b). They are also prepared for typical four PV power output characteristics based on the analysis of the observed PV power output in the past. The four patterns of MF-CL can be expressed to range from high MF to no MF (i.e. uniform output) modes. Thus, instead of forecasting the exact MF_i^{CL} and Avg_i^{CL}, the prediction of the modes to which these values can be categorized are needed. By predicting the PV power output behavior (i.e. Avg and MF modes), CL is adjusted and the resultant Avg_{agg}^{CL} can even be

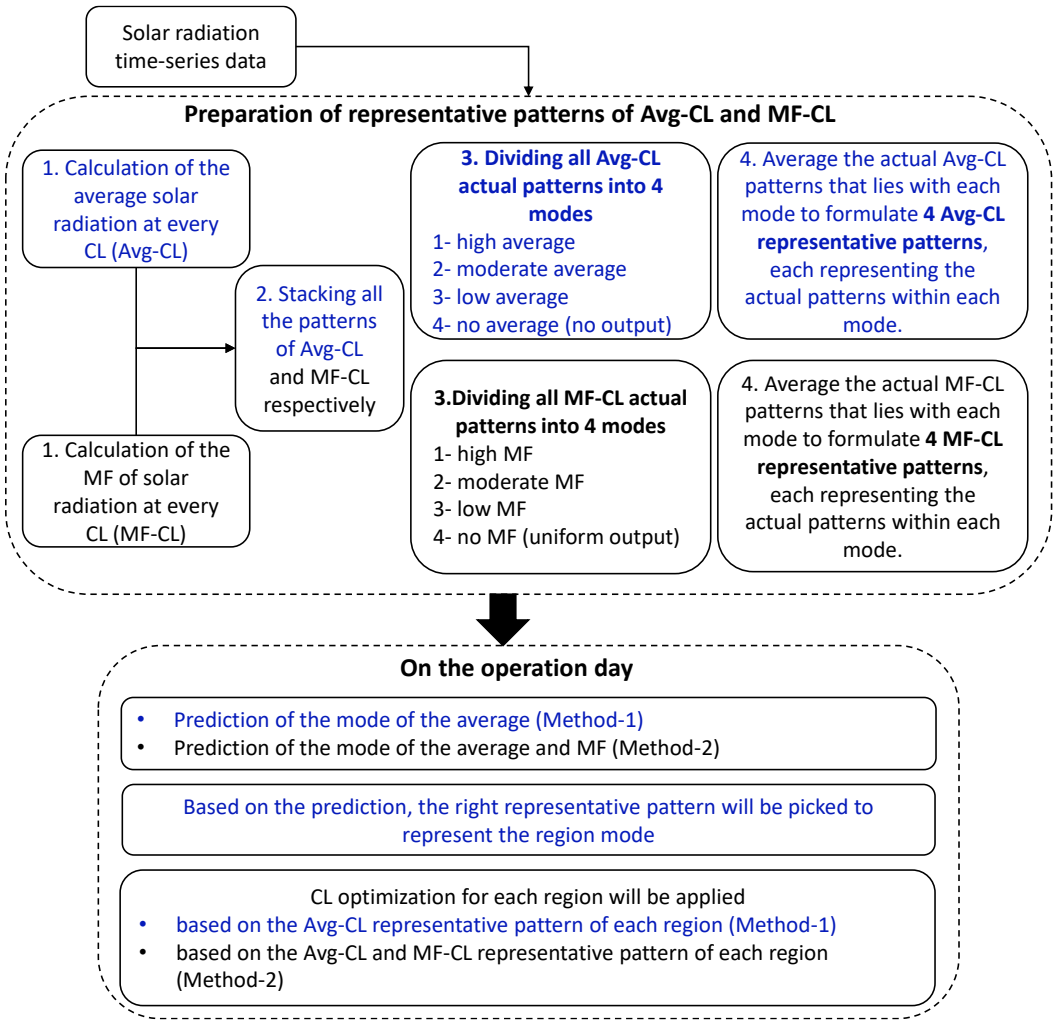

Figure 3-3 High level schematic of the procedures of the preparation of data and usage of the data on the operation day for the proposed methods of CL adjustment.

closer to the Avg_{pre}. The short-term forecasting of Avg modes and MF modes are addressing a simple categorization of the regions from high Avg to low Avg modes and high MF to no MF. The entire Figure 3-3 shows the two main steps of preparation of Avg-CL and MF-CL in Section 3.3, and the utilization of both Avg-CL and MF-CL patterns to apply the CL adjustment methods on the day of operation in Section 3.4.

3.3.2. Comparative CL setting methods

Method-0: No curtailment

Method-0 represents the case when no curtailment is enforced. This is when the entire PV power output is used to balance out the demand along with other generation resources. Whereas frequency regulation can be achieved effectively by mechanisms such as battery energy storage and demand response, without any requirement for PV power curtailment.

Method-3: Same CL for all regions

When the curtailment of PV power output is requested by the current UC scheduling a day-ahead, it merely applies the same CL to all the regions in the power system regardless of each region's behavior of PV power output for each hour on the next day, and no adjustment of CL is applied. Consequently, this might lead to unsatisfying the Avg_{pre} scheduled by the UC to meet the demand especially when the PV power output is fluctuating. This method can be efficient in situations where the PV power output is uniform only.

Method-4: Short-term adjustment of CL based on perfect forecasting of average and fluctuations

In Method-2, short-term forecasting of Avg modes and MF modes are addressing a simple categorization of the weather mode of each region. In Method-4, it is assumed that the perfect short-term forecasting of the time-series of PV power output in each region is available. This kind of zero-error forecasting is challenging and nearly impossible. Therefore, Method-4 is assumed to be an ideal situation and merely used for the comparison with the proposed methods.

3.4. Data preparation for the representative Avg-CL patterns and MF-CL patterns

The data preparation procedure of the proposed methods is applied to the 61 regions for every hour in each month. As an example, this section shows the data preparation of the representative patterns for one hour (from 12:00 to 13:00) in September. In each step, an

example of four regions was used to demonstrate the concept and calculation output in each method. Figure 3-4(a) shows the raw PV power output time-series data of the four regions on 1st September and their Avg_{agg}^{CL}. The different PV power output behaviors of the four regions for corresponding weather modes are identified as the following:

- Region (R) 1 has a high Avg and moderate MF.
- R11 has a high Avg and no MF, i.e. uniform PV power output.
- R29 has a moderate Avg and low MF.
- R51 has a low Avg and high MF.

3.4.1. Method-1

Step 1: Application of LPF to past measured PV power output time-series data.

As described in 3.2, each of the 61 points represents the spatial average PV power output in each of the 61 regions. In Figure 3-4 (b) the filtered PV power output data of the four regions on 1st September and their Avg_{agg}^{CL} are also shown. The filter gain of the LPF depends on the area of each region, i.e. the smaller the area, the smaller the filter gain applied and hence less reduction of fluctuations is witnessed. As R51 is a region with small area, the raw data and LPF data in Figure 3-4(a) and Figure 3-4(b) are almost similar.

Step 2: Application of different CL.

For the 61 regions, different CL are applied on their observed time-series PV power output data ranging from 0 to 1.0 p.u. with an increment of 0.01 p.u. No curtailment is applied at 1.0 p.u. level, and 100% of curtailment is applied at 0 p.u. level. Figure 3-5 shows an example of this step using the time-series data of R51 with an increment of 0.1 p.u. only.

Step 3: Computation of Avg_i^{CL} for each region.

The Avg_i^{CL} will be computed at each CL for every hour of interest at every day of the month. The actual Avg-CL patterns for 61 regions at one hour (here, from 12:00 to 13:00) for the entire days of September are plotted in Figure 3-6(a). The actual Avg-CL patterns of the four regions on 1st September are shown separately in Figure 3-6(b).

Step 4: Formation of the representative patterns of Avg-CL.

The Avg-CL patterns of the 61 regions for 30 days for one hour are stacked. Figure 3-6(a) shows the Avg-CL patterns (1,830 patterns) of the 30 days of September for one hour (from 12:00 to 13:00). The maximum and minimum Avg-CL patterns are detected, then, all the patterns that lie within them are divided into three equal parts horizontally. These parts represent three modes; mode 1, mode 2 and mode 3 indicate low Avg, moderate Avg, and high Avg, respectively. The patterns that lie in each mode are averaged to get a single representative Avg-CL pattern for each mode, as shown in Figure 3-6(c). Figure 3-6(c) is shown as a dotted line as it reflects a prepared table of representative values of Avg against each increment of CL.

Since predicting the actual pattern of Avg-CL for the next hours can be challenging, then by just acknowledging the behavior of PV power output for the next hour, the Avg-CL representative patterns of Figure 3-6(c) can be used instead of the actual patterns in Figure 3-6(a). After that, optimization will be operated using these Avg-CL representative patterns.

As shown in Figure 3-6(c), it is difficult to express the relation between Avg and CL by using a simple function. Therefore, as described below, the optimization problem is formulated with a mixed-integer linear programming (MILP) by preparing a look-up table regarding the relation between Avg and CL. Therefore, in Figure 3-6(c), plots showing the relation between Avg and CL are used instead of lines used in Figure 3-6 (a) and Figure 3-6 (b).

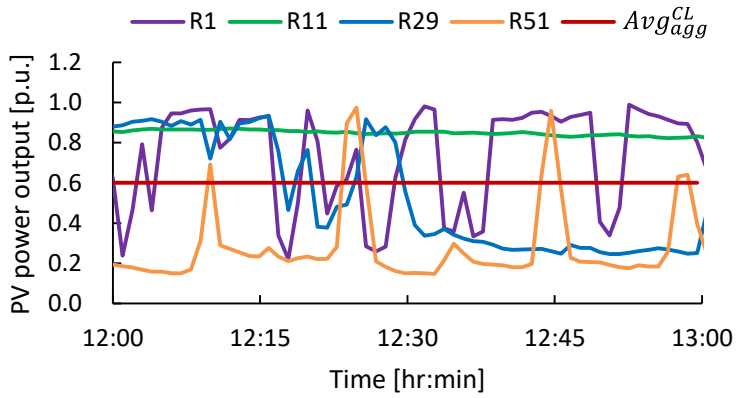

(a) Raw data

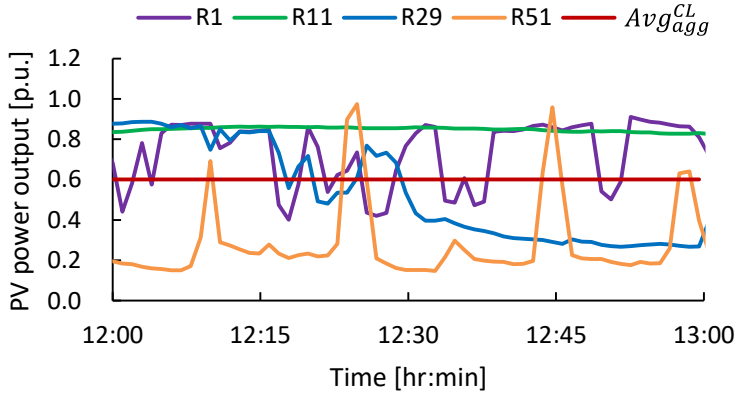

(b) LPF data

Figure 3-4 PV power output of the 4 regions on the 1st September

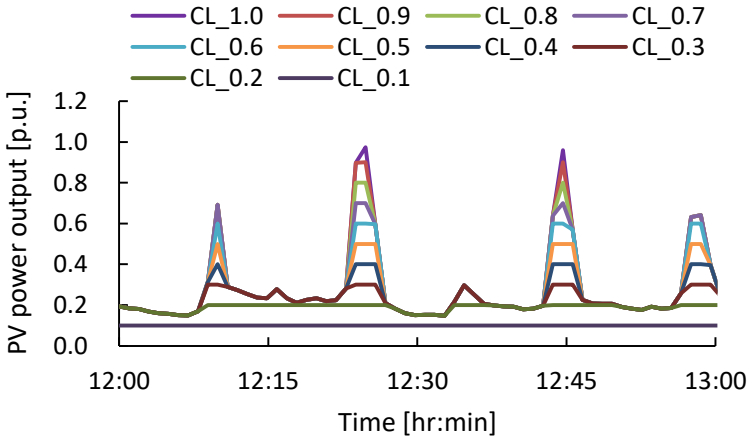

Figure 3-5 Different CL applied on R51 data on 1st September.

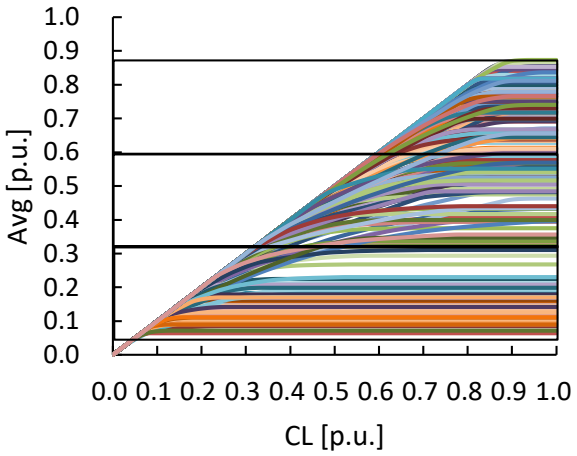

(a) The stacking of the actual patterns of the 61 regions for the entire month of September

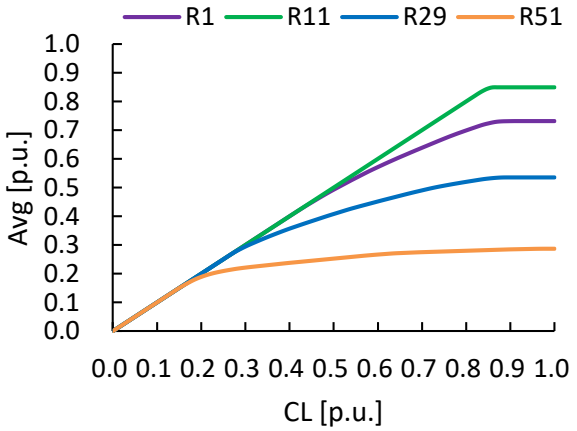

(b) The actual patterns of the four regions only on 1st September

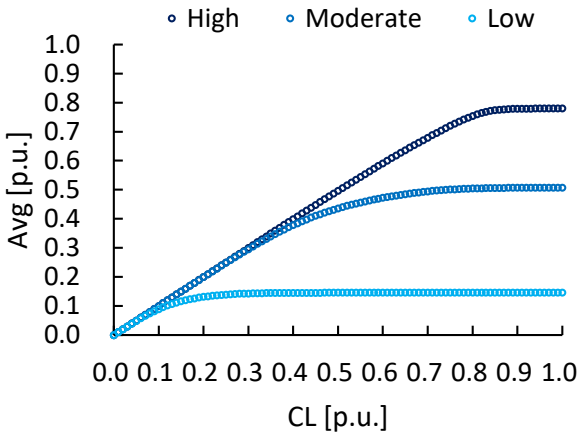

(c) The representative patterns used for 61 regions from 12:00 to 13:00 for the month of September

Figure 3-6 Avg-CL patterns.

3.4.2. Method-2

Step 1: Application of LPF to past measured PV power output time-series data.

The procedure in this step is the same as that in Method-1 described above.

Step 2: Application of different CL

The procedure in this step is the same as that in Method-1 described above.

Step 3: Application of high-pass filter (HPF) on every curtailed PV power output data.

HPF function with a cut-off frequency of 32 minutes is applied to the time-series data calculated in steps 1 and 2. This is implemented to highlight the fluctuations and hence, maximum fluctuation of the HPF data will be calculated in the next step. Figure 3-7 shows an example of the HPF data applied on the curtailed data of R51 on 1st September.

Step 4: Computation of MF_i^{CL} using the HPF data of each region based on a few parameters.

The MF is the difference between the maximum and minimum points of fluctuations calculated in 20-minute-moving-window, and this parameter represents the short-cycle fluctuation in the time-series data. It varies with days and is independent of the season, because the movement of clouds is the reason for the short-cycle fluctuations.

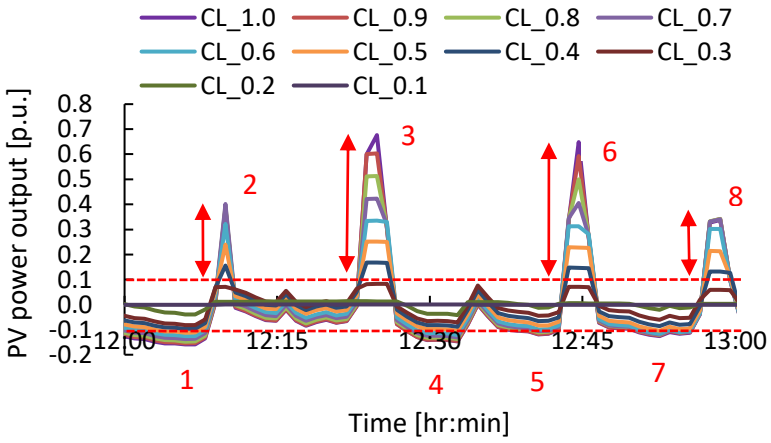

Figure 3-7 Application of HPF to different curtailed PV power data of R51 on 1st September

To consider whether a region's PV power output behavior is fluctuating or not, this study sets some parameters to distinguish the fluctuating behavior such as threshold, count and range. Firstly, the threshold is an initially assumed value of PV power output. When the fluctuations cross this value for a number of times (count) shown in Figure 3-7, they get recorded. In addition, the range is the sum of the heights of crossing fluctuations shown by the red arrows in Figure 3-7. Crossings can be frequent as it can be very short in terms of power changes, then the sum of the heights of crossings becomes a crucial parameter and it gets recorded instead. The total number of times the threshold is passed and the sum of heights of these crossings contain essential information to capture the fluctuations.

When the PV power output changes comply with the pre-set number of count and range, it is characterized as fluctuating. Consequently, MF_i^{CL} is calculated and plotted against each corresponding CL. When the threshold is 0.1 p.u., count is 3, and range is 0.1 p.u., the MF_i^{CL} for the 61 regions at every CL is plotted in Figure 3-8(a). The actual MF-CL patterns of the four regions on 1st September are shown separately in Figure 3-8(b).

Step 5: Formation of representative patterns of MF-CL.

The MF-CL patterns of the 61 regions for 30 days for one hour are stacked. Figure 3-8(a) shows the MF-CL patterns (1,830 patterns) of the 30 days of September for one hour (from 12:00 to 13:00). The maximum and minimum start of MF-CL patterns are detected, then, all the patterns that lie within them are divided into three equal parts vertically. These parts represent three modes; mode 1, mode 2, and mode 3 indicate low fluctuations, moderate fluctuations, and high fluctuations, respectively. While, mode 0 is representing regions with no fluctuations (uniform output). We average the patterns that lie in each mode to get a single representative MF-CL pattern for each mode as shown in Figure 3-8(c). Figure 3-8(c) is shown as a dotted line as it reflects a prepared table of representative values of MF against each increment of CL.

Since predicting the actual pattern of fluctuation for the next hours can be challenging, then by just acknowledging the characteristics of fluctuations for the next hour, the MF-CL representative pattern of Figure 3-8(c) can be used instead of the actual pattern in

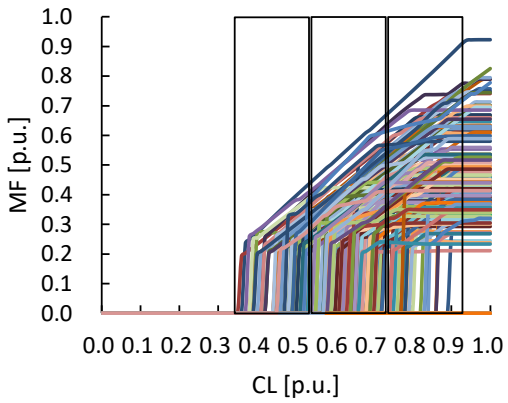

(a) The stacking of the actual patterns of the 61 regions for the entire month of September

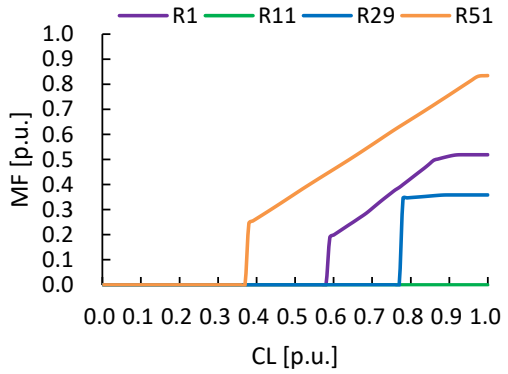

(b) The actual patterns of the four regions only on 1st September

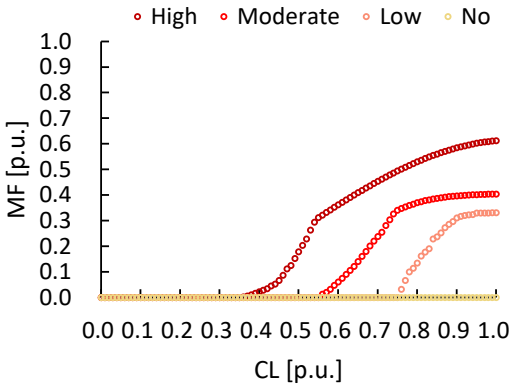

(c) The representative patterns used for 61 regions from 12:00 to 13:00 for the month of September

Figure 3-8 MF-CL patterns.

Figure 3-8(a). After that, optimization will be operated using these representative patterns. As mentioned below, the proposed optimization method is formulated with MILP in consideration of complicated relation between MF and CL. In Figure 3-8(c), therefore, plots are used instead of lines as in Figure 3-6(a) and Figure 3-8(a) due to the same reason for Figure 3-8(c) so as to show the discrete relation between MF and CL.

3.5. Application of CL adjustment methods in the actual operation period

3.5.1. Proposed CL adjustment methods

- **Method-1**

The distinctive representative Avg-CL patterns for each region are used for the actual operation period. Hence, the CL will be optimized among each region so that Avg_{agg}^{CL} equals to the predetermined average by the system operator. For practical application, discrete values of CL are applied as the values of Avg_i^{CL} and MF_i^{CL} corresponding to CL in Figure 3-6 (c) and Figure 3-8(c) are also discrete. The MILP problem is expressed in Eqs. (4) to (8) where the objective is to minimize the gap between the Avg_{pre} and resultant Avg_{agg}^{CL} per hour. Although any kinds of solver for MILP problem can be used, in this study, the optimization process is operated by MATLAB Intlinprog function.

$$\min \left| Avg_{pre} - Avg_{agg}^{CL} \right| \quad \textbf{(3.4)}$$

It is formulated into linear optimization equations

$$\min Avg_{pre} - Avg_{agg}^{CL} \quad \textbf{(3.5a)}$$

$$\min Avg_{agg}^{CL} - Avg_{pre} \quad \textbf{(3.5b)}$$

i.e. $$Avg_{pre} = constant \quad \textbf{(3.6)}$$

$$Avg_{agg}^{CL} = \sum_{i=1}^{61} \sum_{k=0}^{100} n_i^k \omega_i Avg_i^k \quad \textbf{(3.7)}$$

Subject to $$\sum_{k=0}^{100} n_i^k = 1, \qquad n_i^k \in \{0,1\} \quad \textbf{(3.8)}$$

In the proposed method, one of the Avg-CL pattern is selected based on the short-term forecasting of weather mode for each region *i*. Therefore, Avg_i^{CL}(*k* = 0 – 100) in (7) corresponds to individual plots of the selected Avg-CL pattern. The number of possible CL applied is referred to as *k* and there are 101 candidates ranging from 0 to 1.0 p.u. with an increment of 0.01 p.u. By using the constraint in (8), one of the *k* values is selected and hence Avg_i^{CL} is selected among the 101 candidates. In (7) and (8), *n* is a decision variable. The lower bound of *n* is 0 meaning that one of the possible CL is not selected and the upper bound is 1 meaning that one the possible CL is selected. At every iteration for each region, only one CL is chosen to be 1 leaving the other possible CL with 0. Hence, the sum of the decisions will always be 1.

For the four regions, R1, R11, R29 and R51, the short-term forecast of Avg-CL patterns from 12:00 to 13:00 on 1st September provides information that R1 and R11 have a high Avg, R29 has a moderate Avg and R51 has a low Avg. Hence, they are given the corresponding representative Avg-CL patterns that were prepared previously in Figure 3-6 (c).

As a result of the optimization assuming Avg_{pre} value of 0.5 p.u., Figure 3-9(a) shows CL allocated on the four regions where R1 and R11 of the high Avg had the highest CL while R29 and R51 of lower Avg had lower CL. The resultant Avg_{agg}^{CL} is 0.54 p.u. and it is close to the $Avg_{pre.}$

- **Method-2**

Both the distinctive patterns of MF-CL and Avg-CL for each region are used for the actual operation period, and the CL is optimized among each region. The optimization objective is to minimize the MF_{agg}^{CL} based on the different candidates of allocated CL as long as the Avg_{pre} is achieved. A buffer of 0.01 p.u. is added to the Avg_{pre} as CL are applied at an

increment of 0.01 p.u. In this step, the optimization problem is also a MILP problem and it is shown in (9) to (11) to minimize the MF_{agg}^{CL}. MF_{agg}^{CL} is expressed as the root mean square (RMS) of MF of each region per hour. The RMS value is used in this optimization as the MF_i^{CL} values are not dependent or coherent. Avg_{agg}^{CL} and Avg_{pre} are expressed previously in (6) and (7).

$$\min MF_{agg}^{CL} = \sqrt{\sum_{i=1}^{61}\sum_{k=0}^{100}(n_i^k \omega_i MF_i^k)^2} \quad \textbf{(3.9)}$$

Subject to

$$Avg_{agg}^{CL} = Avg_{pre} \pm 0.01 \quad \textbf{(3.10)}$$

$$\sum_{k=0}^{100} n_i^k = 1, \qquad n_i^k \in \{0,1\} \quad \textbf{(3.11)}$$

In the same manner with Avg-CL pattern, one of the MF-CL pattern is selected based on the short-term forecasting of weather mode for each region *i*. Then, MF_i^k (k = 0 – 100) in (9) corresponds to individual plots of the selected MF-CL pattern. By using the constraint in (11), one of the k value is selected and hence MF_i^k is optimally selected among the 101 candidates.

For the four regions, R1, R11, R29, and R51, the short-term forecast of fluctuations from 12:00 to 13:00 on 1st September provides information that R5 has high MF, R1 has moderate MF, R29 has low MF and R11 has no MF. Hence, they are given the corresponding representative MF-CL patterns that were prepared previously and their patterns are shown in Figure 3-8(c).

As a result of the optimization in the case where Avg_{pre} is equal to 0.5 p.u., CL allocated on the four regions are as shown in Figure 3-9(b); where R11 of the no MF had the highest CL; R51 of highest MF had a lower CL. The resultant Avg_{agg}^{CL} is 0.53 p.u. and it is close to the Avg_{pre}.

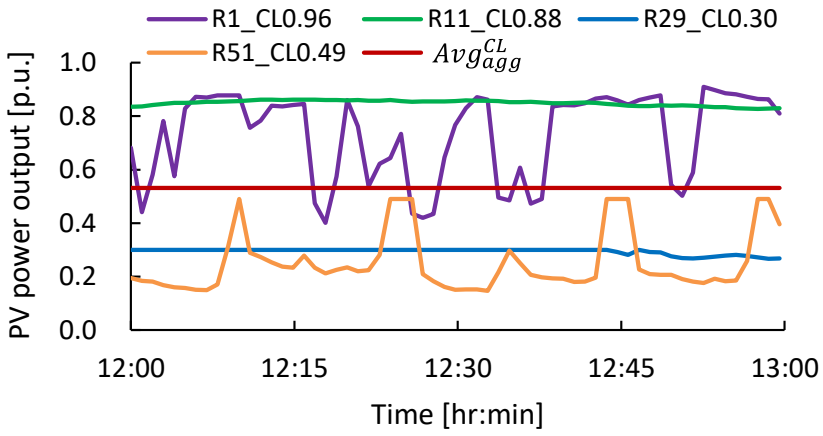

(a) Method-1

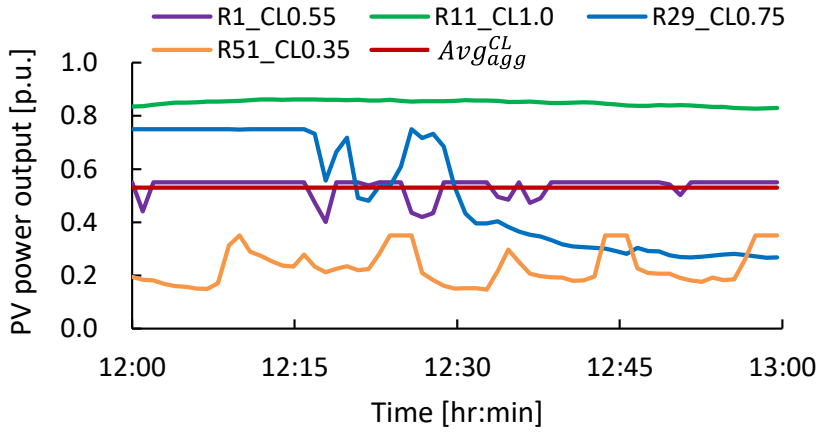

(b) Method-2

Figure 3-9 Application of the proposed CL adjustment methods.

3.5.2. Comparative CL setting methods

- **Method-3**

This method allocates the same CL to each region for the actual operation period. For the four regions, R1, R11, R29, and R51, from 12:00 to 13:00 on 1st September, when the Avg_{pre} is 0.5 p.u., the result is as shown in Figure 3-10(a). The same CL led to a resultant Avg_{agg}^{CL} of 0.41 p.u. lower than Avg_{pre}, this is because, except for R11, the available output is below 0.5 p.u.

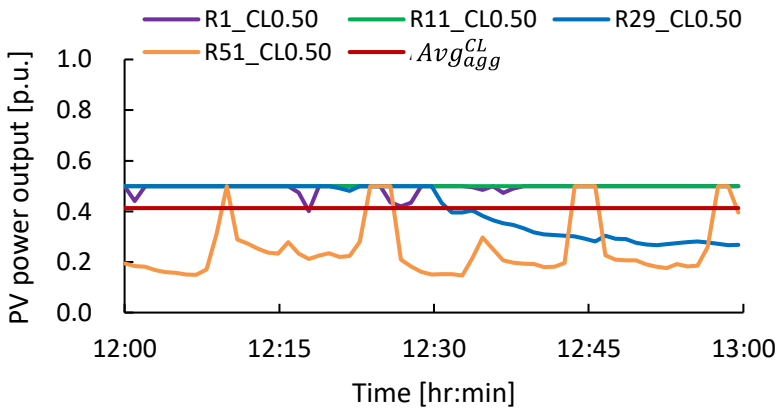

(a) Method-3

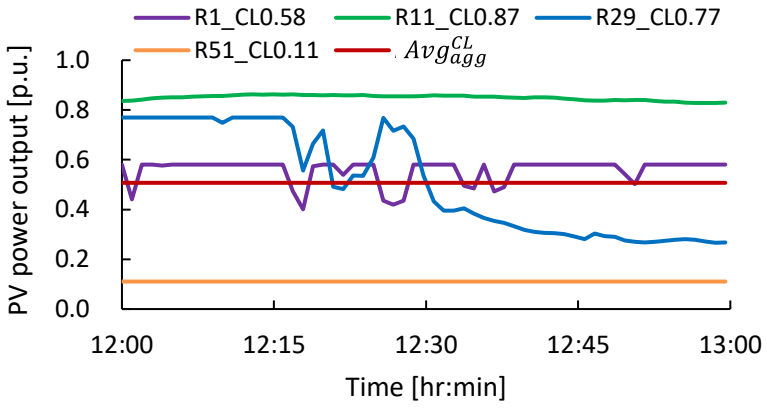

(b) Method-4

Figure 3-10 Application of the comparative methods.

- **Method-4**

The CL allocation is carried out perfectly using the actual patterns of MF-CL and Avg-CL for the actual operation period. For the four regions, R1, R11, R29, R51, from 12:00 to 13:00 on 1st September, the actual patterns of Avg-CL and MF-CL as shown in Figure 3-6(b) and Figure 3-8(b) are used for optimization. The result is shown in Figure 3-10(b). The resultant Avg_{agg}^{CL} is 0.51 p.u. and it is extremely close to the Avg_{pre}.

3.5.3. Comparison of all methods for the sample day

The time-series of curtailed PV power output on 1st September in the four regions were shown above for method-0 to method-4. The resultant Avg_{agg}^{CL} and MF_{agg}^{CL} of each method are plotted in Figure 3-11. This gives a general overview on the differences between each method prior to the demonstration of the results of the 61 regions. The summary of the results when the target Avg_{pre} is 0.5 p.u. is as follows:

- Method-0 has the highest deviation from Avg_{agg}^{CL} and the highest MF_{agg}^{CL}. That is when no curtailment is applied at high PV power output, the resultant Avg_{agg}^{CL} deviated from the target Avg_{pre} and fluctuations were not suppressed.
- Method-1 has a very low deviation from Avg_{agg}^{CL} and lower MF_{agg}^{CL} than Method-0. This proposed method focused mainly on reducing the gap between the resultant Avg_{agg}^{CL} and Avg_{pre} along with that fluctuations were reduced.
- Method-2 has a sufficiently low deviation from Avg_{agg}^{CL} and very low MF_{agg}^{CL} that is very close to the ideal Method-4. This proposed method focused on reducing the fluctuations as well as the gap between the resultant Avg_{agg}^{CL} and Avg_{pre}.
- Method-3 has a very high deviation from Avg_{agg}^{CL} and very low MF_{agg}^{CL}. When severe curtailment suppressed the fluctuations, the resultant Avg_{agg}^{CL} majorly deviated from the target Avg_{pre}.
- Method-4 is the closest to Avg_{agg}^{CL} and it has the lowest MF_{agg}^{CL}. Due to the perfect short-term forecasting, the CL was precisely allocated to reduce the fluctuations and achieve the closest resultant Avg_{agg}^{CL} to Avg_{pre}. Despite the perfect forecast used in Method-4, a deviation is witnessed between the resultant Avg_{agg}^{CL} and the Avg_{pre}. This is because CL applied in this method have an increment of 0.01 p.u. and the actual

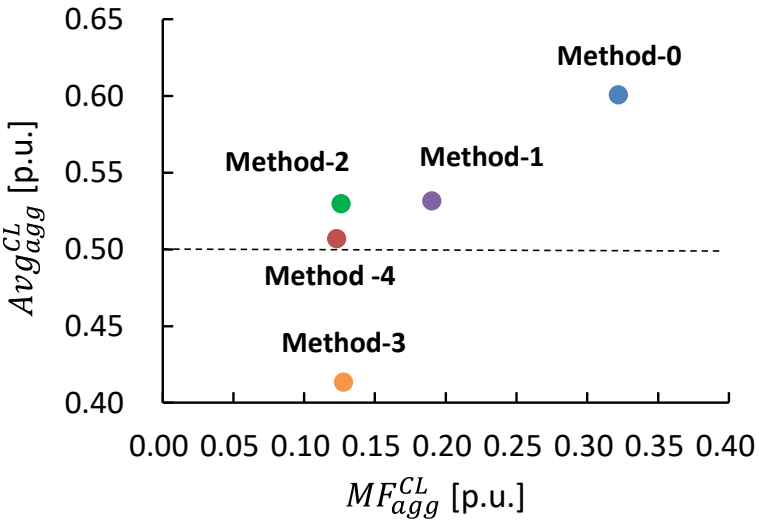

Figure 3-11 MF_{agg}^{CL}- Avg_{agg}^{CL} of all the CL adjustment methods.

patterns of MF-CL and Avg-CL are plotted based on this incremental value. To achieve less deviation, less incremental value can be utilized, however, the assumed value of 0.01 p.u. proved to be effective in forming reasonable MF-CL and Avg-CL patterns.

3.6. Case study of CL adjustment using 61 regions in central Japan

In the practical operation, requested Avg_{pre} is set based on the load forecasting for each hour of the next day. In this study, we directly assume different levels of requested Avg_{pre} that indirectly reflects various levels of electricity demand that has to be met by the Avg_{pre} and other generation resources. Thus, we test the effectiveness of the proposed methods at different levels of Avg_{pre} without necessarily deducing the exact electricity demand levels.

In Japan, the four common weather seasons exist, and September is considered to be in the autumn season. The autumn season tends to have many semi-cloudy days, i.e. fluctuating PV power output days. All the methods are applied on all the regions of all days of September at one hour from 12:00 to 13:00. In the proposed method, Avg-CL and MF-CL patterns are prepared for each hour in every month, accordingly for each hour under investigation, the prepared Avg-CL and MF-CL patterns will be used in the operation period. Therefore, for 12:00 to 13:00 in the entire days of September, the previously

prepared patterns in Figure 3-6(c) and Figure 3-8(c) will be used. The resulting MF_{agg}^{CL} and Avg_{agg}^{CL} for all the methods are plotted in Figure 3-12 at different Avg_{pre} such as 0.7 p.u., 0.5 p.u., and 0.3 p.u.

It is noted that at some data points such as the 12th Sep and 13th Sep, Method-1, Method-2 and Method-4 results are similar to that of Method-0. That happens when the Avg_{agg}^{CL} before CL application is lower than the Avg_{pre}, meaning that there is no adequate PV power output to reach the Avg_{pre} requested in advance. Accordingly, the methods used for adjusting CL in short-term such as Method-1, Method-2 and Method-4 will not be required in such cases, and their output will be similar to Method-0. However, Method-3 where the CL application determined a day-ahead can still apply. Hence, Method-3 seems to be performing the best as it has the lowest MF, however, due to its severe curtailment resultant Avg_{agg}^{CL} becomes the furthest. Apart from these cases, Method-4 is shown to perform that best on days where the short-term CL adjustment is needed.

For the MF_{agg}^{CL} data in Figure 3-12, Method-3 mostly has the lowest MF_{agg}^{CL} due to the severe CL applied, while the MF_{agg}^{CL} of Method-0 without CL is always the highest. The MF_{agg}^{CL} of the proposed Method-2 is almost overlapping the ideal Method-4 trends, which proves that Method-2 can replace the usage of Method-4 which is based on challenging perfect forecasting. While, the proposed Method-1 is constantly lower than Method-0, the proposed Method-2 is closer to the ideal Method-4. Since September days are mostly fluctuating, Method-2 suppresses fluctuations along with maintaining the requested Avg_{pre}. Method-1 is less effective than Method-2 at higher Avg_{pre} however, the overall MF_{agg}^{CL} is decreased as the Avg_{pre} decreases from 0.7 p.u. to 0.3 p.u.

For the Avg_{agg}^{CL} data in Figure 3-12, while the ideal Method-4 always has the closest resultant Avg_{agg}^{CL} to the Avg_{pre}, the least deviation in the other methods is found to be by the proposed methods. The lowest Avg_{agg}^{CL} is Method-3 due to the severe CL applied. As the Avg_{pre} decreases from 0.7 p.u. to 0.3 p.u., the resultant Avg_{agg}^{CL} of all methods except Method-0 are having less deviation from the ideal Method-4.

The proposed methods are evaluated by the difference between the Avg_{agg}^{CL} of the CL adjustment methods respectively and the ideal Method-4 ($\triangle Avg_{agg}^{CL}$). $\triangle Avg_{agg}^{CL}$ is plotted against the difference between the MF of the CL adjustment methods respectively and the ideal Method-4 ($\triangle MF_{agg}^{CL}$) in Figure 3-13, Figure 3-14 and Figure 3-15 for Avg_{pre} of 0.7 p.u., 0.5 p.u., and 0.3 p.u., respectively. The data points in the figures show the relationship between $\triangle Avg_{agg}^{CL}$ and $\triangle MF_{agg}^{CL}$ for the one hour from 12:00 to 13:00 in the entire year in all the regions. It is noted that more data points are found as the Avg_{agg}^{CL} decreases from 0.7 p.u. to 0.3 p.u. This is because the proposed methods are not required when the reliable output before the curtailment is lower than the Avg_{pre}. Generally, Method-1 has a slightly right-leaning horizontal distribution. This means that Method-1 does not suppress the MF as the ideal Method-4. Method-2 has a distribution centered at the origin, which indicated a small deviation between the proposed method-2 and the ideal Method-4 in terms of both Avg_{agg}^{CL} and MF_{agg}^{CL}. Method-3 has longitudinal distribution, which means that the application of equal CL to all the regions majorly deviates the Avg_{agg}^{CL} from Avg_{pre}.

Therefore, Figure 3-13, Figure 3-14 and Figure 3-15 indicate that Method-2 can reduce the fluctuations and be close to the ideal Method-4. While centralized data points of Method-1 represent the less fluctuating days that do not necessarily need the operation of Method-2. In Figure 3-13, Figure 3-14 and Figure 3-15, as the Avg_{pre} decreases from 0.7 p.u. to 0.3 p.u., the data points of the proposed methods, Method-1 and Method-2, become concentrated on a horizontal ellipse centered around the origin because more severe CL is applied. Hence, less MF_{agg}^{CL} is expected and the requested Avg_{pre} is easily reached.

Figure 3-16 gives an overview on the resulting $\triangle MF_{agg}^{CL}$ and $\triangle Avg_{agg}^{CL}$ of each method respectively against the changing Avg_{pre} using the entire data points of the year. Figure 3-16 is also used a collective representation of Figure 3-13, Figure 3-14 and Figure 3-15 including additional results at different Avg_{pre} values. Figure 3-16(a) reflects the ratio of the data points that lie within $|\triangle MF_{agg}^{CL}|$ of 0.01 p.u. and the total data points at a certain Avg_{pre} (MF_{agg}^{CL} ratio). Figure 3-16(b) reflects the ratio of the data points that lie within $|\triangle Avg_{agg}^{CL}|$ of 0.04 p.u. and the total data points at a certain Avg_{pre} (Avg_{agg}^{CL} ratio).

As the trends of the resulting MF_{agg}^{CL} and Avg_{agg}^{CL} ratios of any method approach 1, it implies that this method is close to ideal Method-4 output. The trends in Figure 3-16(a) show that Method-2 is the most efficient at reducing the MF_{agg}^{CL} at any Avg_{pre}. Method-3 shows its efficiency at reducing MF_{agg}^{CL} as the Avg_{pre} decreases, i.e. when severe CL is applied, MF_{agg}^{CL} is reduced drastically. Method-1 is mostly deviated from ideal Method-4 at every Avg_{pre} as reduction of MF_{agg}^{CL} is the least priority of this method and it works the best in non-fluctuating days. The trends in Figure 3-16(b) show that Method-1 and Method-2 are the most effective in meeting the target Avg_{pre} at the medium and low Avg_{pre}. In addition, Method-3 has the most deviation from ideal Method-4, however, this deviation reduces as Avg_{pre} decreases, making this method more feasible at low Avg_{pre}.

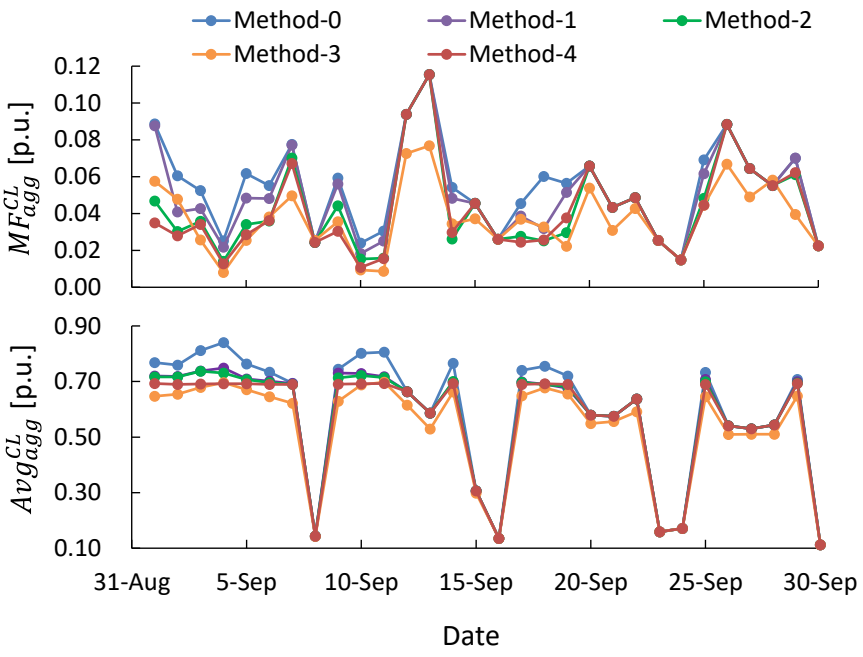

(a) At Avg_{pre} 0.7 p.u.

Figure 3-12 Comparison between all the methods from 12:00 to 13:00 for the 30 days of September 2010.

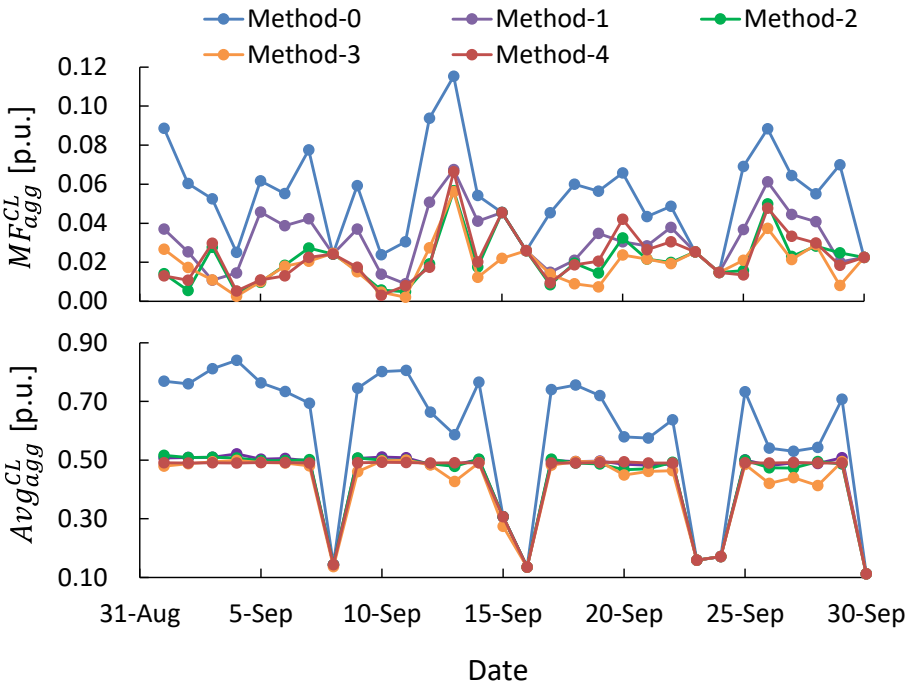

(b) At Avg_{pre} 0.5 p.u.

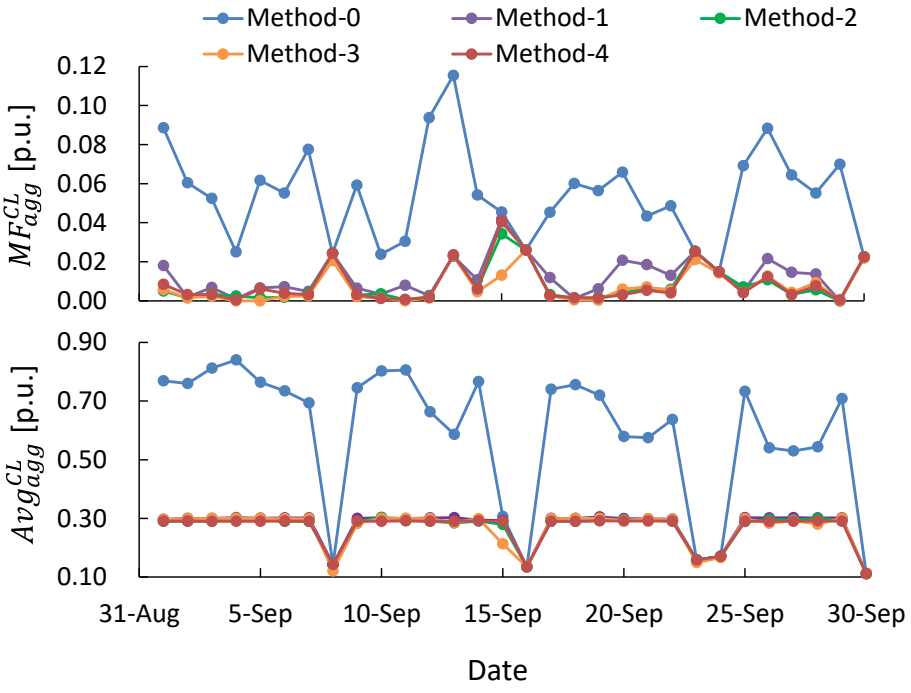

(c) At Avg_{pre} 0.3 p.u.

Figure 3-12 Comparison between all the methods from 12:00 to 13:00 for the 30 days of September 2010.

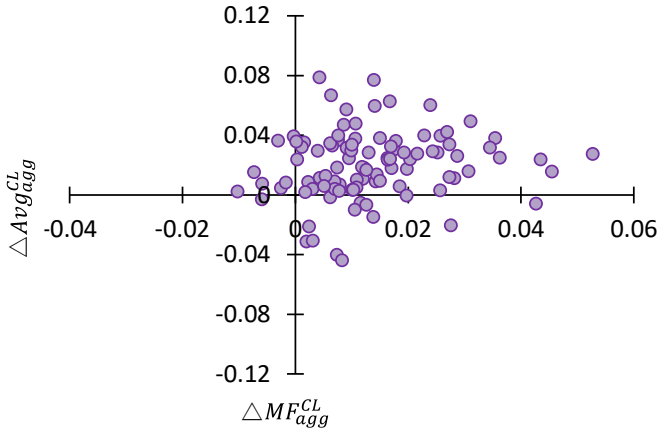

(a) Method-1 and Method-4

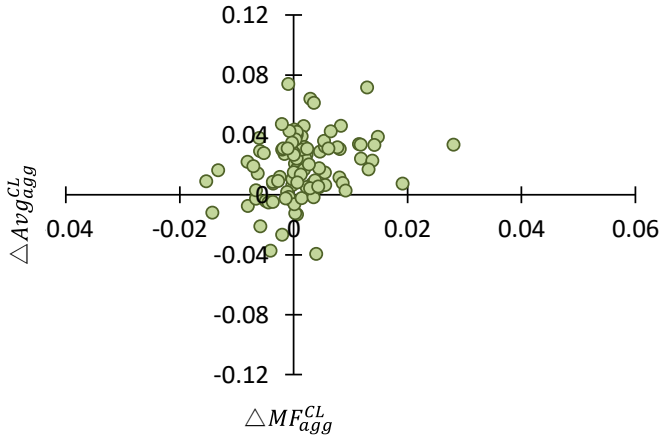

(b) Method-2 and Method-4

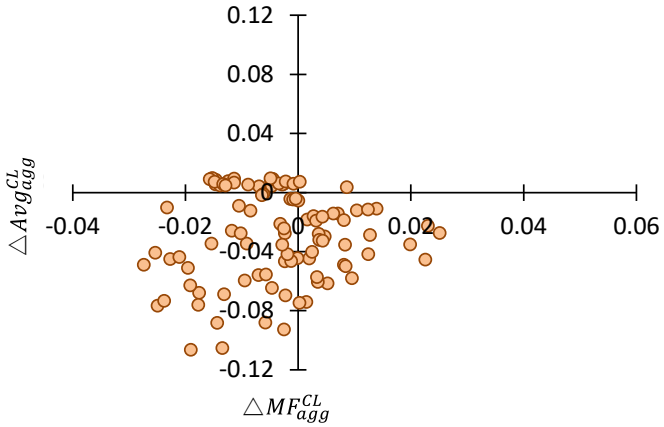

(c) Method-3 and Method-4

Figure 3-13 Comparison between CL adjustment methods at Avg_{pre} 0.7 p.u. from 12:00 to 13:00 in one year.

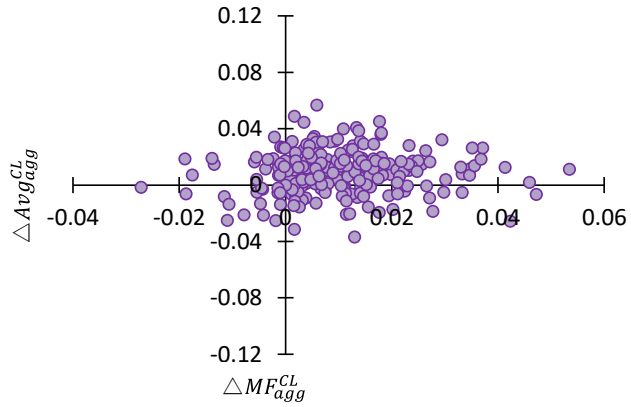

(a) Method-1 and Method-4

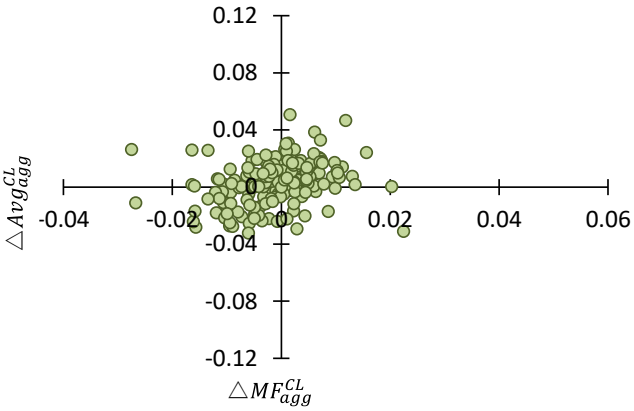

(b) Method-2 and Method-4

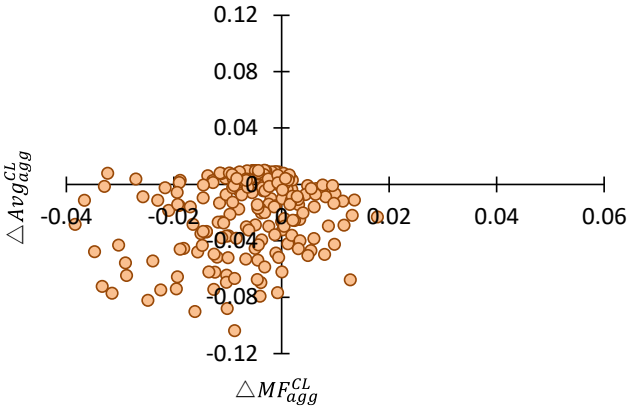

(c) Method-3 and Method-4

Figure 3-14 Comparison between CL adjustment methods at Avg_{pre} 0.5 p.u. from 12:00 to 13:00 in one year.

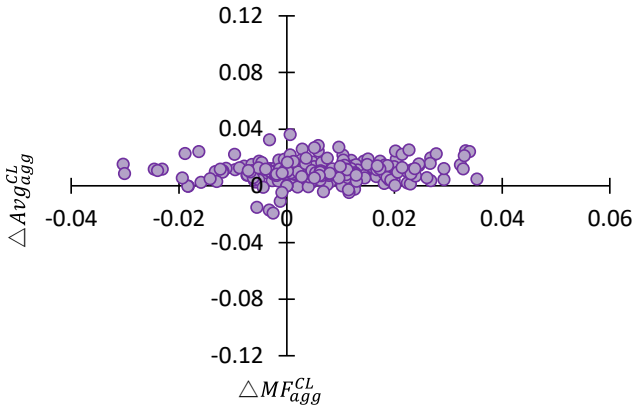

(a) Method-1 and Method-4

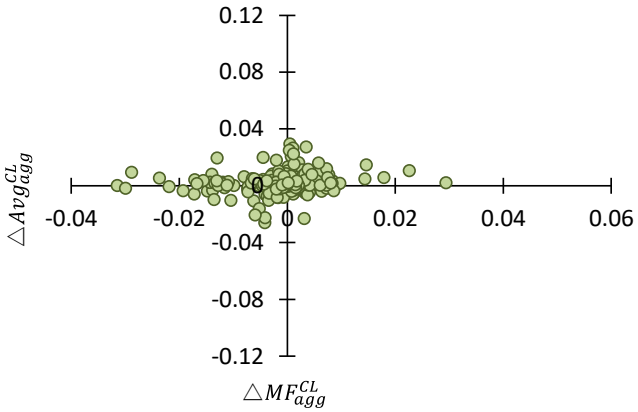

(b) Method-2 and Method-4

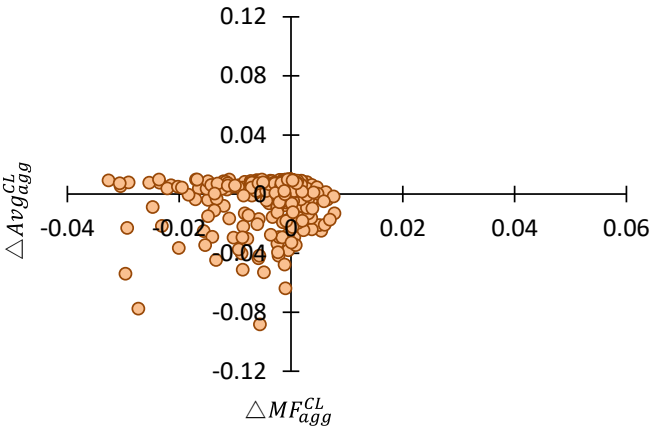

(c) Method-3 and Method-4

Figure 3-15 Comparison between CL adjustment methods at Avg_{pre} 0.3 p.u. from 12:00 to 13:00 in one year.

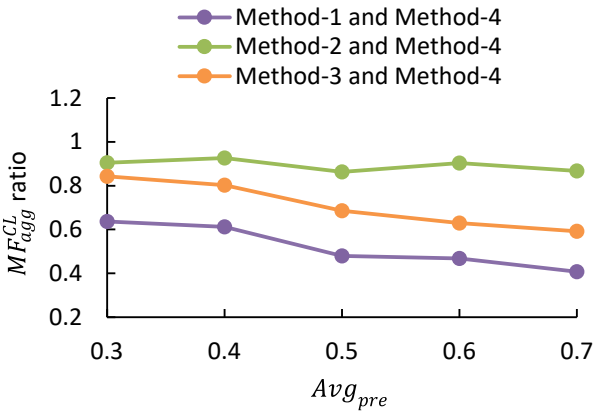

(a) MF_{agg}^{CL} ratio

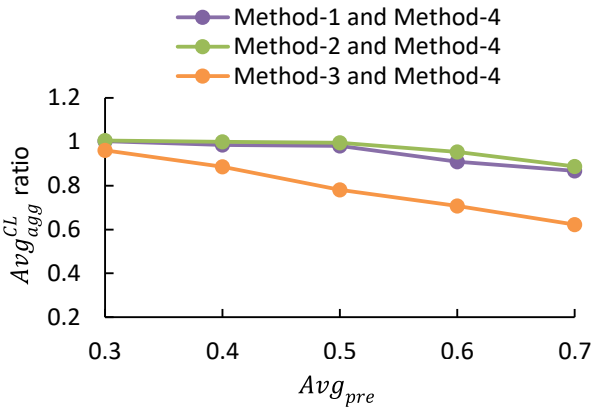

(b) Avg_{agg}^{CL} ratio

Figure 3-16 Ratio of the data points of the resultant $\triangle MF_{agg}^{CL}$ and $\triangle Avg_{agg}^{CL}$ within a certain threshold, respectively, to the total data points at every Avg_{pre}.

3.7. Conclusion

This study proposes methods for the optimal short-term allocation of CL among each region. The allocation of the CL is based on the short-term forecasting of the fluctuation mode of individual PV power output. The proposed method can also reduce the fluctuations in aggregated PV power output.

The proposed method employs two functions, i.e. the relationship between CL and MF, and between CL and Avg prepared for typical fluctuation modes based on statistical data of past PV irradiance observations. Accordingly, the optimal CL is allocated to minimize the fluctuations in aggregated PV power output by merely identifying the region's MF and average modes instead of precisely observing the short-term time-series PV power output.

The proposed methods were tested using the time-series of PV power output at 61 observation points in the central region of Japan for one year. The main results are as follows:

- The proposed methods resulted in optimal CL allocation that majorly reduced MF_{agg}^{CL} and targeted the requested PV output by the operator Avg_{pre}. This will reduce the fluctuations of aggregated PV power output, which contributes to the reduction of the requirement of frequency regulation and required CL of aggregated PV power output itself.
- The results of the proposed methods were found to be almost as effective as the method using perfect short-term forecasting of PV power output. This has been shown through the calculation of the deviation of the proposed methods from the ideal Method-4 and the gaps are manifested to lie within $|\triangle MF_{agg}^{CL}|$ of 0.01 p.u and $|\triangle Avg_{agg}^{CL}|$ of 0.04 p.u.
- The proposed methods becomes functional when there are regions with different modes of power output ranging from fluctuating to non-fluctuating, and high average to low average regions meaning that different modes of MF-CL and Avg-CL are utilized for optimizing the CL allocation. However, for days with similar modes among different regions, for instance in summer days with high and uniform power output, the same CL application in Method-3 can be sufficient.

Additional study can be conducted to use statistical data for creating more classifications of MF-CL and Avg-CL patterns to reflect more different PV power output behaviors, hence, providing highly accurate CL allocation. Also, by enhancing the short-term forecasting accuracy, more specific MF-CL and Avg-CL patterns can be chosen among the various patterns available.

Another issue which is the interconnection between PV power curtailment and grid congestion can be a potential issue that can be investigated in future work. As congestion management can impact PV power curtailment when transmission capacity is limited. Curtailment of some PV systems will then be required to avoid overloading transmission lines.

References

[1] L. Montero, A. Bello, and J. Reneses, “A Review on the unit commitment problem: approaches, techniques, and resolution methods,” in *Energies*, vol. 15, no. 4, p. 1296, Feb. 2022.

[2] H. Sangrody, N. Zhou and Z. Zhang, “Similarity-Based Models for Day-Ahead PV PV Generation Forecasting,” in *IEEE Access*, vol. 8, pp. 104469–104478, Jun. 2020.

[3] B. Lu and M. Shahidehpour, “Unit commitment with flexible generating units,” in *IEEE Transactions on Power Systems*, vol. 20, no. 2, pp. 1022–1034, May 2005.

[4] Udagawa et al., “Analysis of photovoltaic power yield curtailment in day-ahead unit commitment,” in *IEEJ Transactions on Power and Energy*, pp. 520–529, Jul. 2017.

[5] T. Masuta et al., “Evaluation of unit commitment based on intraday few-hours-ahead photovoltaic generation forecasts to reduce the supply-demand imbalance,” in the *Proceedings of the 8th International Renewable Energy Congress (IREC)*, 2017, pp. 1–5.

[6] U. K. Das et al., “Forecasting of photovoltaic power generation and model optimization: A review,” in *Renewable and Sustainable Energy Reviews*, vol. 81, pp. 912–928, Jan. 2018.

[7] L. Gigoni et al., “Day-ahead hourly forecasting of power generation from photovoltaic plants,” in *IEEE Transactions on Sustainable Energy*, vol. 9, no. 2, pp. 831–842, Apr. 2018.

[8] E. Lorenz et al., “Irradiance forecasting for the power prediction of grid-connected photovoltaic systems,” in *IEEE Journal of Selected Topics in Applied Earth Observations and Remote Sensing*, vol. 2, no. 1, pp. 2–10, Mar. 2009.

[9] J. H. Kim et al., “The WRF-PV ensemble prediction system to provide PV irradiance probabilistic forecasts,” in *IEEE Journal of Photovoltaics*, vol. 12, no. 1, pp. 141–144, Jan. 2022.

[10] J. Shi et al., “Forecasting power output of photovoltaic systems based on weather classification and support vector machines,” in *IEEE Transactions on Industry Applications*, vol. 48, no. 3, pp. 1064–1069, Jun. 2012.

[11] H. -T. Yang et al., “A weather-based hybrid method for 1-Day ahead hourly forecasting of PV power output,” in *IEEE Transactions on Sustainable Energy*, vol. 5, no. 3, pp. 917–926, Jul. 2014.

[12] I. Kaaya, and J. Ascencio-Vásquez, “Photovoltaic power forecasting methods,” in PV Radiation - Measurement, Modeling and Forecasting Techniques for Photovoltaic PV Energy Applications. London, United Kingdom, Intech Open, Apr. 2021. [Online]. Available: https://www.intechopen.com/chapters/76055

[13] W. Hu, X. Zhang, L. Zhu and Z. Li, “Short-term photovoltaic power prediction based on similar days and improved SOA-DBN model,” in *IEEE Access*, vol. 9, pp. 1958–1971, Dec. 2021.

[14] J. Yan et al., “Frequency-domain decomposition and deep learning based PV PV power ultra-short-term forecasting model,” in *IEEE Transactions on Industry Applications*, vol. 57, no. 4, pp. 3282–3295, Aug. 2021.

[15] Z. Zhen et al., “Deep learning based surface irradiance mapping model for PV PV power forecasting using sky image,” in *IEEE Transactions on Industry Applications*, vol. 56, no. 4, pp. 3385–3396, Aug. 2020.

[16] M. S. Hossain and H. Mahmood, “Short-term photovoltaic power forecasting using an LSTM neural network and synthetic weather forecast,” in *IEEE Access*, vol. 8, pp. 172524–172533, Sep. 2020.

[17] C. -J. Huang and P. -H. Kuo, “Multiple-input deep convolutional neural network model for short-term photovoltaic power forecasting,” in *IEEE Access*, vol. 7, pp. 74822–74834, Jun. 2019.

[18] B. D. Dimd, S. Völler, U. Cali and O. -M. Midtgård, “A review of machine learning-based photovoltaic output power forecasting: Nordic context,” in *IEEE Access*, vol. 10, pp. 26404–26425, Mar. 2022.

[19] T. Kato et al., “Modelling of aggregated power output of photovoltaic power generation in consideration of smoothing effect of power output fluctuation around observation point,” in *Renewable Energy and Power Quality Journal*, vol. 1, pp. 456-461, Apr. 2018.

4. Conclusion and future work

4.1. Conclusion

4.1.1. Autonomous dual active power-frequency control in power system with small-scale photovoltaic power generation

In order to realize a carbon neutrality by 2050, Japanese government has set targets to achieve a substantial increase in renewable energy capacity by 2030, encouraging the development of renewable projects and the deployment of advanced technologies. As PV will be most dominant renewable energy source, it is expected to provide ancillary services in the power system to support the grid frequency

To improve the contribution of high penetration of PV systems to the grid frequency regulation, it would be more effective to perform a combination of different control schemes in a single PV-based control synthesis problem. The PV system can contribute to the power system by firstly, to mitigate frequent fluctuations of load or generation disturbances and secondly, to suppress frequency deviations in contingencies.

As the number of small-scale PV systems are increasing in the future, they can provide ancillary services to support the grid frequency as contributing to the normal and emergency operations in a power system. To create a simple and autonomous active power control for these small-scale PV systems, an active power control based on a dual power-frequency (*p–f*) droop control is proposed which is capable of changing the droop characteristics depending on the magnitude of frequency change. Two simple control methods (Method-1 and Method-2) of dual *p-f* droop control are designed to achieve a smooth transition between slow to fast responses according to the change in frequency.

Method-1 is an enhanced design of dual *p-f* droop control where besides the simple turning on one frequency control while turning off the other, as the frequency deviation changes, it has an additional control such as transition signal as well as switching of

frequency thresholds. However, Method-2 provides a complementary simpler idea to improve the operation of fast-frequency and slow-frequency controls, i.e. both frequency controls can operate simultaneously.

Two simulation models were conducted to highlight the importance of slow and fast responses of both methods. The first simulation test highlights the importance of slow-frequency response in mitigating the normal frequency fluctuations over a period of time. Whereas the second test shows the influence of fast response in both methods in the case of a dropout of one generator in the system.

The results revealed that the slow and fast frequency controls can work in coherence. As for Method-1, the fast frequency control enabled the mitigation of the frequency deviations that violated the frequency threshold in a quick manner. However, during the recovery of frequency, this method was effective in leading a smooth recovery due to the introduction of the transition signal and the switching of the thresholds. Whereas, Method-2 of dual *p-f* droop control that was anticipated to have a delay of reaction to the frequency violation, proved that that delay was insignificant in the simulation tests. It also provided smoother transitions than Method-1 from slow to fast controls in the recovery phase. That proves that Method-2 outperforms Method-1 in its simplicity as the main purpose of this study is creating the simplest version of dual *p-f* droop control.

4.1.2. Optimal allocation of curtailment levels of PV power output in different regions in consideration of reduction of aggregated fluctuations

The contribution of PV system to the grid frequency regulation is based on the curtailed power output operation of PV system. The curtailment level (CL) of the aggregated PV power output is determined in a day-ahead UC scheduling of required generation resources based on a day-ahead forecast of electricity demand and various renewable power generation. Currently, in the actual application of PV power output curtailment in Japan, the CL of the aggregated PV power output is determined regardless of the distinctive fluctuating behavior of each region in the power system service area. However, different

CL among each region should be applied to reduce the fluctuations in the aggregated PV power output. This will contribute to maintaining the frequency variations within the acceptable ranges determined by the grid codes, reducing the requirement of frequency regulation.

On the other hand, the forecasting of time-series change in PV power output still remains challenging with a considerable amount of error even though machine learning algorithms and other advanced modeling techniques are used. However, the fluctuation characteristics such as fluctuation range can be practically feasible. If available, the forecasted fluctuation characteristics of each region can be used to allocate optimal CL value for each region. Depending on the number of regions to which the optimal CL value is allocated, the allocation process can still be time-consuming, and needs a sophisticated but practically feasible approach.

Therefore, the main objective of this study is to propose methods for the optimal short-term allocation of CL among each region. The allocation of the CL is based on the short-term forecasting of the fluctuation mode of individual PV power output. The proposed method can also reduce the fluctuations in aggregated PV power output.

The proposed method employs two functions, i.e. the relationship between CL and MF, and between CL and Avg prepared for typical fluctuation modes based on statistical data of past PV irradiance observations. Accordingly, the optimal CL is allocated to minimize the fluctuations in aggregated PV power output by merely identifying the region's MF and average modes instead of precisely observing the short-term time-series PV power output.

The proposed methods were tested using the time-series of PV power output at 61 observation points in the central region of Japan for one year. The main results are as follows:

- The proposed methods resulted in optimal CL allocation that majorly reduced MF_{agg}^{CL} and targeted the requested PV output by the operator Avg_{pre}. This will reduce the fluctuations of aggregated PV power output, which contributes to the reduction of the

requirement of frequency regulation and required CL of aggregated PV power output itself.

- The results of the proposed methods were found to be almost as effective as the method using perfect short-term forecasting of PV power output. This has been shown through the calculation of the deviation of the proposed methods from the ideal Method-4 and the gaps are manifested to lie within $|\Delta MF_{agg}^{CL}|$ of 0.01 p.u and $|\Delta Avg_{agg}^{CL}|$ of 0.04 p.u.
- The proposed methods becomes functional when there are regions with different modes of power output ranging from fluctuating to non-fluctuating, and high average to low average regions meaning that different modes of MF-CL and Avg-CL are utilized for optimizing the CL allocation. However, for days with similar modes among different regions, for instance in summer days with high and uniform power output, the same CL application in Method-3 can be sufficient.

4.2. Practical Aspects of the Proposed Ideas

4.2.1. Autonomous dual active power-frequency control in power system with small-scale photovoltaic power generation

The deployment of smart inverters with droop control has significant impacts on both the practical and business aspects of the energy sector. Here are some key implications:

- **Practical Impact**
  - Grid Stability: Smart inverters with dual *p-f* droop control help maintain grid frequency, ensuring a balanced distribution of power and reducing fluctuations.
  - Enhanced Grid Resilience: The increased number of small-scale PV systems can provide ancillary services such as regulating the grid frequency through a simple and autonomous control.
- **Business Impact**
  - Ancillary Services: Smart inverters with dual *p-f* droop control can provide ancillary services, such as frequency regulation, creating new revenue streams

for distributed energy resource owners.

- Grid Services Market: The participation of smart inverters in grid services markets opens up opportunities for energy resource owners to monetize their grid support capabilities.
- Business Models: The adoption of smart inverters may drive changes in business models, encouraging the growth of energy service providers that offer aggregated control and optimization of distributed energy resources.
- Regulatory Adjustments: Regulatory frameworks may need to be adjusted to accommodate the functionalities of smart inverters and ensure fair compensation for grid services.

In summary, the deployment of smart inverters with droop control brings practical benefits such as grid stability and enhanced grid resilience. On the business side, it creates opportunities for revenue generation through ancillary services and participation in grid services markets, while also driving changes in business models and necessitating regulatory adjustments. Overall, these advancements contribute to a more reliable, flexible, and sustainable energy system in both the practical and business realms.

4.2.2. Optimal allocation of curtailment levels of PV power output in different regions in consideration of reduction of aggregated fluctuations

The optimized curtailment of PV power, which refers to intentionally reducing or limiting the power output of PV systems, can have several impacts on the business and practical world in the context of the energy sector. Here are some key implications:

- **Practical Impact**
  - Grid Flexibility: Effective curtailment of PV power facilitates better integration of renewable energy into the grid. By strategically managing PV generation, grid operators can accommodate a higher penetration of PV power without compromising grid stability and operational efficiency.

- System Balancing: Curtailing PV power allows for better coordination between intermittent renewable sources and other controllable generation or energy storage systems. This enables a more reliable and balanced power supply, reducing reliance on conventional power sources.

- **Cost Optimization and Revenue Management**
  - Grid Management Efficiency: Curtailment strategies can help optimize grid management and reduce operational costs. By curbing PV power during periods of low demand or grid congestion, utilities can avoid or delay expensive grid infrastructure upgrades.
  - Revenue Generation: In some cases, PV power curtailment can be monetized through various mechanisms such as grid services or demand response programs. This creates potential revenue streams for PV system owners or operators.

- **Regulatory and Policy Implications**
  - Market Incentives and Regulations: Policies and market mechanisms that encourage or require curtailment of excess PV power can be implemented to ensure grid stability and incentivize efficient renewable energy integration.
  - Curtailment Limits and Compensation: Establishing appropriate curtailment limits and compensation mechanisms becomes important to strike a balance between grid management needs and the economic viability of PV projects.

It is important to note that while curtailment reduces the immediate utilization of PV power, it can still be a valuable strategy for grid management and long-term sustainability. Striking the right balance between PV power curtailment and maximizing renewable energy utilization is a key consideration for the successful integration of PV power into the energy landscape.

4.3. Future work

4.3.1. Autonomous dual active power-frequency control in power system with small-scale photovoltaic power generation

There are different aspects that can be created as a progression to the idea of dual *p-f* droop control. These aspects involve the application of dual *p-f* droop control in microgrids, using the *p-f* droop control along with reactive power- voltage (*Q-V)* droop control and finally supporting these mentioned numerical simulation with experimental studies for more validation.

- **Impact assessment of proposed method using a more realistic power system model**

The proposed dual *p-f* droop control should be tested using a detailed model in consideration of the existence of various types of generators, different irradiance fluctuations among different regions, different control schemes such as dual *p-f* droop control and other direct controls by the system operator, etc. Then, a sensitivity analysis will be also done for some factors such as the used frequency threshold, PV curtailment ratio, numbers of cycles of frequency measurement and the droop setting. Accordingly, the impact of this variability on the system frequency deviation will be investigated. Finally, various changes in demand data especially their surge will reflect the future inflation of demand, thus the effectiveness of the proposed control under this condition should be tested.

- **Grid Multiple-Area Model Simulation**

Next step will consider the emulation of multiple-area model replicating the equipment used in single-area model. Accordingly, additional synchronizing power model is implemented to merge the multiple areas together. Then, this model will simulate a fault that might occur in a system geographically and hence separate the accident occurrence point and allow PV unit to supply adequate active power compensating the isolation of the fault and hence adjusting frequency of the system.

- **Implementation of dual *p-f* droop control in microgrids**

In this study the application of dual *p-f* droop control proved its effectiveness in supporting LFC and mitigating the frequency deviations while the generators can eliminate the remaining fluctuations. On the other hand, virtual inertia control proved its effectiveness in microgrids in terms of quick reactions to frequency deviations [1]. For the purpose of mitigating normal and emergency frequency deviations in a microgrid, dual *p-f* droop control can be applicable, as the fast frequency response of this control can be realized to be of quick response as the virtual inertia and slow frequency response mitigate the normal frequency deviations. This proves that dual *p-f* droop control has an additional functionality over the virtual inertia control.

- **Voltage issue at high penetration of PV systems**

In the present work, the regulation active power (dP_{reg}) is adjusted according to the increment of measured frequency using *P-f* droop control. The amount of active power injected or absorbed by the PV system may affect the voltage and reactive power dynamics of the network accordingly. To accommodate these changes, additional droop control such as *Q-V* must be used as more PV installations will exist in the distribution network where line impedance is resistive. In this droop control, the voltage changes can be adjusted by absorbing or injecting reactive power by the PV system and therefore maintain a nominal voltage level. Due to different dynamics nature and timescale, the overlap between frequency/active power and voltage/reactive power in power systems is not so strong, and this fact allows to design *p-f* and *Q-V* droops, separately. Considering the mentioned dynamic overlap, recently some research works have been done on the simultaneous frequency and voltage control design. For example, in [2], voltage and frequency droop controls were operating simultaneously by a new control method. Moreover, frequency and voltage control, including mitigation of voltage harmonics, are achieved without the need for any common control circuitry or communication between inverters. That approach has a superior behavior regarding the mitigation of voltage harmonics, short-circuit behavior and the effectiveness of the frequency and voltage control. While in [3], a technique was proposed based on the droop control method that uses locally measurable feedback signals. This method is usually applied to achieve good

active and reactive power sharing when communication between the inverters is difficult due to its physical location.

- **Experimental study supporting numerical simulation of the dual *p-f* droop control**

The proposed control should be tested by using the experimental setup described to approve its efficiency in realistic situations and conduct a comparison between numerical simulation and experimental results. Therefore, a supply-demand balancing simulation model using hardware-in-the-loop simulation (HILS) can reflect the frequency variation in the network involving one area model of grid. HILS experimental environment enables PV simulation power supply of a real machine to be connected to a computer simulation model will simulate a power system phenomenon in real-time. HILS is crucial to construct computer simulation model operates in real time and each area model is composed of generator model and an inertia model.

4.3.2. Optimal allocation of curtailment levels of PV power output in different regions in consideration of reduction of aggregated fluctuations

Optimal allocation of CL among each region is accomplished by forming statistical patterns of average value and maximum fluctuation against different CL (Avg-CL and MF-CL patterns) to distinguish each region PV power output behavior in short-term. Using these relations, different CL to be allocated to each region. Thus, the optimal CL in each region will minimize the fluctuation of aggregated PV power output without precisely forecasting the time-series of PV power output.

By enhancing the short-term forecasting accuracy, more specific MF-CL and Avg-CL patterns can be prepared and chosen among the various patterns available. Based on the assumption that further improvement of short-term forecasting accuracy, additional study can be conducted to use statistical data for creating more classifications of MF-CL and Avg-CL patterns to reflect more different PV power output behaviors, hence, providing highly accurate CL allocation.

Another issue is to allocate optimal CL in consideration of the transmission capacity is limited. This means that the congestion management plays a crucial role in determining the extent of PV power curtailment. In situations where the available transmission infrastructure is insufficient to handle the full output of PV power, congestion can occur, posing risks to grid stability. To prevent overloading and ensure reliable operation, grid operators may implement curtailment measures. PV power curtailment serves as a congestion management tool by selectively reducing or limiting the power generation from PV systems located in congested areas. This approach helps balance the power supply and demand within the constraints of the transmission infrastructure, optimizing the utilization of available transmission capacity. By strategically curtailing PV generation, grid operators can regulate the flow of power, minimize transmission bottlenecks, and maintain a stable grid. However, it is essential to consider alternative solutions, such as grid upgrades, energy storage systems, and demand response programs, to mitigate congestion and minimize the need for frequent or prolonged curtailment. A comprehensive approach that combines curtailment with infrastructure enhancements and innovative grid management techniques is necessary to effectively manage congestion, ensure reliable PV power integration, and maximize the utilization of renewable energy resources.

4.3.3. Expansion of the proposed ideas of this dissertation

Hydrogen plants and battery energy storage systems can indeed absorb the surplus power generated by renewable energy sources such as PV systems. The response of battery energy storage system can be faster than that of hydrogen plants which makes battery energy storage system more effective in areas with high and quick fluctuations of power. The system operator will have the coordinate the operation of battery energy storage system or hydrogen plants. Another difference between hydrogen plants and battery energy storage system is that hydrogen plants will have higher energy density which makes the energy stored for a longer time horizon and used for different applications rather than supplying demand. Hence, based on the application, system operator would choose the appropriate storage system.

PV systems convert sunlight directly into electricity, and this electricity can be used to power various applications, including hydrogen production. Hydrogen production typically involves a process called electrolysis, where water is split into hydrogen and oxygen using electricity.

The electricity required for this process must come from various sources, including PV systems. When a PV system generates excess electricity that is not immediately needed, it can be used to power the electrolysis process in a hydrogen plant, which splits water into hydrogen and oxygen. There are major types of electrolysis available today i.e. alkaline type and solid polymer type. The later one has a quicker response. The hydrogen can then be stored and used as a clean and versatile energy carrier. It can be used for various applications, such as fueling hydrogen fuel cells for vehicles or as a source of energy for industrial processes.

Based on the proposed study in Chapter 2, similar to high penetration of small-scale PV, high penetration of hydrogen power plants will be expected. Hence, the smart inverters of hydrogen power plants can adopt the same control scheme of dual *p-f* droop control to regulate the frequency. Since solid polymer electrolysis hydrogen plant has faster response, the droop control can be applicable to use it for frequency regulation

Based on the proposed study in Chapter 3, there can be different scenarios to the utilization of optimal allocation of curtailment and integrating PV systems with hydrogen plants. One potential scenario is portrayed through this simple example. If there are two regions; one has fluctuating power output and the other has uniform power output, hydrogen power plant can be following the fluctuating PV power output to utilize the fluctuating PV power. However with implementing the scheme of optimal allocation curtailment levels to different regions, the fluctuations will be mostly eliminated that will reduce the requirement of hydrogen power plants utilizing fluctuating PV power and also reduce the burden of generators reducing the frequency fluctuations caused by high penetration of PV in the power system.

References

[1] R. Ofir, U. Markovic, P. Aristidou and G. Hug, “Droop vs. virtual inertia: Comparison from the perspective of converter operation mode,” in the *Proceeding of 2018 IEEE International Energy Conference (ENERGYCON)*, Limassol, Cyprus, 2018, pp. 1-6, doi: 10.1109/ENERGYCON.2018.8398752.

[2] L. Montero, A. Bello, and J. Reneses, “A Review on the unit commitment problem: approaches, techniques, and resolution methods,” in *Energies*, vol. 15, no. 4, p. 1296, Feb. 2022.

[3] H. Sangrody, N. Zhou and Z. Zhang, “Similarity-Based Models for Day-Ahead PV Generation Forecasting,” in *IEEE Access*, vol. 8, pp. 104469–104478, Jun. 2020.

Acknowledgments

I would like to sincerely thank Professor Takeyoshi Kato for his guidance and support along every step of my Masters and PhD degrees. I saw a professor with vision and plan, who is able to lead his students on a concretely planned path to fulfill their objectives. My undeniable appreciation also goes to Assistant Professor Masaki Imanaka and Assistant professor Chiyori T. Urabe, who helped in setting a conductive atmosphere for students to enhance their knowledge and expertise, which is the epitome of our laboratory.

I would like to express my appreciation to the PhD committee members; Prof. Naoki Hayakawa, Prof. Masayoshi Yamamoto, and Prof. Yuzuru Ueda for their constructive comments and revisions.

I thank each and every member of my laboratory for an admirable intercultural workspace, thereby, facilitating constant learning among another on both academic and personal level.

My research is financially supported by the Ministry of Education, Culture, Sports, Science and Technology of Japan through providing MEXT scholarship funding. I was able to have a good work-life balance for which I am grateful. The Power Energy Professional (PEP) training program, part of Waseda University's graduate programs, is a collaborative effort involving 13 prominent Japanese universities. Through this program, I have had the opportunity to delve into a diverse range of studies, spanning from electrical engineering to humanities and social sciences. This holistic approach has significantly contributed to fostering energy innovation and has greatly benefited my learning experience.

My family, my support system, I could not have done this without them. My father who had always believed that whatever path you choose, you have to excel in it. He encouraged me to travel to pursue further education and enhance my expertise. My mother had always cared about my mental and physical state the entire way. My siblings, the care they gave, the phone calls they made, to hear them growing and prospering, it all cheered me up. My extended family member who made sure that I am doing well through my life abroad, I truly value their connection.

My friends here in Japan, my family abroad, we have created memories of merriment and joy. Yet, we have each other in the hardships and difficulties. My other friends scattered all over the world, keeping in touch made me feel I have friends to talk to in all time zones. These connections were valuable in the completion of my work, thank you.

Submissions

Paper Titles	Method and Timing of Publication	Authors
I. Academic Journals		
1. Optimal Allocation of Curtailment Levels of PV Power Output in Different Regions in Consideration of the Reduction of Aggregated Fluctuations	IEEE Access (early access, published July 2023) DOI:10.1109/ACCESS.2023.3296091	N. Harag, T. Urabe, T. Kato
2. Autonomous Dual Active Power-frequency Control in Power System with Small-scale Photovoltaic Power Generation	Journal of Modern Power Systems and Clean Energy, vol. 10, No. 4, pp. 941-953, July 2022. DOI:10.35833/MPCE.2020.000700	N. Harag, M. Imanaka, M. Kurimoto, S. Sugimoto, H. Bevrani, T. Kato
II. International Conference		
1. Optimal Allocation of Curtailment Level of PV Power Output in Different Regions in Consideration of the Reduction in Aggregated PV Power	International Conference on Renewable Energy and Power Quality 2023 (ICREPQ'23). Paper No. 265, Madrid, Spain, May 2023.	N. Harag, T. Urabe, T. Kato
2. Optimal Allocation of Curtailment Levels of the PV Power Output in Consideration to the	International Council on Electrical Engineering (ICEE) Conference. Paper No. F20220315-0971, Online (Korea), July 2022.	N. Harag, T. Urabe, T. Kato

	Reduction of the Total Fluctuations in Different Regions		
3.	An Experimental Study on Dual Power-frequency Droop Control of Photovoltaic Power Generation for Supporting Grid Frequency Regulations	International Council on Electrical Engineering (ICEE) Conference. Paper No. ICEE19J-050, Hong Kong, July 2019.	N. Harag, M. Imanaka, M. Kurimoto, S. Sugimoto and T. Kato

Appendix

Example to highlight the electricity demand level and its variability, and thermal units needed for meeting the demand as well as providing flexibility for the anticipated variability of the demand, a simple example is demonstrated as follows:

1. Assuming an electricity demand of 10 GW in a one hour time period and given that the variability of demand is 2%, then the demand variability corresponds to 0.5 GW. Also, assuming the capacity of one thermal unit to be 0.5 GW, the LFC reserve flexibility will be 5% of its capacity that corresponds to 0.025 GW. Then the number of units needed to provide this LFC flexibility is 0.5/0.025 = 20 units. Since these units will be operating at 0.475 GW to provide this flexibility, their total power output will be 20 units x 0.475 = 9.5 GW, which leaves 0.5 GW shortage to balance out the 10 GW of demand. Hence, an additional thermal unit operating at 0.5 GW will be needed. In summary, 20 units of 0.475 GW and 1 unit of 0.5 GW are needed to balance the demand and provide the required flexibility.

2. Adding another supply resource to the previous example such as PV of average power output of 5 GW will yield the following scenario. As mentioned previously the variability of PV power output accounts for 10% which corresponds to 0.5 GW in this example. The variability of the demand and PV power output is independent which yields a higher flexibility requirement for the demand that is equal to $\sqrt{0.5^2 + 0.5^2} = 0.7$ GW. Hence, the number of thermal units needed are 0.7/0.025 = 28 units. If the thermal units operate at 0.475 GW, the total power of thermal units will be 0.475 x 28 = 13.3 GW which exceeds the electricity demand level (10 GW). Then, the assumption of the minimum capacity of a thermal unit to be 30% is introduced, this corresponds to 0.15 GW of minimum capacity of a single thermal unit. However if the thermal unit operates at 0.15 GW, there will not be enough room for a downward flexibility of 0.025, then the realistic minimum capacity of single unit should be 0.175 GW. For 28 units operating at 0.175, the total capacity becomes 4.9 GW, adding the

average PV power output of 5 GW, the resultant supply power becomes 9.9 which does not balance out the demand. Further adjustment is needed by the thermal units to compensate for the 0.1 GW shortage which is raising the each unit's power by 0.1 GW/28 units = 0.0035 GW to balance out the demand.

3. In the case where 8 units out the 28 units of the thermal units are nuclear units where each has the same rated capacity of thermal unit (0.5 GW), and that nuclear units in Japan do not provide LFC reserve, the scenario will change accordingly. The total power of the supply resources will be 12.5 as for 20 thermal units) at 0.175 GW each will give 3.5 GW, 8 of nuclear units of 0.5 GW will give 4 GW and the average PV power output is 5 GW. This exceeds the electricity demand by 2.5 GW and since the thermal units are already adjusted to operate at their minimum capacity, the next adjustment according to the previously mentioned curtailment rule of power plants in Japan is the curtailment of PV power output. Therefore, the PV power output will be curtailed by 2.5 GW (from 5 GW to 2.5 GW, accounts for 50% of PV power output curtailment) for the supply to balance out the demand. If the average PV power output is more than 5 GW used in this example, more curtailment will be applied to reach the 2.5 GW that will balance out the demand beside the other supply resources.